DEVELOPMENT AND APPLICATION OF ANALYTICAL INSTRUMENTATION FOR MONITORING FUNCTION OF ISLETS OF LANGERHANS

by

Kendra Rae Reid

A dissertation submitted in partial fulfillment
of the requirements for the degree of
Doctor of Philosophy
(Chemistry)
in The University of Michigan
2009

Doctoral Committee:

Professor Robert T. Kennedy, Chair
Professor Raoul Kopelman
Professor Mark E. Meyerhoff
Professor Michael D. Morris
Associate Professor Shuichi Takayama

To Mom and Dad, for their constant guidance, support, and love, without which this Ph.D. would not have been possible.

ACKNOWLEDGEMENTS

I would like to sincerely thank, first and foremost, my advisor and dissertation chair, Dr. Robert T. Kennedy for his contributions to this research, and for all of his guidance and support during my time at the University of Michigan. I am grateful for the mentorship that Bob has provided me in the field of analytical chemistry. Bob's encouragement throughout graduate school was invaluable. Second, I would like to thank the remaining members of my committee, Dr. Raoul Kopelman, Dr. Mark E. Meyerhoff, Dr. Michael D. Morris, and Dr. Shuichi Takayama, for their additional ideas and suggestions, and for taking the time to serve on my committee. I would also like to thank my collaborators, Dr. Rohit N. Kulkarni and associates for their work with the ObRKO project and Dr. Ayyalusamy Ramamoorthy, Dr. Jeffrey Brender, and associates for our partnership in the IAPP project.

I wish to express genuine gratitude to current and former members of the Kennedy lab who taught me countless invaluable skills and lessons. Specifically, I would like to thank Dr. Gabriella M. Dahlgren and Dr. Jonathan G. Shackman for teaching me the foundation of skills necessary for my thesis work. I would like to thank all the other members of the Kennedy Lab, past and present, for their general guidance and suggestions and for their company throughout my graduate school career.

I am wholeheartedly grateful for the dear friends who have supported me throughout this endeavor. In Ann Arbor, I am particularly thankful for the support and love that my good friends, Ms. Amberlyn M. Wands, Dr. Tasneem H. Lira, and Dr. Sarah

J. Bethune, provided me. Afar, I would like to first extend thanks to my fantastic and supportive undergraduate advisor, Dr. Eric C. Conte, for introducing me to the world of analytical chemistry, and for his encouragement before and throughout graduate school. I would like to thank Ms. Emily R. Causey, Ms. Amanda J. Cummins, Dr. Paul D. Kelsey, and Ms. Melissa L. Bieber, all long-standing friends who supported me throughout my graduate career.

I would also like to extend my gratitude to my church families in Ann Arbor and back home. In particular, I would like to thank Rev. Melissa Anne Rogers, of First Presbyterian Church of Ann Arbor, for her guidance and support throughout the second half of my graduate school career. I am also thankful for the members of my church back home, First Christian Church of Bowling Green, KY, for their prayers and support.

I would like to give very special thanks to my wonderful family. I would first like to express gratitude to my parents, Dr. Sherry M. Reid and Mr. Ronald V. Reid. I will forever be grateful for their belief in me and for their encouragement. I am also thankful for my brothers, Mr. Carl E. Reid, Mr. Chris S. Reid, my sister, Ms. Kerri L. Brodersen, as well as my sisters-in-law, Ms. Wanda Reid and Ms. Lori Reid, and my brother-in-law, Mr. Jason Brodersen, for their love and support.

Finally, I would like to thank Dr. Charles R. Evans, for his love and companionship. I am extremely blessed to have a fiancé as loving and sincere as Charles. Thank you, Charles, for your suggestions in lab and for your constant encouragement, support, and love throughout my final stride of graduate school.

TABLE OF CONTENTS

LIST OF FIGURES

Figure

LIST OF TABLES

Table

LIST OF APPENDICES

Appendix

LIST OF ABBREVIATIONS

Ab	Antibody
ADP	Adenosine diphosphate
ATP	Adenosine triphosphate
B/F	Bound-to-free ratio
BSA	Bovine serum albumin
BSS	Balanced salt solution
CCD	Charge-coupled device
CE	Capillary electrophoresis
CE-LIF	Capillary electrophoresis – laser-induced fluorescence
EDTA	Ethylenediaminetetraacetic acid
ELISA	Enzyme-linked immunosorbent assay
EOF	Electroosmotic flow
FFA	Free fatty acid
FITC	Fluorescein isothiocyanate
G	Glucose
GLP-1	Glucagon-like peptide-1
HFD	High fat diet
HV	High voltage
Hz	Hertz
K_{ATP}	ATP-sensitive potassium channels
kHz	Kilohertz
kD	kiloDalton
K_d	Dissociation constant
LIF	Laser induced fluorescence
LOD	Limit of detection
mM	Millimolar
µg	Microgram
µL	Microliter
NA	Numerical aperture
nM	Nanomolar
pL	Picoliter
pM	Picomolar
PMT	Photomultiplier tube
R^2	Coefficient of determination of a linear regression
RFU	Relative fluorescence units
RIA	Radioimmunoassay
RSD	Relative standard deviation
SD	Standard deviation

SEM	Standard error of the mean
S/N	Signal-to-noise ratio
UV	Ultraviolet
kV	Kilovolts
W	Watts

ABSTRACT

Impaired insulin secretion is a hallmark of type 2 diabetes. Numerous reports of long-term kinetics of insulin secretion from islets have been reported, but potentially underlying fast kinetics of the phenomena are difficult to study using conventional insulin measurement techniques. To monitor long-term insulin secretion from islets of Langerhans, a microfluidic chip capable of long-term operation was designed. All buffers and reagents were continuously perfused into the chip, ensuring only fresh reagents were used for analysis. The device performed a capillary electrophoresis-based competitive immunoassay every 6 s and operated for 24 h, resulting in the completion of 14,400 assays in 24 h.

A microfluidic chip was developed to perform intracellular calcium measurements on islets. With the chip, rapid changes were made to the islet environment by perfusing glucose, peptides or other stimulants over the islets. The chip was used in a collaborative effort to investigate the membrane-disrupting effects of islet amyloid polypeptide. Application of the peptide to islets resulted in the flux of calcium into islets, presumably due to the membrane-disrupting effects of the peptide. The results, corroborated by results from experiments performed on model membranes, identify a role of the His18 residue of the peptide for the demonstrated membrane-disrupting effects.

The intracellular calcium chip was also used in a collaborative effort to investigate leptin signaling in islets. By monitoring a number of parameters, including islet cell mass, insulin secretion, and intracellular calcium concentration, islets from

pancreas-specific leptin receptor knock-out mice were compared with control islets. The effects of leptin, palmitic acid, and glibenclamide on intracellular calcium concentration and insulin release were explored. The results from the investigation demonstrate the inhibitory effect of leptin on calcium flux into islets and on glucose-stimulated insulin secretion and suggest a role of leptin-signaling on islet behavior.

Oscillations in oxygen consumption by islets have been observed to correlate with insulin release levels, and it is of interest to study the pathway that links the two parameters in islets. To investigate the link between metabolism and glucose-stimulated insulin secretion, a fiber optic nanosensor was developed to monitor oxygen consumption by islets. The submicron dimensions of the sensor enabled high spatial resolution for oxygen measurements, and the sensor demonstrated good reversibility, good stability, and high sensitivity compared with previously-reported optical oxygen sensors. Such characteristics make the sensor a potentially good candidate for measuring oxygen consumption by islets.

CHAPTER 1

INTRODUCTION

Diabetes is of increasing interest due to the growing prevalence of the disease; for instance, the total prevalence of diabetes in the United States increased 13.5% from 2005 to 2007.[1] In fact, 1 in 3 Americans will develop the disease during his/her lifetime if the present trends persist. In 2007, approximately 23.6 million people in the U.S., or 7.8% of the population, were estimated to suffer from diabetes, and the disease was estimated to cost the U.S. $174 billion in direct and indirect expenditures. It is reported that well over 200,000 U.S. citizens died because of diabetes, making diabetes the 5th deadliest disease in the U.S. Additionally, because diabetes is generally under-reported on death certificates, it is believed that the death toll of diabetes is significantly higher than officially reported. Due to the devastating impact of the disease, further investigations into the pathology of the disease are warranted.

Diabetes can be classified into two types. Type 1, or insulin-dependent, diabetes mellitus arises from an absolute deficiency of insulin due to the autoimmunological destruction of β-cells.[2] Type 2, or non-insulin-dependent, diabetes mellitus, results from a combination of impaired insulin secretion and the resistance of skeletal muscle and adipose tissue to insulin.[3] Type 2 diabetes accounts for 90-95% of diagnosed diabetes cases in the U.S.[4] The pathogenesis of type 2 diabetes is not well-understood. Several

factors, including obesity and genetic predisposition, are implicated in the development of type 2 diabetes. The purpose of this work is to develop new analytical tools with the hope that they may be used to better study the root causes of diabetes.

Islets and Glucose-Stimulated Insulin Secretion. Pancreatic islets of Langerhans are microorgans composed of 2000-4000 cells and are approximately 50-300 μm in diameter. An adult human pancreas has approximately 1 million islets, comprising 1-2 % of the pancreas. Two images of typical mouse islets are shown in Figure 1.1 depict a section of pancreas showing a single islet (left)[5] and an image of a single isolated islet (right).

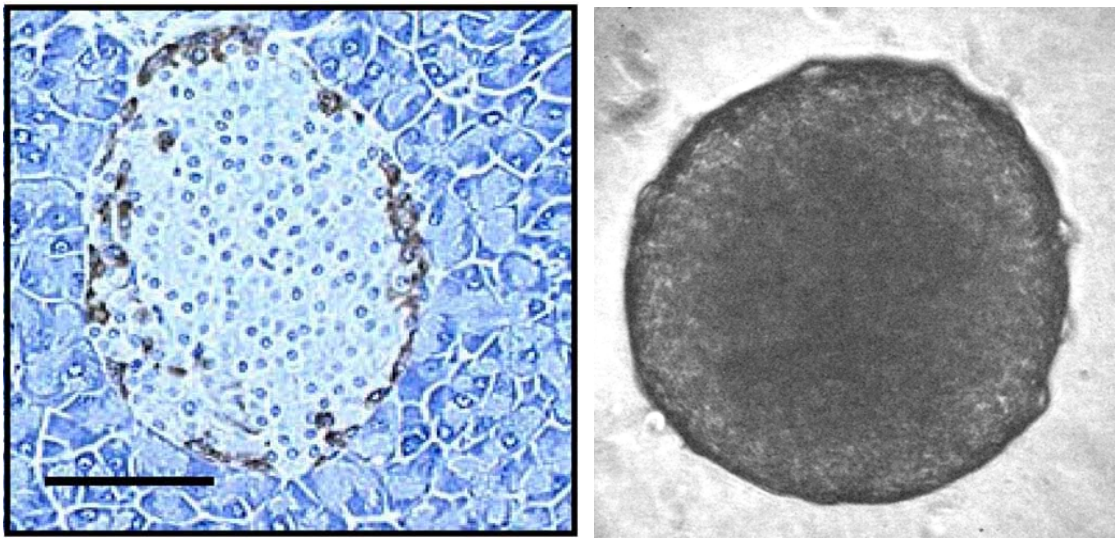

Figure 1.1. Images of pancreatic islets of Langerhans. (A) A section of pancreas showing a single islet stained to illustrate a core of β-cells (nuclei stained in blue). Scale bar = 50 μm. Reproduced with permission from reference 5. (B) A photomicrograph image of a single isolated islet.

Islets are composed of four cell types: α-cells, which secrete glucagon; β-cells, which, depending on the species, compose nearly 70-80% of an islet and are responsible for secreting insulin; δ-cells, which secrete somatostatin; and PP-cells, which secrete

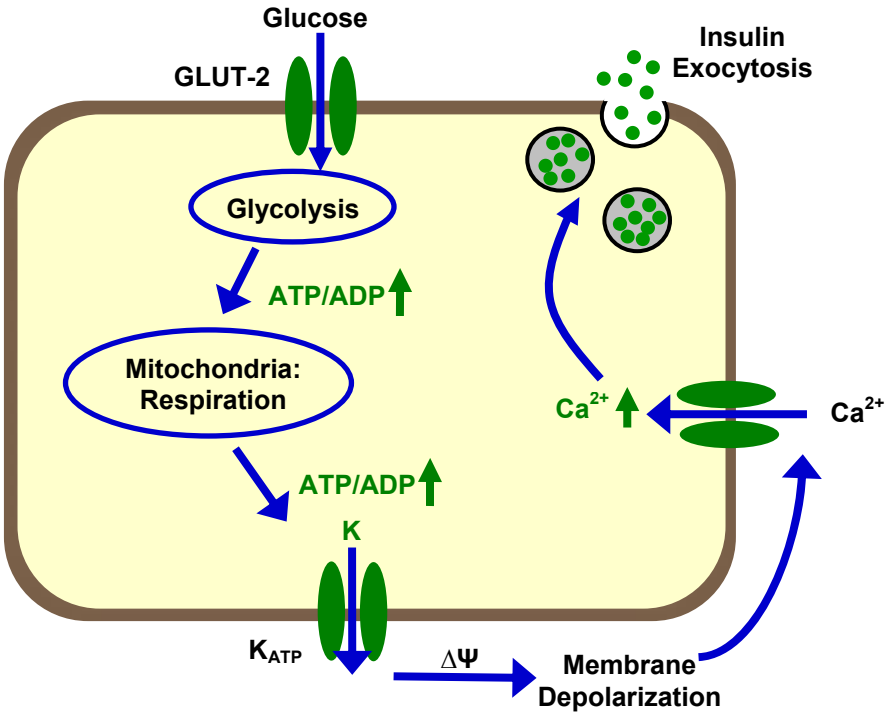

Figure 1.2. Simplified schematic of GSIS. β-cells are stimulated with glucose, which enters the cells through the Glut-2 transporter on the cell membrane. Subsequent metabolism results in an increase in ATP, which causes the K_{ATP} channels to open. The resulting membrane depolarization causes the voltage-sensitive Ca^{2+} to open. The influx of Ca^{2+} ultimately results in exocytosis of insulin.

Pancreatic Polypeptide.[5] At elevated levels of glucose, β-cells are stimulated to secrete insulin. Insulin is then carried by the bloodstream throughout the body, and it works tomaintain glucose homeostasis.[6] Glucose-stimulated insulin secretion (GSIS) involves metabolism of the sugar to generate appropriate intracellular signaling events. While the coupling of metabolism with insulin secretion is not yet clear, the present model suggests that glucose is rapidly transported into the β-cell through glucose transporter-2, after which time glycolysis occurs. Glycolysis produces ATP and the mitochondrial substrates, NADH and pyruvate. Mitochondrial respiration then produces a large amount of ATP. The further increase in the ATP/ADP ratio activates K_{ATP} channels causing the cell to depolarize, opening L-type Ca^{2+} channels, and allowing Ca^{2+} to enter. The rise in

intracellular Ca^{2+} concentration leads to the subsequent triggering of insulin secretion.[6] Figure 1.2 illustrates some of the known molecular pathways of GSIS from the pancreatic β-cell. Failure of β-cells due to a decrease in β-cell mass and to the decline of β-cell function, including GSIS, is a hallmark of diabetes.[3] Consequently, much effort has been placed on investigating the molecular and biochemical mechanisms leading to β-cell failure.

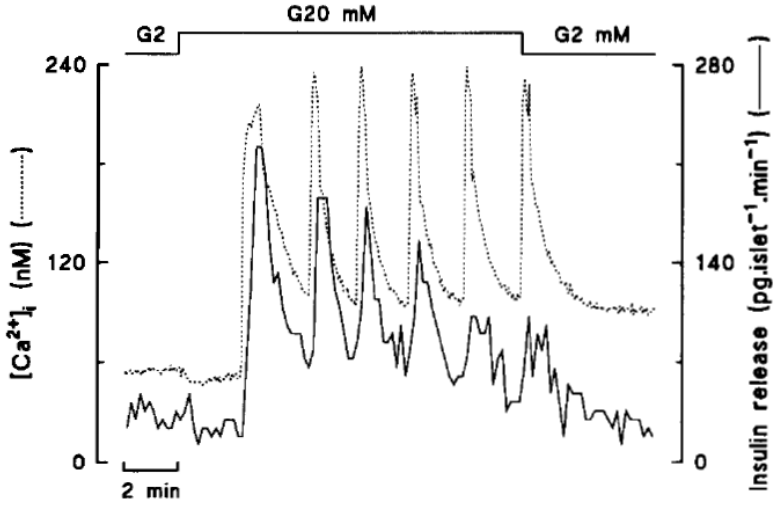

Figure 1.3. Biphasic and pulsatile insulin secretion. Insulin secretion is characterized as biphasic. Stimulate with glucose results in a "first phase" spike of insulin secretion followed by a "second phase" of less insulin secretion. The second phase may gradually rise and is often pulsatile. Reproduced with permission from reference 7.

Insulin Secretion Dynamics. GSIS both *in vivo* and in isolated islets is characterized by a biphasic and pulsatile nature, as illustrated in Figure 1.3.[8] The 1st-phase consists of a sharp spike in insulin release that typically occurs within 2-5 min of glucose administration. It is theorized that the "1st phase" results from the GSIS model shown in Fig 1.2. The length and profile of the "2nd phase" varies from species to species. The 2nd phase in mammals is characterized by a gradual rise in insulin release for several minutes often accompanied by pulsatile behavior.

In vivo oscillations have a period of 5-15 minutes, depending on the species, and the pulsatile release of insulin accounts for 75% of all insulin secretion in humans.[9] Several studies suggest the oscillatory secretion patterns are important for optimal insulin action[10-12] and insulin secretion.[13, 14] Furthermore, the loss of the pulsatile secretory patterns is implicated in the development of type 2 diabetes.[15-17] In fact, the loss of insulin secretion oscillations in healthy relatives of type 2 diabetic individuals and in obese non-diabetics suggest that loss of oscillations may be one early sign of type 2 diabetes.[18, 19] The impairment of oscillatory secretory patterns in type 2 diabetics as compared to healthy individuals is illustrated in Figure 1.4.[17] The figure demonstrates that healthy individuals secrete insulin in an oscillatory manner with a period of 10 min, whereas type 2 diabetics exhibit more irregular insulin secretion oscillations and elevated serum insulin concentrations.

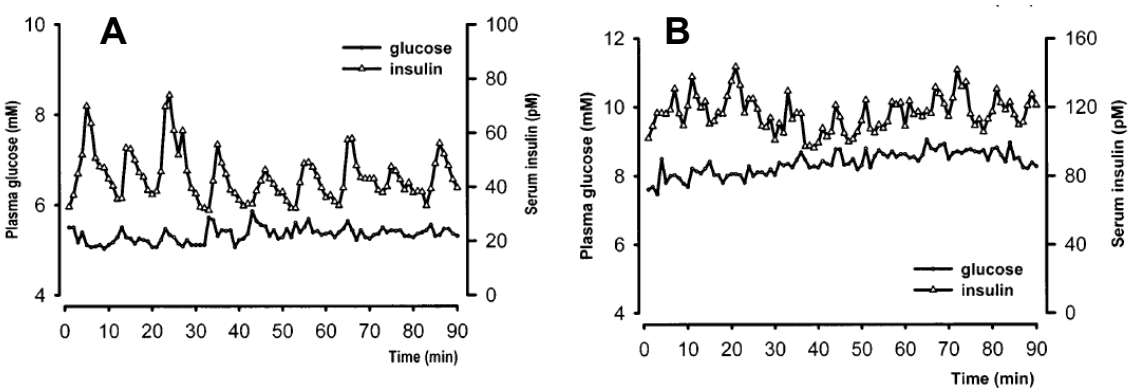

Figure 1.4. Plasma glucose and serum insulin levels in normal (A) and diabetic subjects (B). Subjects were infused with 6 mg kg^{-1} glucose for 1 min every 10 min. The normal subjects exhibited pronounced oscillations in serum insulin level, while the diabetic subjects did not. Reprinted with permission from The American Diabetes Association and reference 17.

Long-term Physiological Phenomena of Islets. In addition to the short-term (<2 h) trends described above, islets also exhibit numerous long-term insulin secretion phenomena. While short-term secretion dynamics of islets, including oscillatory patterns of periods <15 min, have been closely studied and are better characterized, much remains

to be clarified regarding the mechanisms of long-term insulin secretion phenomena. A brief review of long-term islet studies performed to date is included below. A major thrust of the work in this thesis is directed towards design and development of improved analytical technologies to investigate long-term islet secretion phenomena.

Slower ultradian insulin secretion oscillations of periods ranging from 50-120 min have been reported.[20] The ultradian rhythms have been described in both humans and animals and have been observed under multiple conditions, including during intravenous glucose infusion[21] and during continuous enteral nutrition.[22] Figure 1.5 represents plasma insulin concentration and corresponding insulin secretion rate profiles in an individual monitored with a 2-min blood sampling method during continuous enteral nutrition.[20] Spectral analysis of the two profiles shown in Figure 1.5 identified the existence of one rhythmic component with a periodicity of 48-96 min and another rhythmic component with a periodicity of 6-12 min.

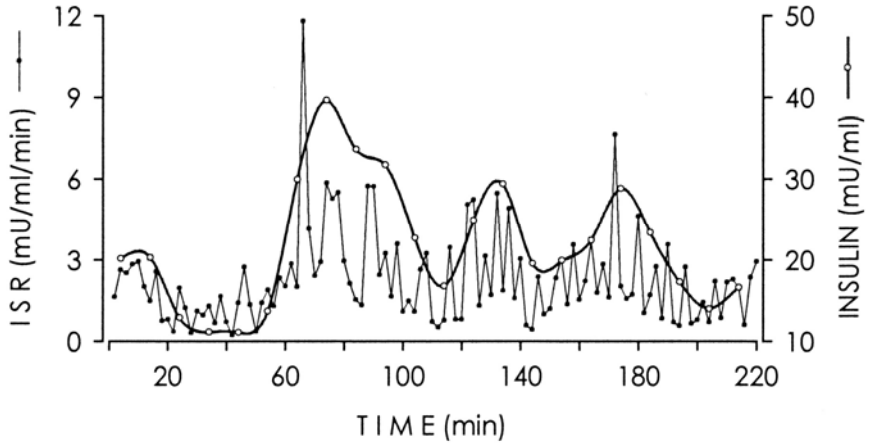

Figure 1.5. Ultradian rhythms in insulin secretion. Plasma insulin concentration and ISR profile in one subject studied during continuous enteral nutrition demonstrate the existence of a slower rhythmic component (period = 48-96 min) and a more rapid rhythmic component (period = 6-12 min). Reprinted with permission from The American Diabetes Association and reference 20.

Like the more rapid oscillations, ultradian oscillations are associated with improved insulin action,[23, 24] and are lost or altered upon insulin secretion impairment.[25-

[27] In fact, alterations in the ultradian slower pulsatile insulin rhythms have been reported in patients with type 2 diabetes, as demonstrated in Figure 1.6.[26] Figure 1.6 depicts an insulin secretion rate (ISR) profile in a control subject during continuous enteral nutrition (Figure 1.6A) and an ISR profile during continuous enteral nutrition in a type 2 diabetic patient (Figure1.6B). The clear ultradian rhythms present in the control subject are not present in the ISR profile from the type 2 diabetic individual. Due to the demonstration that the ultradian patterns are altered in type 2 diabetics, the ultradian insulin secretory patterns are of interest when investigating the pathogenesis of type 2 diabetes.

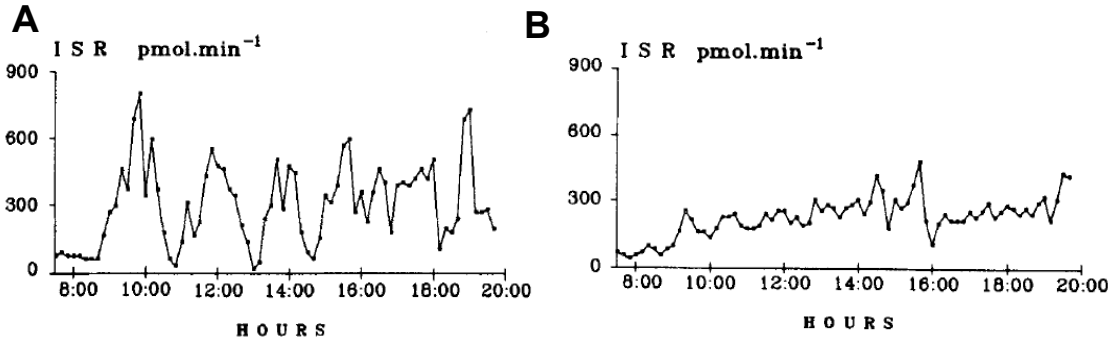

Figure 1.6. ISR profiles collected from a control subject and a type 2 diabetic patient during continuous enteral nutrition. While the control subject (A) exhibited defined ISR rhythms, the ISR pulses in the diabetic subject (B) were significantly less defined and lower in amplitude. Reproduced with permission from reference 27.

Additionally, circadian patterns in insulin secretion have been demonstrated.[28-30] The circadian insulin secretion rhythms appear important for maintaining glucose homeostasis.[21, 31-34] Figure 1.7 depicts plasma insulin concentration over the course of ~72 h (Figure 1.7A).[29] Following quadratic trend elimination, the data are fit with a cosine function (Figure 1.7B) making the oscillatory pattern with period ~ 24 h more apparent.

While multiple groups have reported the presence of circadian rhythms in insulin secretion, the mechanism causing the patterns is not yet elucidated. One group claimed

that the oscillations are regulated by an endogenous circadian oscillator located within the islets[29] or pancreas.[35] Another group reported findings that suggested that circadian oscillations in insulin secretion are a result of other neuroendocrine factors regulated by circadian rhythms in the central nervous system.[28]

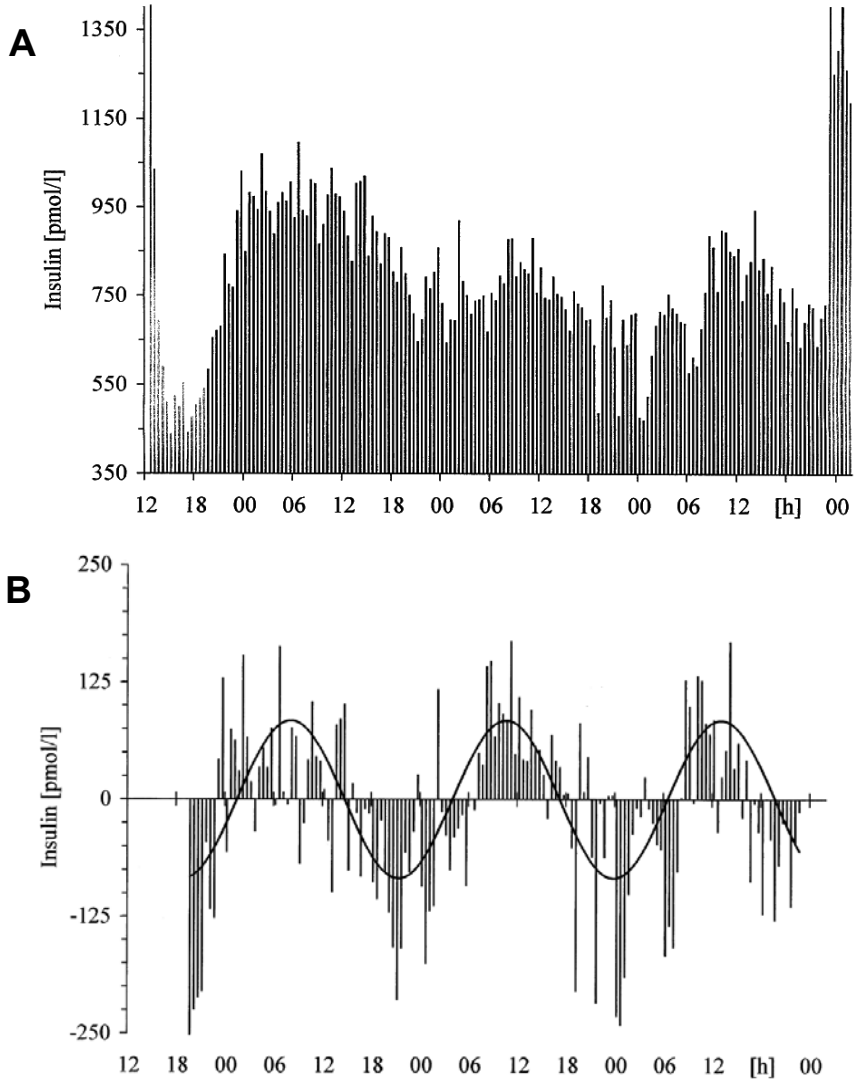

Figure 1.7. Circadian rhythms of insulin secretion from isolated islets. Rhythms with a period approximately equal to 24 h are apparent in the insulin secretory profile (A) from a batch of 300 islets. Media samples of the perfused islets were collected at 30 min intervals and analyzed using RIA insulin detection. Following trend elimination (quadratic trend), the data were fit with a cosine function (B), further illustrating the circadian rhythms. Reproduced with permission from reference 29.

The bulk of the reported studies of both ultradian and circadian rhythms have been performed *in vivo*. Although some investigations have been performed on isolated islets, these experiments were performed with batches of hundreds of islets.[29] Similar studies on single islets may reveal additional interesting dynamics, but it is not known whether single islets exhibit long-term oscillations, and if single islets do exhibit the long-term rhythms, it is not clear whether they will after culture. Furthermore, the evidence depicted in Figure 1.5 suggests that the ultradian rhythms may exist due to increasing and decreasing amplitude of the more rapid pulses, but the data were collected *in vivo*. Simplifying the experiment by performing similar studies on single islets may help to elucidate the mechanisms of the ultradian rhythms. Interestingly, it is not clear how the more rapid oscillations change over the course of 24 h, nor how alterations in the amplitude or the period of the oscillations may affect long-term secretion rhythms. Additionally, it has been suggested that the circadian rhythms are diurnal (meal-related);[28] thus, it may be of interest to investigate whether single islets can maintain the long-term rhythms under constant glucose conditions or whether variations in glucose are necessary. Methods devised to monitor single islets over longer periods are required to address these questions.

In addition to ultradian and circadian insulin secretion oscillations, other long-term islet phenomena have been reported. It has been demonstrated the culture conditions and duration can affect islet behavior.[36-38] One group demonstrated that intracellular Ca^{2+} concentration patterns in islets were influenced both by the culture duration (1 day vs. 2-4 days) and by glucose concentration (5-10 mM vs. 15 mM glucose).[36] It has also been reported that prolonged culture in low glucose (3-5 mM

glucose vs. 10 mM glucose) induces apoptosis of islet β-cells.[38] Such effects must be considered when performing experiments on isolated islets. A method capable of monitoring islets during culture may help to optimize culture duration and conditions.

Another example of long-term phenomena is the effect of metabolic overload in β-cells. GSIS is enhanced after acute exposure to fatty acids.[39] It was reported that GSIS (12.5 mM G) from a perfused pancreas is enhanced 65 fold after acute exposure to 0.5 mM stearate.[39] Conversely, chronic (~48 h or more) exposure of islets to elevated levels of fatty acids results in impaired GSIS.[40] Interestingly, however, it has been demonstrated that fatty acid-induced impairment of GSIS does not occur unless the islets are cultured in ~8 mM glucose or higher, as described by the concept of glucolipotoxicity.[41, 42] The effects on GSIS after chronic exposure of islets to 0.125 mM palmitate and oleate are illustrated in Figure 1.8; GSIS is significantly impaired after exposure to the fatty acids.

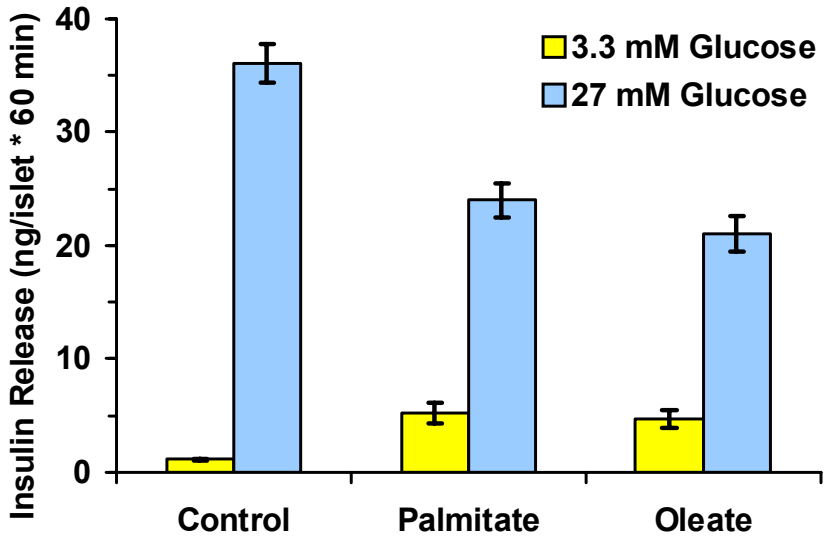

Figure 1.8. GSIS from islets after chronic exposure to fatty acids. Islets were cultured for 48 h with 0.125 mM of the indicated fatty acid. After chronic exposure to palmitate and oleate, basal insulin release was increased and GSIS (27 mM glucose) was impaired. Chart created from data from reference 40.

Despite the demonstration of the varying effects of fatty acids on insulin secretion, the mechanisms of the contradictory effects on insulin secretion after acute and chronic exposure to fatty acids are not yet elucidated. For instance, it is of interest to investigate how the kinetics of insulin secretion change over time with exposure to fatty acids. To date, insulin secretion has not been monitored with sufficient sampling rate and duration to observe the slow and fast kinetics of insulin secretion from islets exposed to FFA. The effects of FFA, however, are particularly relevant when investigating the link between obesity and type 2 diabetes. Numerous studies suggesting various physiological parameters may link the disease states of obesity and type 2 diabetes have been reported,[43-47] but, still, the specific mechanisms are not clear and thus warrant further investigation.

As already described, the mechanisms of long-term insulin secretion phenomena are understudied. Using conventional insulin monitoring techniques, the data collection and analysis from investigations of both slow *and* fast long-term insulin secretion patterns are exceedingly laborious and expensive. For example, faster insulin secretion oscillations are best observed by assaying secretion no less frequent than every 30 s. To monitor insulin release every 30 s for 24 h with conventional assays, it would cost $14,400, assuming a price of $5/assay. Furthermore, such a study would require the offline analysis of 2,880 fractions. If one were to increase the sampling rate to 10 s, *one* experiment would involve the analysis of 8,640 fractions and would cost $43,200. As a result, such methods are not conducive to simple, long-term studies. The development of an automated insulin assay capable of long-term operation could significantly further the investigation of the long-term events.

Various Methods for Insulin Detection. Insulin secretion patterns may be investigated *in vivo*,[9] in the perfused pancreas,[48] and with isolated islets.[7] Performing investigations on isolated islets may help to help to elucidate mechanisms of long-term insulin secretion trends because such experiments simplify the biological system as compared to *in vivo* experiments. Furthermore, secretory dynamics are best observed with single isolated islets, as illustrated in Figure 1.9. While a perfused pancreas (Figure 1.9A)[48] can be used to observe differences in GSIS, only the biphasic nature of insulin secretion is observed; however, when an isolated islet is stimulated with glucose, several potentially important oscillatory dynamics are observed in the second phase in addition to the first phase response (Figure 1.9B).[7]

It is difficult to monitor long-term insulin secretion patterns with high temporal resolution using conventional techniques. The most common methods of measuring insulin secretion from islets are radioimmunoassays (RIA) or enzyme-linked immunosorbent assays (ELISA). While these techniques are quite sensitive, the need for off-line fraction analysis makes the methods labor and time intensive and requires large sample volumes. An alternative method entails collecting the fractions, performing an assay to measure the C-peptide levels, and creating an insulin secretion rate (ISR) profile from the C-peptide levels using a two-compartmental model; the technique, however, allows only indirect measurement of insulin secretion and also requires off-line fraction analysis.[49]

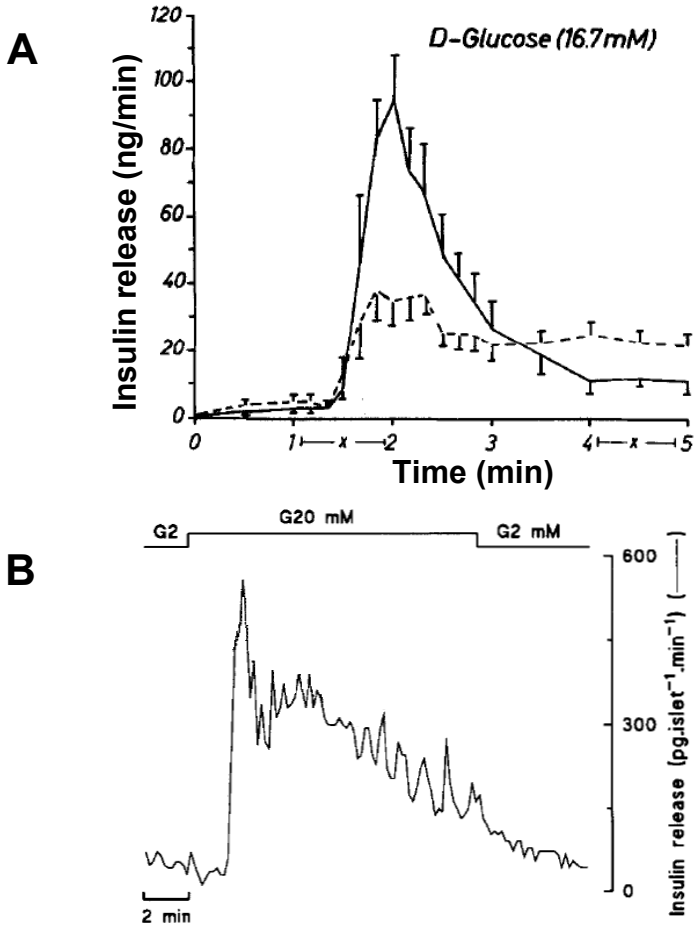

Figure 1.9. Insulin release from a perfused pancreas and a perfused islet. (A) The effect of D-glucose on acute insulin secretory response (1-5 min) of the perfused pancreas from thyroxine treated rats (——) and controls (-----) (B) Insulin secretory dynamics from a single, isolated, perfused islet. While the biphasic nature of insulin release from a perfused pancreas is apparent (A), much more secretory dynamics are observed from a single isolated islet (B). Reproduced with permission from reference 48 (top) and adapted from reference 7 (bottom).

Our lab previously developed a capillary system for monitoring of insulin secretion using an on-line capillary electrophoresis (CE) competitive immunoassay.[50] This system was later implemented on a microfluidic device. [51, 52] In the insulin immunoassay microchip, single islets were continually perfused and perfusate was sampled by EOF. The perfusate stream was monitored with 6 s temporal resolution and a limit of detection of 0.8 nM insulin was achieved. The microfluidic CE immunoassay device vastly improved insulin secretion monitoring by enabling 600 automated assays in

1 h of operation. Encouraged by the success of this chip for short term insulin measurements, we became interested in the possibility of using similar devices for longer term measurements to address the mechanisms responsible for the long-term insulin secretory patterns as well as the means of the impairment of the long-term phenomena.

Long-term Analysis of Living Cells on Microfluidic Chips. Interest in the use of microfluidic devices for cellular studies has increased dramatically in the last decade. There are several motives for performing cellular analyses on microfluidic devices. Microfluidic devices enable automation and integration of several functions important for cellular studies, including sampling, reactions with, injection, and detection of secretions from living cells. Additionally, the dimensions (10-100 μm) of typical microfluidic channels are compatible with cell sizes, and the devices are capable of manipulating large number of cells simultaneously. The tiny channel dimensions in microfluidic devices can also result in increased sensitivity due to less analyte dilution. Furthermore, should high applied voltages be necessary, Joule heating is less significant. Perhaps the primary reason for cellular studies on microfluidic devices, however, is the precise control over the cells' environments. The micro-environment in which the cells are housed is conducive for making rapid changes in concentrations of stimulants or other chemicals delivered to the cells via perfusion. Perfusion also allows for constant replenishment of nutrients and fresh buffer to the cells, which helps to maintain cell viability over time. Furthermore, with continuous perfusion, it is possible to monitor cell activity on-line and real-time. Such advantages also make microfluidic devices suitable for long-term culture and analysis of living cells.

Several studies have been performed that examine the feasibility of using microfluidics for long term cell culture and analysis. One system was used for long-term culture and monitoring of immobilized HFF11 cells, which originate from a cell line based on genetically modified HeLa cells.[53] The system consisted of a microchip flow cell unit housed beneath a photomultiplier tube, used for luminescence detection, as depicted in Figure 1.10. The application of the system to monitor luciferase reporter gene activity in HFF11 cells via a stop-flow injection-based chemiluminescent assay. The results demonstrated the possibility of long-term real-time monitoring of cellular events using a microfluidic system, but temporal resolution was limited to 1 h.

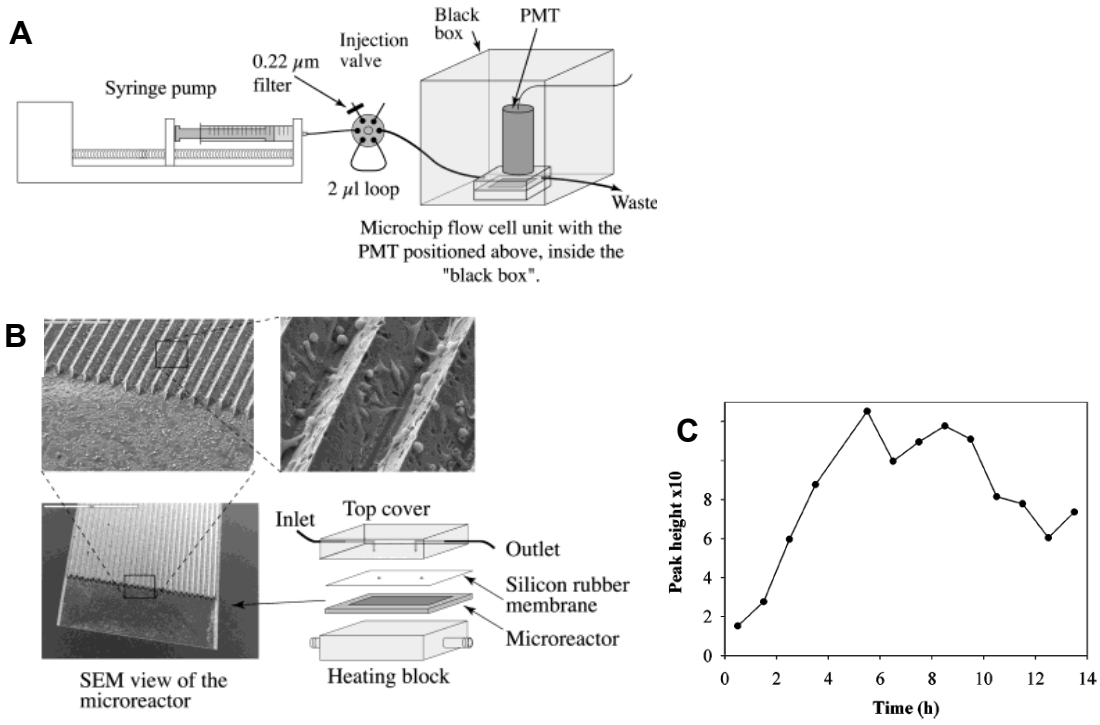

Figure 1.10. Long-term monitoring of HFF11 cells. (A) Microfluidic system. Cells were housed in a microfluidic flow cell unit and perfused with buffer via a syringe pump. The microchip was placed below a PMT for chemiluminescence detection. (B) Microchip flow cell with temperature control. The chip was composed of multiple V-channels, (71 µm deep, 100 µm wide, and 10 mm long) which lead into a basin at each end. The three insets show the chip with increasing magnification. (C) Long-term monitoring of dynamic changes in of HFF11 cells. The microfluidic flow cell unit was used to monitor dynamics of photinus luciferase expression level in HFF11 cells for 13 h. Reproduced with permission from reference 53.

Another group reported the development of an integrated microfluidic device for long-term culture and monitoring of Caco-2 cells.[54] Stirred-based micropumps for perfusion of media over cells were embedded into the system, which contained a two-compartment cell culture chamber. The device also incorporated an optical fiber detection system for on-line pharmacokinetic monitoring. Caco-2 cells were cultured and immobilized on the device for several days. The device was used to monitor polarized transportation activities of Caco-2 cells for 24 h after several days in culture. Like the system developed for long-term culture and analysis of HFF11 cells, however, detection of the cellular events is only performed once per h.

Long-term Capillary Electrophoresis Operation. For our work, we sought to use CE-based monitoring. CE offers several advantages as a separation technique, including its high efficiency and short analysis time, the capability for on-line detection, the small sample volume requirement, the capability for automated instrumentation, and its overall simplicity.[55, 56] Despite the strong advantages CE offers for separations, conventional capillary electrophoresis is not conducive for long-term separation-based analyses. Several sources of instability hamper long-term CE operation on commercial instruments.[57] A significant source of instability is the buffers required for CE operation.[58] Buffers may become depleted and concentrations of buffer constituents may vary over time due to evaporation. Furthermore, the electrochemical reaction that occurs at the electrodes results in both the production of gas, leading to bubble formation, as well as degradation of buffer components.[59, 60] Such outcomes result in unstable CE operation by affecting a variety of parameters, including migration time and signal. Furthermore, the manner in which injection is performed on conventional CE instruments

may result in sample carryover,[61] which, over the course of several hours, may considerably alter the separation buffer composition. Additionally, any slight mechanical disturbances to the instrument and any pressure changes or vibrations may result in significant baseline noise. Another source of variation is the capillary itself;[62] capillaries are fragile and may spontaneously break as a result of mechanical stress during operation. Application of voltage across the capillary can weaken capillaries further increasing this possibility. Furthermore, electroosmotic flow

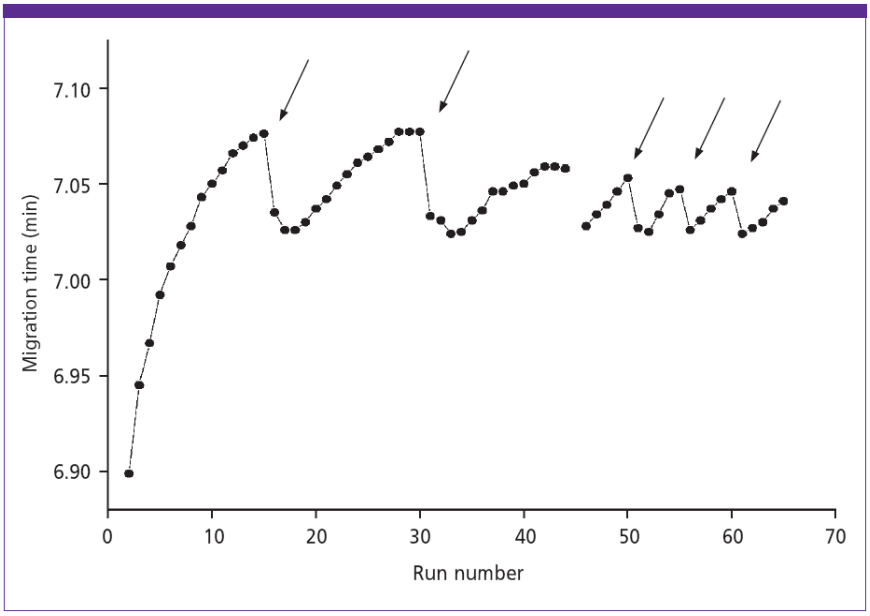

Figure 1.11. Importance of solution replenishment in CE analyses. Migration time increases during serial runs of continuous CE operation, but with replenishment of washing solutions (indicated by arrows), the migration decreases to a constant time. Continuous replenishment of washing solutions is necessary for long-term CE operation. Reproduced with permission from reference 62.

(EOF) is dependent on the chemistry of the inner wall of the capillary.[63-65] EOF depends on the charge at the wall surface, and over time, the charge of the surface may be altered due to fluctuations in pH. Additionally, any adsorption of the analyte or buffer components will alter the capillary surface and a change in EOF will result.[66, 67]

Preventative steps may be taken to lengthen operation time on conventional CE instruments.[68] One preventative measure is periodically replenishing electrophoresis buffers, which may help to prevent variations due to evaporation, electrolysis, or sample carryover. The effect of solution replenishment is illustrated in Figure 1.11. With continuous electrophoresis operation, the migration time of an analyte continuously increased; however, upon renewal of washing solutions, the migration time decreased. In fact, each time the washing solution was replenished, the migration time returned to ~7.03 min. However, many of the suggested preemptive actions, including buffer replenishment, are labor-intensive and are not simply automatable on conventional CE instruments. Furthermore, these preventative measures have not been applied to chip-based CE operation.

For this thesis work, a microfluidic electrophoresis device was developed for culture and analysis of islets of Langerhans for up to 24 h. In the device, all reagents and electrophoresis are continuously perfused into the device with a gas pressure system, ensuring only fresh reagents buffer are used for analysis. The long-term monitoring chip was used to complete 14,400 unattended assays in 24 h. Observation of glucose-stimulated insulin secretion from single islets over this time frame revealed several noteworthy trends in secretion dynamics.

Intracellular Ca^{2+} Imaging on Microfluidic Chips. Fluorescence imaging is a relatively non-invasive technique that can provide spatial information, thus making it a promising and attractive technique for studying living cells. The advent of the cell-permeant fura-2, a Ca^{2+}-sensitive fluorescent dye, revolutionized intracellular Ca^{2+} measurements in the 1980s.[69] Fura-2 exhibits improved selectivity for Ca^{2+} over other

divalent cations compared to its predecessor, and also the quantum efficiency of the dye is much higher. Furthermore, fura-2 is ratiometric, rendering differences in instrumental sensitivity, optical path length, and effective total concentration of dye in the cells insignificant. The dye's excitation wavelength shifts from 380 nm to 340 nm upon Ca^{2+} binding, and the ratio of the integrated intensities of the fluorescence emission from 340- and 380-nm excitation allows for quantitation of intracellular Ca^{2+} following calibration of the system.

Traditionally, fura-2 measurements are performed on cells affixed to a coverslip. The coverslip is typically placed sealed into a chamber of approximately 3 mL volume. The chamber is perfused with a peristaltic pump. A disadvantage of the instrumentation described is that the large volume of the media makes maintaining precise control of the environment around the cells difficult. A microfluidic device incorporating perfusion channels leading to a cell chamber offers an attractive alternative to the 'macro'-perfusion system. The microfluidic cell perfusion chip for Ca^{2+} imaging allows for rapid introduction of stimulants to the cells and assurance that the cells are constantly provided fresh media. In recent years, several groups have reported the use of microfluidic chips for intracellular Ca^{2+} imaging using fura-2.[70-72] Mohammed *et al*. reported the development of a microfluidic device for performing mitochondrial membrane potential and fura-2-based Ca2+ imaging on islets, in addition to insulin secretion measurements via offline ELISA analyses.[73] The Kennedy lab also developed and characterized a microfluidic chip for monitoring the intracellular Ca^{2+} concentration of pancreatic islets using fura-2 fluorescence imaging.

In this thesis work, the Ca2+ imaging device was used to investigate the membrane-disrupting effects of Islet Amyloid Polypeptide (IAPP) on islets. IAPP is a 37-residue peptide cosecreted with insulin by the β-cells of islets of Langerhans.[74] Highly aggregated amyloid deposits of human IAPP (hIAPP) have been observed in islets of more than 90% of type 2 diabetic patients but not in non-diabetic patients.[75] The observation of amyloid deposits and their high prevalence in diabetic patients suggests the formation of amyloid fibers may play a causative role in the development of diabetes.[76, 77] Several reports indicate that the formation of aggregates of the peptide into either amyloid fibers or oligomers may lead to death of β-cells by disrupting the cellular membrane,[78] but whether or not the aggregation of amyloidogenic proteins can disrupt membranes by forming toxic oligomers is disputed.[79, 80] To explore the toxicity of various forms of IAPP on islets, a series of *in vivo* and *in vitro* experiments were performed by collaborating labs.[79] In our lab, we used the Ca^{2+} imaging chip to measure the membrane disrupting effects of IAPP by monitoring fluctuations in intracellular Ca2+ concentration. The experiments were based on a previous report that application of oligomeric forms of amyloid fibers resulted in elevated intracellular Ca^{2+} levels, likely due to membrane disrupting effects.[81]

Additionally, the Ca^{2+} imaging chip was employed to investigate leptin signaling in islets from pancreas-specific leptin receptor knockout mice. Leptin is a 16 kDa hormone primarily secreted from white adipose tissue.[82] Leptin helps to prevent obesity by acting on the hypothalamus to regulate appetite.[83] In addition to the existence of leptin receptors in the brain, they exist throughout several peripheral tissues in the body, including islet β-cells.[84, 85] The expression of leptin receptors on β-cells suggests

potential for a role of leptin in modulating insulin secretion.[86] Indeed, several studies have shown that leptin acts to inhibit insulin secretion from β-cells[86-88], but the mechanism of leptin's function on β-cells is not clear. Numerous investigations of the effects of whole-body genetic leptin receptor knock-out have been reported[89, 90], but these studies do not isolate the effects of leptin receptor knock-out on the islet from various other effects of the lack of leptin receptors throughout the body. In an effort to clarify the mechanism of leptin's effects on β-cells, Morioka *et al*. used the Cre-*LoxP* approach to create pancreas-specific leptin receptor knock-out (ObRKO) and corresponding control (ObRlox) mice.[91] In this dissertation work, a series of experiments to study leptin signaling in β-cells was designed and performed by monitoring Ca^{2+} flux into islets isolated from both ObRlox and ObRKO mice. By exposing islets to various environments, it was possible to probe potential signaling pathways in β-cells.

O_2 Measurements. As already described, diabetics exhibit loss of insulin secretion oscillations[15, 17], and several analyses have been performed to investigate the pathway in which the oscillations are impaired. It has been demonstrated that, in addition to the oscillations in insulin secretion, other pathways and analytes in β-cells oscillate; intracellular Ca^{2+} concentration, membrane potential, glucose consumption, and oxygen oscillations with a period similar to the period of rapid insulin secretion oscillations.[92] The synchronicity of the oscillations suggests that pathways such as glycolysis and respiration are linked to insulin secretion and insulin secretion oscillations. It is of interest to investigate the mechanism in which metabolism and insulin secretion are linked. Thus, measurements of metabolic parameters, such as O_2, may help elucidate the pathway leading to insulin secretion. Currently, electrochemical detection is the most

common method to monitor oxygen consumption by islets. Our lab previously developed an electrochemical microsensor for monitoring oxygen consumption by single islets.[93] Although the electrodes are extremely sensitive and exhibit high spatial resolution, they are difficult and time-consuming to fabricate, and use of the sensors is quite tedious. Spectroscopic methods, such as fiber optic sensors, provide a useful method of measuring oxygen levels in single islets while exhibiting high sensitivity, high spatial resolution, and simplicity.[94] A fiber optic oxygen sensor was developed and characterized.[95] The sensor was used to monitor oxygen consumption at an islet, but further work is necessary to demonstrate the capabilities of the sensor for monitoring oxygen consumption oscillations in living cells.

Dissertation Overview

The overall objective of this research was to design, develop, and apply novel analytical techniques to investigate insulin secretion from islets of Langerhans. The design and characterization of a microfluidic device for monitoring insulin secretion from single islets for 24 h is presented in Chapter 2. The microfluidic device employs a capillary electrophoresis-based immunoassay, and thus Chapter 2 includes a demonstration of the long-term electrophoresis operation of the device. The application of the chip for monitoring long-term insulin secretion from islets is also presented in Chapter 2. Because the chip was capable of monitoring insulin secretion with a 6-s temporal resolution for 24 h, it was used to study insulin secretion dynamics from islets for 24 h. Data and results from Chapter 2 are in preparation for submission to *Analytical Chemistry*.

Presented results in Chapter 3 are from a study investigating the membrane-disrupting effects of Islet Amyloid Polypeptide (IAPP). The work was completed in collaboration with Dr. Ayyalusamy Ramamoorthy and Dr. Jeffrey R. Brender of the Department of Chemistry and Biophysics at the University of Michigan. Work performed by the author was limited to studying the effects of IAPP on single islets via intracellular Ca^{2+} imaging. Data and results in this chapter were originally published in *Biochemistry.*

Chapter 4 presents data and discussion from a study investigating leptin signaling in islets using pancreatic-specific leptin receptor knock-out mice. Results presented in Chapter 4 were collected in collaboration with Dr. Rohit N. Kulkarni and Dr. Tomoaki Morioka of the Joslin Diabetes Center at Harvard Medical School. Work performed by the author was limited to investigating leptin signaling via intracellular Ca^{2+} imaging in islets. Data presented in this chapter are in preparation for submission.

Development and characterization of a fiber-optic oxygen sensor to monitor intracellular oxygen concentration in islets are presented in Chapter 5. The work was completed in collaboration with Dr. Raoul Kopelman and Dr. Edwin J. Park from the Department of Chemistry at the University of Michigan. Results presented in this chapter were published in *The Journal of Materials Chemistry*.

CHAPTER 2

UNATTENDED OPERATION OF MICROFABRICATED ELECTROPHORESIS DEVICES FOR 24 HOURS AND APPLICATION TO CHEMICAL MONITORING OF LIVING CELLS

Introduction

Pancreatic islets of Langerhans are microorgans composed primarily of insulin secreting β-cells.[5] At elevated levels of glucose, β-cells are stimulated to secrete insulin,[6] which helps to maintain glucose homeostasis.[41] Glucose-stimulated insulin secretion (GSIS) from β-cells involves metabolism of the sugar to generate appropriate intracellular signaling events.[6] β-cells and insulin secretion are of interest because they are fundamental in the pathophysiology of diabetes.[41]

Radioimmunoassays (RIAs) or enzyme-linked immunosorbent assays (ELISA) are most commonly used for insulin secretion analyses. While these techniques are quite sensitive, they are labor- and time-intensive and require large sample volumes. Microchip electrophoresis is a popular separation technique, primarily due to its small sample volume requirements, high speed, and efficiency.[55] Electrophoresis chips have been used to perform on-line reactions for sensing applications, including immunoassays.[96] Furthermore, microfluidic electrophoresis devices are amenable for cellular culture because they allow precise control of the cells' environment[97] and enable automation of several integrated, on-chip functions important for cellular studies.[96] Microfluidic electrophoresis devices are typically not used for more than a few hours, but

longer operating capabilities would be helpful for cellular studies, particularly for chemical monitoring of cells over time to monitor slowly evolving phenomenon.

Our laboratory previously developed a microfluidic electrophoresis device capable of monitoring insulin secretion from living cells. In this system, perfusate from the cells was collected and monitored with 6 s temporal resolution.[52] This device offered several advantages over conventional immunoassays, including automation of insulin monitoring with high temporal resolution. The device was modified to allow for higher throughput via parallel measurements, and the parallel device has been used to monitor insulin secretion from multiple independent islets simultaneously.[98, 99] The electrophoresis immunoassay devices were used to perform real-time monitoring of insulin secretion over periods less than 2 h and have generated much useful information about the function of healthy and diseased β-cells.[91, 100]

While the microfluidic devices described above are designed for no longer than 2 h operation, there are indications of several longer-term secretion phenomena of islets that, if better understood, could further the understanding of the impairment in insulin secretion associated with type 2 diabetes. For example, numerous reports suggest that islet behavior, including glucose-stimulated insulin secretion, fluctuates over time in culture.[36-38] Thus, it is desirable to optimize the culture conditions and duration prior to experimentation. Furthermore, oscillations of insulin secretion with periods of approximately 2 h (ultradian rhythms)[20-22] and 24 h (circadian rhythms)[28-30] have been observed using RIAs and ELISAs. The longer-term oscillations are important for optimal insulin action throughout the body[23, 24, 33, 34] and are impaired in diabetics.[27, 31] However, the rhythms are difficult to study using conventional immunoassay techniques due to the

time, labor and cost associated with the techniques. To date, the longer-term rhythms have not been studied on single islets, and it is not known whether individual islets can maintain the oscillations.

The increased temporal resolution and automation of the insulin assay on the previously-reported microfluidic electrophoresis device offer tremendous advantages compared with conventional immunoassays, particularly for long-term insulin studies. However, continuous electrophoresis operating time on the original chip was previously limited by degradation of reagents and electrophoresis buffers on the chip. It is well-documented that conventional capillary electrophoresis operating time is limited by detector and injection fluctuations, buffer instability, and temperature variations.[57, 62] In this work, we demonstrate that buffer degradation and injection failure were two limiting constraints for long-term operation. In order to resolve these issues, a novel microfluidic device was developed in which all reagents are continuously perfused into the device with a gas pressure system, ensuring only fresh reagents are used for analysis. The stability issues associated with conventional capillary electrophoresis are largely resolved with the microfluidic electrophoresis device, which is capable of performing stable electrophoresis for 24 h.

Furthermore, we describe the use of the long-term electrophoresis device for culturing cells and monitoring cellular secretion over periods of 24 h or longer. With the device, insulin secretion from individual islets was monitored for 24 h via completion of 14,400 immunoassays. The improved insulin immunoassay capabilities enabled observation of insulin secretion dynamics virtually impossible to observe with convention immunoassay techniques. The results presented here demonstrate the promise of the

long-term electrophoresis device for elucidating mechanisms behind long-term insulin secretion dynamics and perhaps revealing more interesting trends in secretion.

Experimental Section

Chemicals and Reagents. Tricine, electrophoresis grade, was obtained from MP Biomedicals (Aurora, OH). Fluorescein isothiocyanate-labeled insulin (FITC-ins) was purchased from Molecular Probes (Eugene, OR), and monoclonal antibody (Ab) to human insulin was purchased from Biodesign International (Saco, ME). Cell culture reagents were purchased from Invitrogen (Carlsbad, CA). Collagenase type XI, Tween 20, ethylenediaminetetraacetic acid (EDTA), and insulin were obtained from Sigma (St. Louis, MO). All other chemicals were from Fisher (Pittsburgh, PA). All solutions were made using Milli-Q (Millipore, Bedford, MA) 18 MΩ deionized water and filtered using 0.2 μm nylon syringe filters (Fisher). Stock antibody solution was stored at 4 °C in the manufacturer-provided phosphate-buffered saline. Stock FITC-ins was diluted to 166 μM in immunoassay reagent buffer and stored at -20 °C.

Other solutions were used as physiological, reagent, and electrophoresis buffers. Balanced salt solution (BSS) contained 125 mM NaCl, 5.9 mM KCl, 1.2 mM $MgCl_2$, 2.4 mM $CaCl_2$, 25 mM tricine, and 0.7 mg mL^{-1} bovine serum albumin (BSA), adjusted to pH 7.4. Immunoassay reagent buffer contained 60 mM NaCl, 1 mM EDTA, 20 mM tricine, 0.1% (w/v) Tween 20, and 0.7 mg mL^{-1} BSA, adjusted to pH 7.4. Separation buffer contained 20 mM NaCl and 150 mM tricine, adjusted to pH 7.4.

Microfluidic Chip Fabrication and Preparation. The microfluidic devices were fabricated using a previously described method.[51] Briefly, 1 mm thick Borofloat photomask blanks (2.5 cm X 7.6 cm) were exposed to a collimated UV light source

(Optical Associates, Inc., Milpitas, CA) for 5 s through a patterned photomask (Digidat, Pasadena, CA). The blanks, purchased from Telic Co. (Santa Monica, CA), had a 530 nm layer of AZ1518 positive photoresist on a 120 nm chrome layer. The exposed photomasks were developed in AZ915 MIF developer (Clariant Corp., Summerville, NJ), and the exposed chrome was then developed in CEP-200 chrome etchant (Microchrome Technologies, Inc., San Jose, CA). The exposed glass was etched in 14:20:66 (v/v/v) HNO_3:HF:H_2O for 20 min to create channels 12 μm deep. Diamond-tipped drill bits (Tartan Tool Co., Troy, MI) were used to drill 360 μm-diameter access holes. The remaining photoresist was removed with acetone, and the remaining chrome was removed with the CEP-200 chrome etchant. The etched chips and blank coverplates were placed in piranha solution (3:1, v/v, H2SO4:H2O2) to remove organic oxides, and the plates were subsequently placed in a heated RCA solution (5:1:1, v/v/v, H2O:NH4:H2O2) to increase glass hydrophilicity. The plates were bonded at 640 °C under vacuum in a Neytech Centurian Qex furnace (Pacific Combustion, Los Angeles, CA). To aid in bonding, stainless steel weights were applied during heating. Microfluidic reservoirs (Upchurch Scientific, Oak Harbor, WA) were applied to the device over drilled access holes after bonding. The chip was conditioned prior to experiments by flowing 0.1 M NaOH through the channels, followed by deionized water and then experimental solutions.

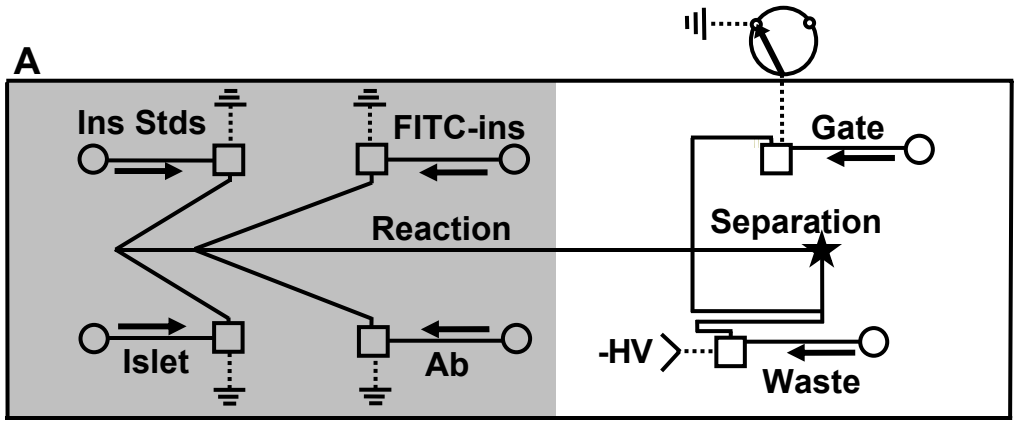
A
Ins Stds
FITC-ins
Gate
Reaction
Separation
Islet
Ab
-HV
Waste

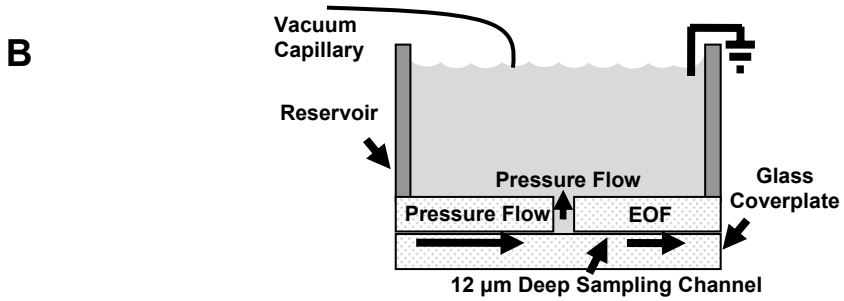
B
Vacuum Capillary
Reservoir
Pressure Flow
Glass Coverplate
Pressure Flow
EOF
12 µm Deep Sampling Channel

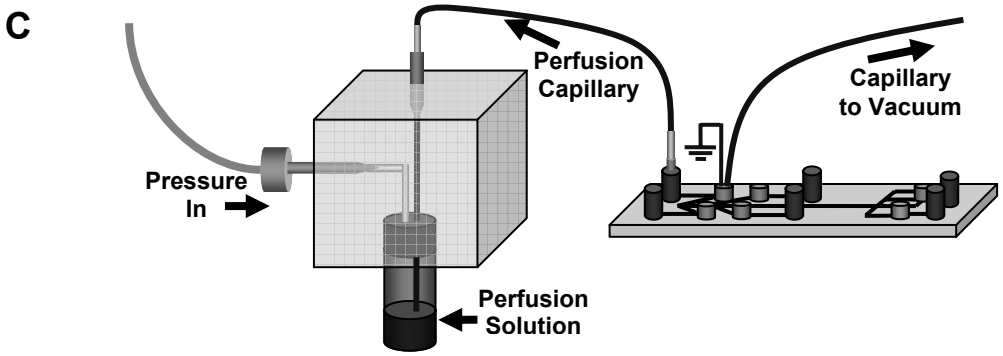
C
Perfusion Capillary
Capillary to Vacuum
Pressure In
Perfusion Solution

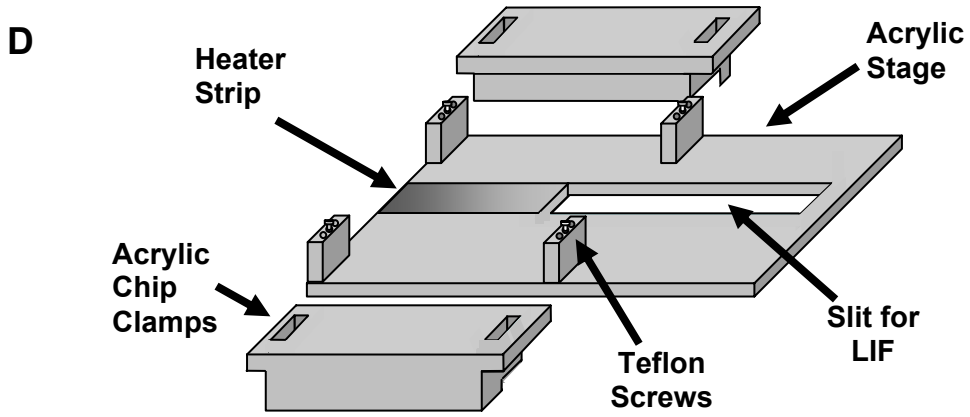
D
Heater Strip
Acrylic Stage
Acrylic Chip Clamps
Slit for LIF
Teflon Screws

Figure 2.1. (previous page) Microfluidic chip for long-term electrophoresis operation and perfusion scheme. (A) Channel layout of a microfluidic device for monitoring insulin secretion for 24 hours. Solid lines indicate microfluidic channels, while electrical connections are indicated by dotted lines. Circles indicate perfusion inlets and squares indicate CE sampling reservoirs. All fluidic access holes are 360 μm in diameter, and all channels are 12 μm deep and have a half-width of 26 μm. The shaded portion of the chip is heated to physiological temperature (37 °C) with a thin film resistive heater taped underneath the chip. Arrows indicate direction of perfusion flow. The operation of the chip is explained in the experimental section. (B) Side view of islet chamber. Pressure-driven fluid is perfused into a 0.1 μL chamber and flows into a 100 μL fluidic reservoir. Solution from the chamber is sampled by electroosmotic flow (EOF) through the sampling channel at a rate of approximately 2 nL min^{-1}. (C) Scheme for perfusing reservoirs. Perfusion buffer supply is pressurized and fluid flows into the chip providing a constant supply of buffer that is sampled by electroosmotic flow. (D) Modified microscope stage for maintaining long-term stability of chip position.

Microfluidic Chip Operation. The layout of the microfluidic channels in the device and a schematic demonstrating chip operation are shown in Figure 2.1. All solutions were filtered prior to use to prevent introduction of particulates to the chip, as well as to prevent degradation of the solutions. During chip operation, all solutions were continuously pumped onto the chip using fused-silica capillaries inserted into vials pressurized with 5-30 psi of helium, allowing only fresh reagents to be used for analysis. Solution in excess of 100 μL in the electrophoresis reservoirs were continuously removed via fused-silica capillaries connected to a vacuum manifold. A high voltage (HV) of -6 kV was applied at the waste reservoir of the device, and all other reservoirs were grounded. Solution sampled electrophoretically from the islet reservoir mixed with 50 nM fluorescein isothiocyanate-labeled insulin (FITC-insulin) (Molecular Probes, Eugene, OR) and 25 nM anti-insulin antibody (Ab) (BioDesign Int'l, Saco, ME) in immunoassay reagent buffer on a heated reaction channel. The electrophoresis buffer was placed in the gate and waste reservoirs. The gate reservoir was connected to ground via a high voltage relay (Kilovac, Santa Barbara, CA). When the relay was opened, sample was allowed to flow onto the 1.5 cm separation channel. Afterward, the gate was returned to ground, and

separation occurred. Laser-induced fluorescence (LIF) detection occurred 1 cm from the injection cross. Each separation resulted in a zone of FITC-ins bound to antibody (B) zone followed by a free FITC-ins (F) zone. The ratios of the heights of the bound and free peaks (B/Fs) were used after calibration to quantify insulin.

Islets were perfused with BSS and glucose at 1.0 μL min^{-1}. For islet experiments, a single islet was placed in the grounded islet reservoir and perfused with BSS and perfusate from the islet was sampled via electroosmotic flow. For calibration, grounding was alternated from the islet reservoir to the insulin standards reservoir, allowing the electrophoretic sampling of insulin standards without flowing exogenous insulin through the islet chamber while the islet was present.

The chip is designed for unattended use requiring the chip to remain still for stable detection; thus, additional measures were taken to ensure the device did not shift location during operation. An acrylic stage was developed to hold the chip in place and the coverslip of the chip was modified to extend 0.25" past each side of the etched piece of glass. The stage, illustrated in Figure 2.1D, contained 2 acrylic pieces that were placed atop the extended coverslip portions of the chip and held in place via Teflon screws.

Detection. The laser-induced fluorescence (LIF) detection was performed with a Zeiss Axiovert 35M inverted microscope equipped with an 814 microscope photometer system (Photon Technology International, Lawrenceville, NJ). A 20 mW optically pumped semiconductor Sapphire laser (Coherent, Santa Clara, CA) was directed onto a 500 nm long-pass dichroic mirror and through a 40X, 0.6 numerical aperture, long working distance objective (Carl Zeiss, Inc., Thornwood, NY). After passing through the dichroic mirror, the emission light passed through a 530 ± 30 nm band-pass filter. The

fluorescence emission was further spatially filtered by an iris diaphragm on the photometer. Instrument control and data collection were performed using LabVIEW software written in-house (National Instruments, Austin, TX), and electropherograms were analyzed using Cutter software.[101]

Islet Isolation Protocol. Pancreatic islets were obtained from 20 to 30 g male CD-1 mice as previously described.[102] Briefly, mice were sacrificed by cervical dislocation and collagenase type XI was injected into the pancreas through the main pancreatic duct. The pancreas was removed and incubated in 5mL of a collagenase solution at 37 °C. A Ficoll gradient was used to separate islets from exocrine tissue. Islets that were used for experiments were 100-200 μm in diameter, had an intact islet membrane, and were oblong to spherical in shape. Islets were placed in tissue culture dishes and incubated in RPMI 1640 containing 10% fetal bovine serum, 100 U/mL of penicillin, and 100 μg/mL of streptomycin at 37 °C, 5% CO_2, pH 7.4. Islets were used 1-6 days following isolation.

Results and Discussion

Microfluidic Device for Stable Long-term Electrophoresis. The microfluidic chip developed for long-term electrophoresis-based insulin secretion monitoring is illustrated in Figure 2.1. All buffers and reagents were continuously perfused into the chip via pressure-driven flow and were subsequently sampled via electroosmotic flow (EOF). In the device, a single islet was placed in a chamber on the chip and continuously perfused with buffer containing glucose as needed for islet analyses.

For long-term operation, it was necessary to build into the device the ability to periodically calibrate the immunoassay even in the presence of cells so that the stability

of calibration could be monitored. To calibrate the device with the islet present, the islet reservoir was ungrounded. The insulin standards were perfused into the calibration channel, and the calibration reservoir was grounded. Once the calibration was complete, the ground was removed from the calibration reservoir and ground was returned to the islet reservoir to return to insulin secretion sampling.

Initial experiments were performed to demonstrate the effectiveness of continuous perfusion of buffers for maintaining long term electrophoresis stability and results are summarized in Figure 2.2. The first experiment was performed without the constant perfusion of fresh buffer; only a 10 nM insulin standard was continuously perfused. The resulting plot of B/Fs calculated from serial electropherograms (Figure 2.2A) demonstrates that without perfusion, the immunoassay became unstable after only two hours of operation. After 2 h, the relative standard deviation (RSD) increased to 7%, and after 3 h, the RSD increased to 20%. Also included in Figure 2.2 is an overlay of an electropherogram collected at the start of the immunoassay operation and an electropherogram collected at 3 h of immunoassay operation. After 3 h of operation without buffer and reagent replenishment, electroosmotic flow was significantly diminished, resolution between the bound and free peaks was decreased, and the peak heights were significantly lower.

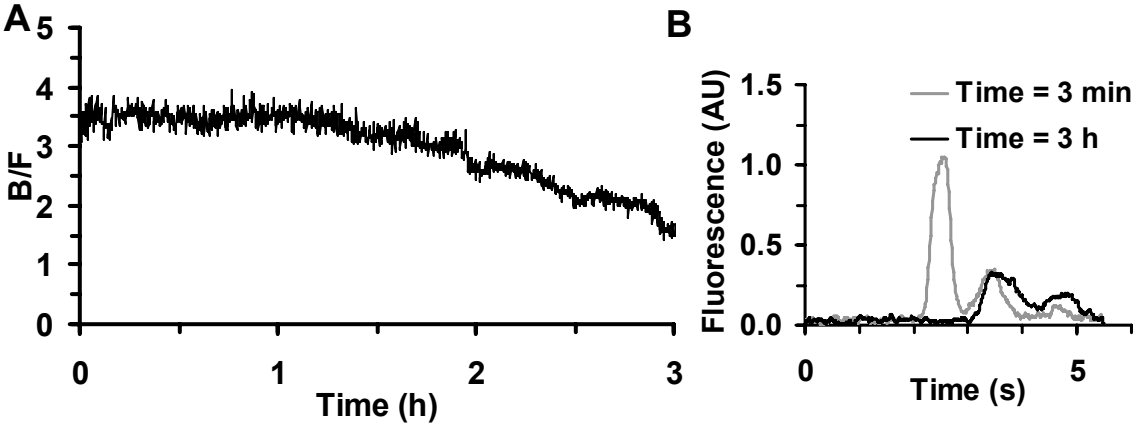

Figure 2.2. Immunoassay instability without solution replenishment. A) Immunoassay stability with no perfusion. By 3 h of chip operation, the RSD increased to 20%. B) Electropherograms collected at 3 min and 3 h of immunoassay operation. At 3 h, migration times of both B and F peaks significantly increased, peak heights decreased, and resolution of the B and F peaks was considerably diminished.

A similar trial was repeated to characterize the new long-term electrophoresis device. A stability test was performed by continuously perfusing 10 nM insulin, along with all other buffers and reagents, into the device. In initial experiments, the B/F was stable for approximately 12 to 15 h, at which point stability was lost due to a gradual, yet significant, decrease in both B and F signals, as illustrated in Figure 2.3.

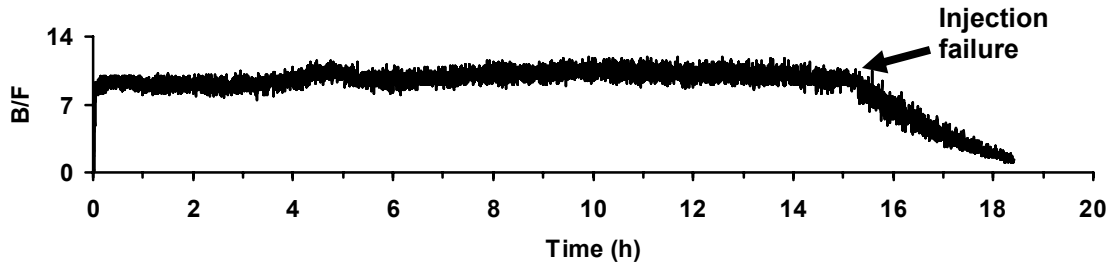

Figure 2.3. Failure of injections after long-term chip operation. After several hours of continuous chip operation, the fluorescence signal began to gradually decrease. The decrease in signal was later determined to be an effect of failed electrokinetic injections, resulted in loss of immunoassay (B/F) stability.

Upon further investigation, it was determined the loss of fluorescence signal was a result of failure of the gated injections due to failure of the high voltage relay necessary for the injections. The gated injection design allows for rapid and automated serial

injections, as well as continuous flow through the reaction channel during injection and separation. Such capabilities are necessary for long-term chip operation. The original, gas-filled relay was not capable of such repetitive l use, and was therefore replaced with a vacuum dielectric relay rated for 1 billion cycles.

Once the relay was replaced, the stability of gated injection was investigated by performing serial injections of Rhodamine 110 and plotting the Rhodamine 110 peak heights vs. time, as depicted in Figure 2.4. The RSD of the peak heights was less than 4% over 24 h of continuous operation. Because the investigation was performed using all the typical immunoassay buffers (less the Ab, FITC-insulin, and insulin), the low RSD value suggests that mixing and sampling are reproducible, the injections are reliable, and the detector is stable over 24 h. Furthermore, the migration time reproducibility for Rhodamine 110 was less than 1% RSD, indicating the chip is reliable for 24 h electrophoresis. Longer (> 24 h) operating time may be limited by a change in surface chemistry of the channels, resulting in decreased sampling and EOF. The effects would cause a change in migration time and fluorescence intensity.

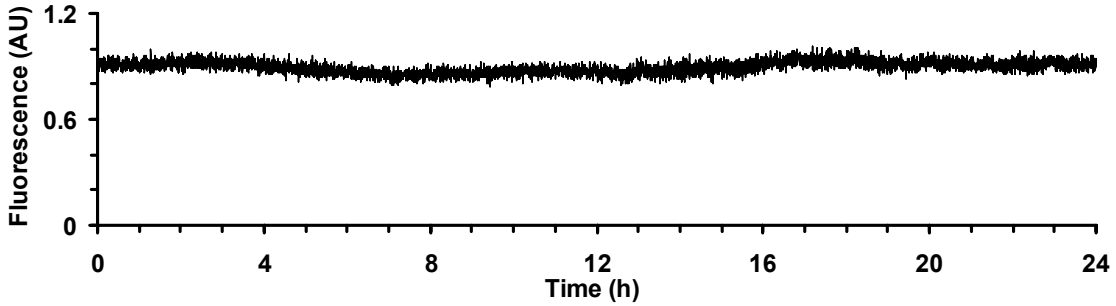

Figure 2.4. Long-term electrophoresis stability. The stability of the normal chip operation was investigated by plotting the peak height of the Rhodamine 110 peak from several electropherograms collected during continuous sampling of 50 nM Rhodamine 110. The RSD of the Rhodamine 110 peak height was less than 4% over 24 h of continuous operation.

In contrast to results shown in Figure 2.2, with constant perfusion of fresh buffers, the immunoassay stability was much improved (Figure 2.5). The RSD of the B/F from the 14,400 electropherograms/immunoassays collected over 24 h was 4%, indicating good stability for this period. The overlay of an electropherogram collected at the start of the immunoassay and an electropherogram collected after 24 h of continuous chip operation demonstrates that with perfusion, the migration time and peak heights were stable over 24 h. The results shown in Figure 2.5 are representative of 5 identical experiments.

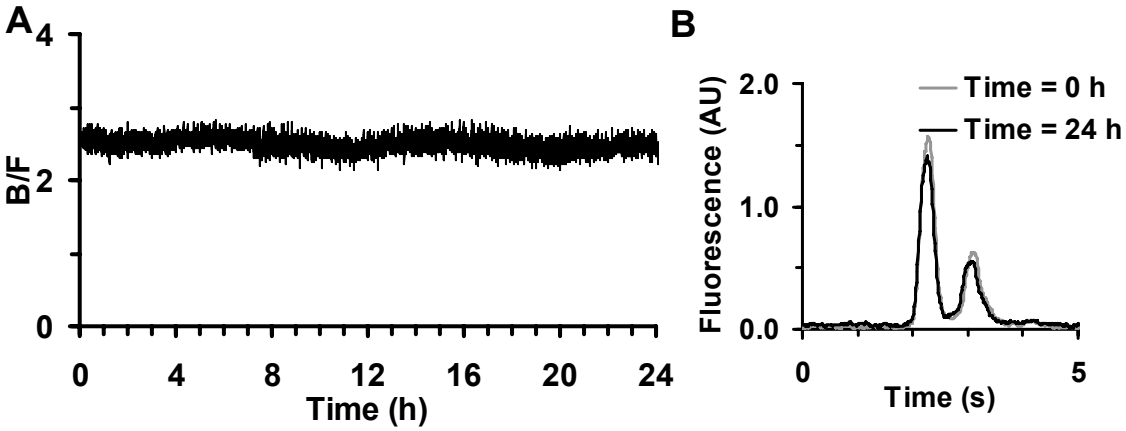

Figure 2.5. Long-term immunoassay stability. A Immunoassay stability during continuous perfusion of 10 nM insulin. The immunoassay device performed 14,400 assays over 24 h with an RSD of 4 %. B) Electropherograms collected at 0 h and 24 h of immunoassay operation. At 24 h, the migration times and heights of both B and F peaks were nearly identical to those at 0 h.

Calibration of Immunoassay. We next evaluated the stability of the immunoassay calibration over 12 h. Fifty nM insulin and all other buffers were perfused into the chip and sampled via EOF for 12 h. A trace of B/Fs calculated from the resulting electropherograms is shown in Figure 2.6A. Figure 2.6 also includes an overlay of the calibration curve formed by calculating B/Fs obtained from the device while perfusing

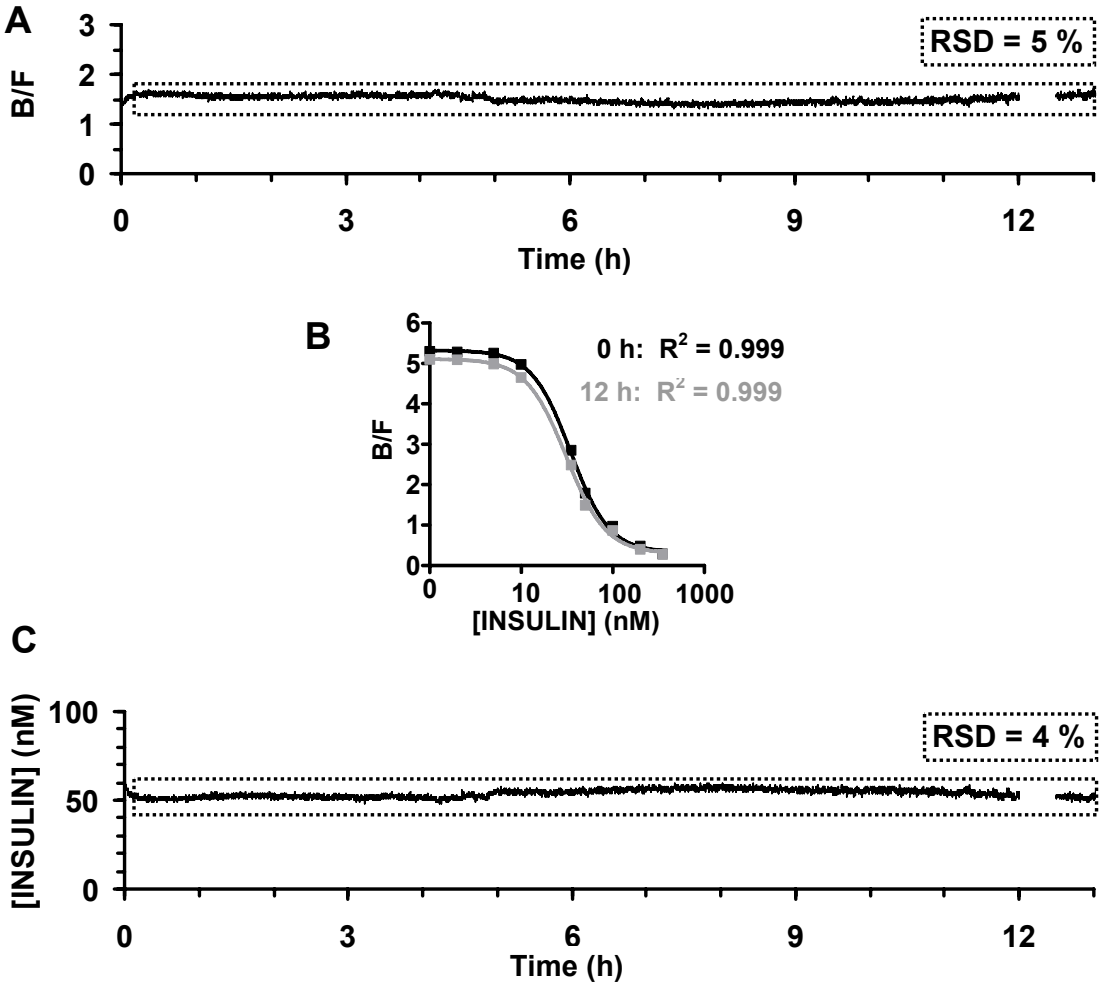

Figure 2.6 Stability of immunoassay calibration over a 12 h period. A) B/Fs calculated from consecutive electropherograms collected while perfusing 50 nM insulin into the chip. The RSD of the B/Fs was 5% over 12 h operation. B) Overlay of calibration data obtained at 0 h and at 12 h of chip operationPoints from both curves were fitted with variable slope sigmoidal dose response functions with $R^2 = 0.999$. Error bars indicate standard deviation of the mean. The similarity of the two calibration curves indicates there is minimal drift in calibration over the long-term operation. C) Calculated insulin concentrations during 12 h perfusion of 50 nM insulin. Insulin concentrations were calculated from the B/Fs shown in A and the calibration data shown in B. The RSD of the calculated insulin concentration was 4% over 12 h operation.

1 nM to 350 nM insulin standards into the chip at 1.0 μL min^{-1} and plotting those ratios versus insulin concentrations at time 0 h and at 12 h. Points were fitted with a variable slope sigmoidal dose response function with $R^2 = 0.999$. The calibration curves were similar over time, indicating there was little drift in calibration over the course of the 12 h experiment. However, any drift in calibration can be detected during immunoassay

operation by recalibrating the system via the insulin standards channel. After completing the calibrations, the insulin concentration was calculated from the B/Fs and is also plotted in Figure 2.6C. The RSDs of the B/Fs and the insulin concentrations in Figure 2.5 are 5% and 4%, respectively.

Islet Culture. Besides the assay, it was also necessary to evaluate the cell culture conditions for 24. Because the islets on the chip are maintained at physiological temperature and constantly perfused with fresh physiological buffer (BSS) they should remain healthy and viable on the chip during 24 h experiments. Islet morphology may be used as an indicator of the viability of the islets in their microfluidic environment. To investigate the viability of perfused islets cultured in the microfluidic device, two islets were placed in 11 mM glucose in a 360 μm drilled microfluidic access hole on the heated device for 24 h. One islet was not perfused while the second islet was continuously bathed with fresh buffer. After 24 h with no perfusion, the first islet's membrane appeared disrupted, and the islet did not appear healthy as illustrated on the left in figure 2.7. In contrast, after being perfused with fresh buffer for 24 h, the second islet's membrane remained intact, and the islet appeared viable, as depicted on the right in Figure 2.7. The morphological evidence suggests that perfusion with fresh media helps to maintain the health of islets while maintained at 37 ˚C. Results from two repeated experiments agreed well with results shown in Figure 2.7. Although the perfused islets appeared healthy after 24 h, it may be necessary to perfuse the islet with true cell culture media, such as RPMI 1640 rather than BSS, which contains no nutrients other than glucose, for longer-term (> 24 h) culture.

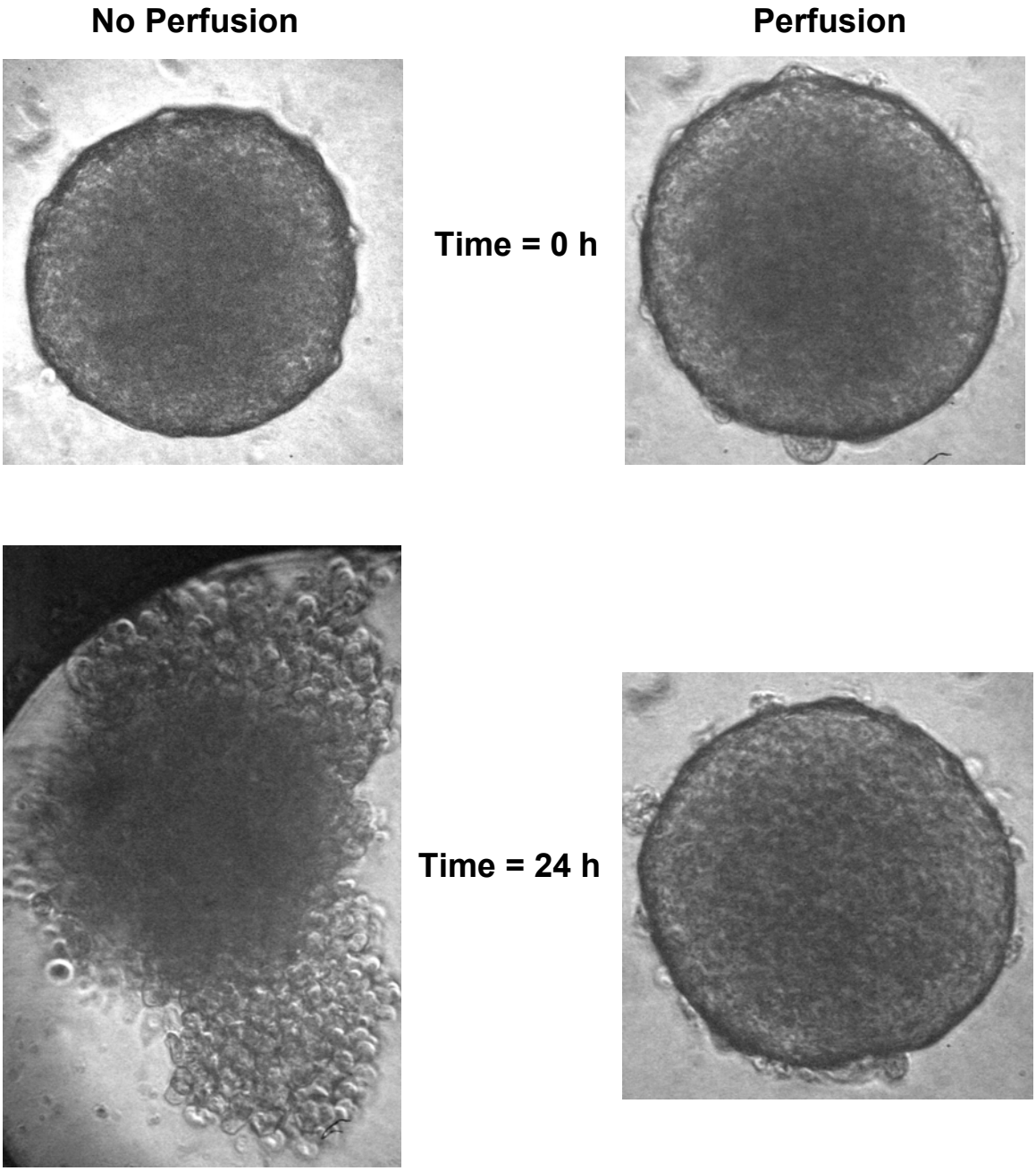

Figure 2.7 Islet morphology. Two islets were placed in 11 mM glucose in a 360 μm drilled microfluidic access hole on a heated long-term microfluidic device for 24 hours. There was no perfusion to one islet, while the second islet was continuously bathed with fresh buffer. After 24 hours with no perfusion, the islet membrane appears seriously disrupted, the islet cells are leaking out from the islet core, and, thus, the islet does not appear healthy. Additionally, there is some evidence of necrosis in the non-perfused islet, as indicated by a dark region in the islet. In contrast, after being perfused with fresh buffer for 24 h, the second islet's membrane remains intact, there is no indication of necrosis, and thus, the islet appears viable. This evidence suggests that perfusion with fresh media helps to maintain islets in a healthy environment.

Long-term Insulin Secretion. To illustrate the potential of the system, we used it to monitor insulin secretion from single islets following a step change from 3 to 11 mM glucose. We monitored 6 islets for up to 39 h. Of the tested islets, 4 were successfully monitored for 12 h or more while others failed more quickly, typically due to clogs in the chip. Examples of insulin secretion from single islets perfused with 3 mM to 11 mM glucose for 6 and 12 h are shown in Figure 2.8. The 6 and 12 h secretion dynamics demonstrate the differences in insulin secretion that can exist between various islets. For example, the 6 h islet exhibited a large first phase of insulin release upon stimulation with 11 mM glucose and insulin secretion oscillations began immediately after the first phase of insulin secretion. Conversely, the insulin secretion from the 12 h islet did not immediately oscillate after the first phase, but rather began to oscillate several hours after continuous stimulation with 11 mM glucose. While the individual islet studies provide much interesting long-term secretion dynamics, insulin secretion from several islets can be averaged to summarize results from several long-term single islet studies. The averaged results can be compared to insulin secretion results from previously reported individual or batch islet studies. Also included in Figure 2.8 is an average of insulin secretion of several islets. While the individual islet traces are preferable for investigating single islet dynamics, the plotted average demonstrates the reliability of the long-term monitoring device. The figure includes results from over 60,000 assays, a feat virtually impossible with conventional immunoassay techniques due to the time, labor, and cost necessary to complete such assays.

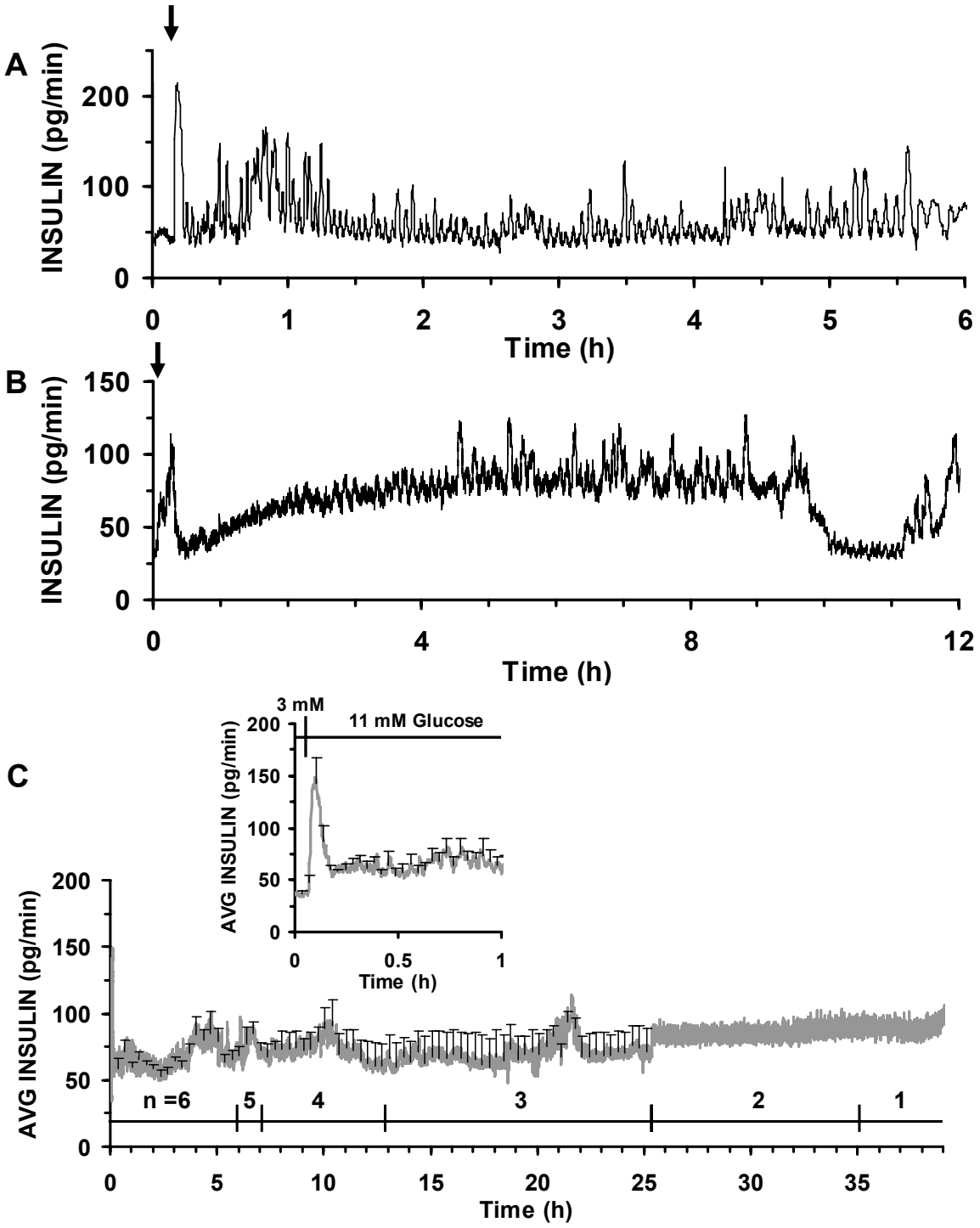

Figure 2.8. Long-term insulin secretion data. The long-term device can be used to observe secretion dynamics from several individual islets. A) 6 h and B) 12 h insulin secretion from single islets monitored as glucose was raised from 3 to 11 mM glucose. C) Average of insulin secretion from up to 6 islets. n indicates the number of islets included in the average, and the error bars indicate the standard error of the mean. The inset is an enlarged version of averaged insulin secretion for the first h.

Figure 2.9 depicts the insulin secretion for an islet that was monitored for 24 h. 3 point calibrations of the assay were performed throughout the monitoring period, specifically at 9.9 h, 12.0 h, 21.5 h, 22.9 h, and 23.9 h. Insulin standards for the calibrations were chosen because the resulting B/Fs fall on the linear portion of the sigmoidal dose response curve. The calibrations are shown in Figure 2.9B. The similar calibrations confirm that the calibration of the immunoassay system was stable over the course of the 24 h experiment.

To better portray the insulin secretion dynamics, every other hour of insulin secretion dynamics are shown in Figure 2.9C. The 6 s temporal resolution and long-term automation of the chip enabled the observation of never-before-seen insulin secretion dynamics. In the experiment, the islet secreted insulin in large oscillatory bursts with a period of 4-6 minutes at approximately 10 h and 20 h of perfusion with 11 mM glucose. Other noteworthy trends observed include a sharp burst in insulin release immediately upon glucose stimulation (first phase), defined oscillatory patterns in second-phase insulin release, and transitions between these organized oscillatory patterns and more disorganized regions over the 24 h monitoring period.

Figure 2.9 (following page). 24 h islet insulin secretion. A) One example of 24 h insulin release from a single islet monitored as glucose concentration was raised from 3 to 11 mM. The islet was perfused with BSS and glucose at 1.0 mL min^{-1}. Time of glucose change is indicated by an arrow. B) Calibrations of the immunoassay were performed at 9.9 h, 12.0 h, 21.5 h, 22.9 h, and 23.9 h to measure any drift in calibration over the course of the 24 h monitoring period. C) Enlarged versions of insulin secretion dynamics shown in A. 1 h insulin secretion every other h is enlarged to better depict the secretion dynamics over the monitoring period.

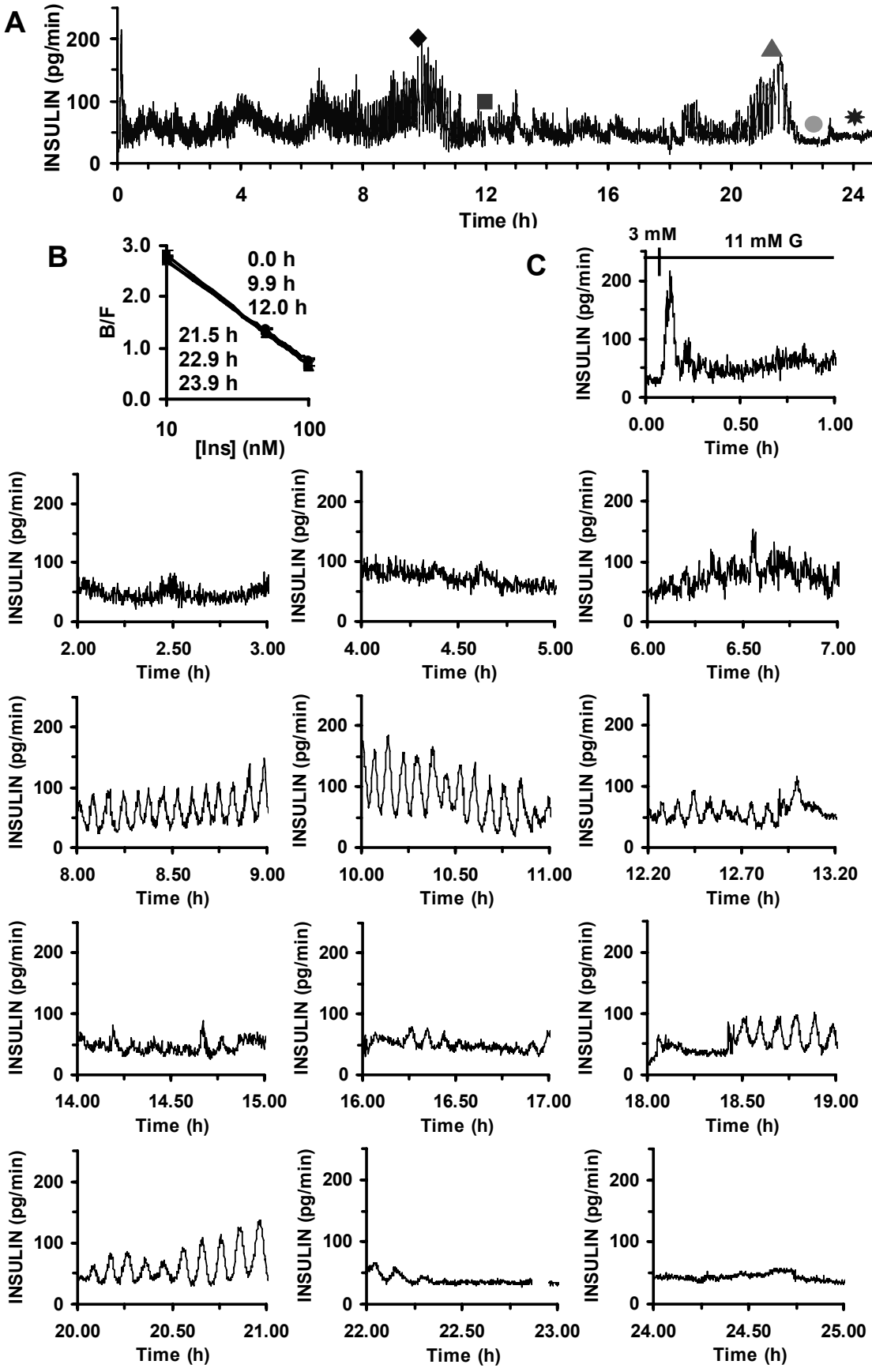
A
INSULIN (pg/min)
Time (h)
B
B/F
[Ins] (nM)
0.0 h
9.9 h
12.0 h
21.5 h
22.9 h
23.9 h
C
3 mM
11 mM G
INSULIN (pg/min)
Time (h)

The 24 h islet insulin secretion data shown in Figure 2.9 may demonstrate the previously-reported ultradian oscillations. Figure 2.10 includes a trace outlining the secretion data; oscillations with a period of 2 to 4 h can be observed for 23 hours. The evidence could indicate that the ultradian oscillations may be a result of higher amplitude of the more rapid oscillations (4-6 min). Although more experiments are necessary to suggest that single isolated islets are capable of maintaining ultradian oscillations, the data presented here demonstrate the capability of the long-term electrophoresis chip for monitoring ultradian secretion dynamics with high temporal resolution.

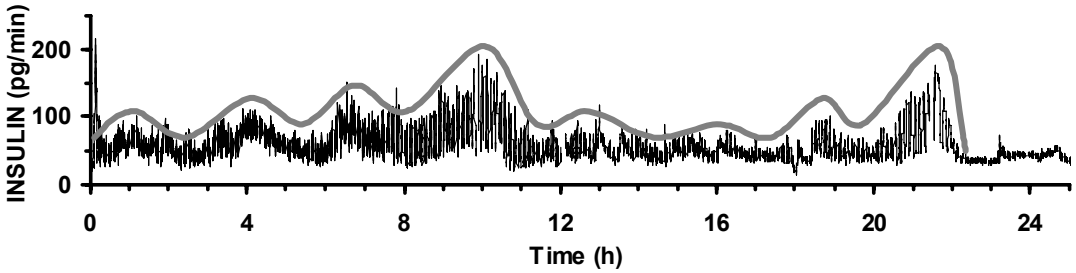

Figure 2.10. Evidence for Ultradian Oscillations. Data from Figure 2.9 were outlined (gray trace). The trace suggests evidence of secretion rhythms with period of 2 to 4 h.

Previously, the significantly more time- and labor-intensive RIAs and ELISAs did not allow for the observation of such long-term insulin secretion phenomena. Results shown in Figure 2.8 and Figure 2.9 demonstrate the potential for the long-term electrophoresis device to serve as a system for monitoring long-term insulin secretion phenomena. Such capabilities may help to elucidate and/or characterize important long-term dynamics in insulin secretion.

The vast increase in insulin secretion monitoring capabilities could significantly further the investigation of long-term insulin secretion phenomena. The device can be used to investigate and optimize islet culture conditions, to examine ultradian and

perhaps circadian rhythms of insulin secretion, and to perform numerous other pharmacological studies. Results of such studies may further elucidate pathways that link impaired insulin secretion and type 2 diabetes.

Conclusions

We have developed a microfluidic cell culture device capable of long-term unattended electrophoresis operation. To our knowledge, the presented work is the first demonstration of stable 24 h electrophoresis operation. With the automated device, 14,400 serial electrophoretic insulin immunoassays were completed in 24 h, and the device allowed for the observation of never-before-seen dynamics of insulin secretion in response to long-term glucose stimulation. The device resulted in considerable time and cost savings compared with the conventional insulin assay techniques. With modifications, the long-term measurement device may be used to monitor chemical secretions from other living cells. To increase the throughput of the long-term device, it would be beneficial to design the long-term monitoring device to perform the serial immunoassays in parallel.

CHAPTER 3

INVESTIGATION OF MEMBRANE-DISRUPTING EFFECTS OF ISLET AMYLOID POLYPEPTIDE ON ISLETS

Introduction

Islet amyloid polypeptide (IAPP or amylin) is a 37-residue peptide cosecreted with insulin by the β-cells of islets of Langerhans.[74] Highly aggregated amyloid deposits of human Islet Amyloid Polypeptide Protein (hIAPP) have been found in islets of more than 90 % of type 2 diabetic patients but not in non-diabetic patients, suggesting the formation of amyloid fibers plays a causative role in the development of diabetes.[76, 78] The formation of aggregates of the peptide into either amyloid fibers or oligomers has been implicated in the death of β-cells during type 2 diabetes through disruption of the cellular membrane; however, it is not clear which form of the peptide is responsible for β-cell death. Several reports indicate that the formation of aggregates of the peptide into either amyloid fibers or oligomers may lead to death of β-cells by disrupting the cellular membrane,[103, 104] but whether or not the aggregation of amyloidogenic proteins can disrupt membranes by forming toxic oligomers is disputed.[79, 80] Previous reports have indicated that the N-terminal region of the peptide (residues 1-19) is primarily responsible for the membrane-disrupting effect of the hIAPP peptide and that it disrupts membranes to a similar extent as the full-length peptide without forming fibrils when bound to membranes.[79] The rat version of the peptide is both non-amyloidogenic and non-cytotoxic but differs from the human peptide by only one amino acid residue.[105] The

18th residue in the rat version is arginine (Arg) and histidine (His) in the human peptide, as shown in Figure 3.1[105]

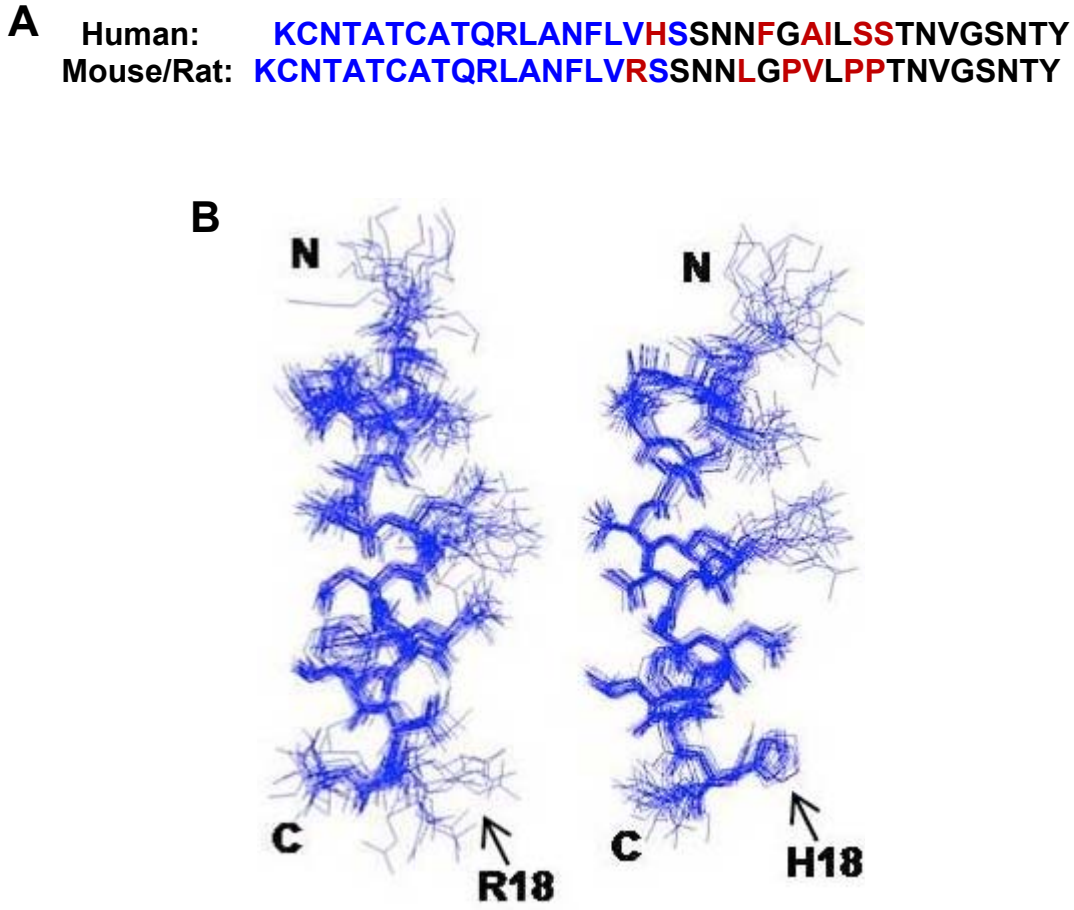

Figure 3.1. IAPP structures. (A) The amino acid sequences of rat and human IAPP. The 1-19 fragment used in this study is shown in blue, and the differences between the two sequences are shown in red. A disulfide bond exists between residues 2-8. The N-termini are amidated to mimic the naturally occurring peptide. (B) An ensemble of conformers for rat (left) and human (right) $IAPP_{1-19}$, demonstrating the convergence of the conformers for side chain atoms. B is reproduced with permission with permission from reference 105.

To explore the toxicity of the two peptide fragments, $hIAPP_{1-19}$ and $rIAPP_{1-19}$, a series of *in vivo* and *in vitro* experiments were performed by collaborating labs. The assays were designed to assess the ability of the peptides to permeabilize the membranes of both islets and model membranes. Circular dichroism experiments and dye leakage assays were performed on model liposomes and differential scanning calorimetry was

used to probe and compare the modes that the human and rat versions of the peptides use to bind to the membranes.

One useful method of investigating the membrane-disrupting effects of different versions of IAPP on islets is monitoring changes in intracellular Ca^{2+} concentration via fluorescence microscopy. Ca^{2+} signaling disruptions have been implicated in amyloid toxicity. It was previously reported that application of oligomeric forms of amyloid fibers resulted in elevated intracellular Ca^{2+} levels, likely due to membrane disrupting effects.[81] To explore the membrane permeabilizing effects of IAPP on islets, fluorescence imaging microscopy was used to monitor influx of Ca^{2+} to the islets. The fluorescence measurements were performed using fura-2, a ratiometric, Ca^{2+}-sensitive dye.

Conventional fura-2-based Ca^{2+} measurements are performed on cells in a chamber designed to hold approximately 3 mL of physiological buffer. With the large volume of the cell chamber, it was difficult to rapidly introduce stimulants to cells and to provide them with fresh media. In an effort to better control the cellular environment, we developed and characterized a simple microfluidic chip for monitoring the intracellular Ca^{2+} concentration of pancreatic islets.

Experimental Section

Dye Leakage Assays. In dye leakage assays, carboxyfluorescein-containing POPG vesicles were prepared by rehydrating a dried lipid film in 50 mM sodium phosphate buffer (pH 7.5) containing 40 mM carboxyfluorescein, adjusted to pH 7.5. Size exclusion chromatography using a PD-10 column (Amersham Pharmacia Biotech,

Uppsala, Sweden) was used to filter out free (Nonencapsulated) carboxyfluorescein from the vesicles. Experiments were performed immediately following vesicle formation, and a fresh vesicle solution was used for each assay. Fluorescence measurements were collected at an excitation wavelength of 493 nm and an emission wavelength of 518 nm. A baseline fluorescence measurement of the solutions was collected prior to the addition of the peptide. The fluorescence intensity was recorded 100 s after injection, allowing interaction between the peptide and the vesicles. The resulting fluorescence signal was later normalized to the total possible fluorescent signal, collected upon addition of Triton X detergent, which causes all vesicles present to release any remaining dye.

Circular Dichroism Spectroscopy. Lyophilized peptide dissolved in sodium phosphate buffer (10 mM, pH 7.3), was briefly vortexed and sonicated (approximately 15 s), and was then transferred to a 0.1 cm cuvette. After recording the initial spectrum of the peptide in solution, POPG vesicles from a 40 mg/ml stock solution were titrated into the cuvette. Spectra were collected at 1 nm wavelength intervals from 185-260 nm with a scanning speed of 50 nm/min and a bandwidth of 5 nm. The baseline spectrum of the buffer and vesicles, collected with peptide present, was subtracted from all spectra. Each spectrum reported is the average of four scans.

Differential Scanning Calorimetry.

Multilamellar vesicles of DMPC and DMPG (70% DMPC; 30% DMPG) were prepared as described for the dye leakage experiments. Sodium phosphate buffer (10 mM) with 150 mM NaCl at pH 7.3 was used to hydrate the samples. The total molar concentration of lipid was held constant (5.9 mM) for each sample while the molar peptide concentration was varied as indicated. Scans were performed on a Calorimetry

Sciences N-DSC II over a temperature range of 5 to 45 °C with a total of four heating and four cooling scans. The heating scans were run at 0.25 °C/min while the cooling scans were run at 1.0 °C/min, in between each of which there was a 10 min equilibration period. The buffer solution without the sample was used as the reference cell. The data was converted to molar heat capacity using the average molecular weight of the lipids, the lipid concentration, and a partial specific volume of 0.988 mL/g. Excess heat capacity was calculated by subtracting a baseline with buffer in both the reference and sample cells at the same scanning rate.

Islet Isolation Protocol. Pancreatic islets were obtained from 20 to 30 g male CD-1 mice as described previously.[102] The isolation procedure is also described in more detail in Appendix A. Briefly, mice were sacrificed by cervical dislocation and collagenase type XI was injected into the pancreas through the main pancreatic duct. The pancreas was removed and incubated in 5 mL of a collagenase solution at 37 °C. Islets that were used for experiments were 100-200 μm in diameter, had an intact islet membrane, and were oblong to spherical in shape. Islets were placed in tissue culture dishes and incubated in RPMI 1640 containing 10% fetal bovine serum, 100 U/mL of penicillin, and 100 μg/mL of streptomycin at 37 °C, 5% CO_2, pH 7.4. Islets were used 1-6 days following isolation

Microfluidic Chip Fabrication. The microfluidic devices used for monitoring Ca^{2+} flux and insulin secretion were fabricated using a previously described method. Fabrication of microfluidic chips is described in detail elsewhere.[51] Briefly, chips were prepared using photolithography and wet chemical etching.

Ca^{2+} Measurements. Ca^{2+} flux measurements were performed on islets following a 40 min incubation with 2 μM of the Ca^{2+}-sensitive fluorescence dye, fura-2. Individual islets were then loaded into an open cell chamber on a microfluidic chip, where islet media and stimulants were perfused over the islet at a rate of 0.6 μL/min. The chip was placed atop the stage of a Nikon Diaphot 300 microscope. The instrumentation and methods used to monitor intracellular Ca^{2+} concentration are described in more detail in Appendix B. Briefly, the fura-2 was alternately excited using a filter wheel with 340 and 380 nm light from a Xenon-arc lamp. The fluorescence emission from both excitation wavelengths was collected through a 510 ± 10 nm bandpass filter. Fluorescent images of the islet were collected at 1 Hz, and Metamorph software was used to ingrate the intensity over the islet area. Intracellular Ca^{2+} concentration was determined following calibration of the system by calculating the ratio of the emission at 340 and 380 nm excitation.

Results and Discussion

Microfluidic Device for Calcium Measurements. We designed a simple microfluidic system for performing intracellular Ca^{2+} imaging in islets. To confirm the chip is suitable for islet measurements, we investigated how rapidly changes in glucose, peptide, or other drug concentrations can be made in the cell chamber. Additionally, we examined whether solution from a channel with no applied pressure would leak or diffuse into the cell chamber at a problematic rate. Results from the experiments are summarized in Figure 3.2. While perfusing non-fluorescein-containing buffer into the cell chamber through channel y (Figure 3.2A), there was no detectable fluorescence in the chamber.

The lack of detectable fluorescence confirmed that there was no significant leakage through channel x while perfusing through the y channel. At approximately 23 min, pressure-driven flow of the non-fluorescein buffer was halted and pressure was applied to drive flow of the fluorescein solution. With flow of fluorescein through channel x, fluorescence signal in the chamber increased; fluorescence maxed within 1 min (Figure 3.2B). To confirm that the fluorescein was flushed from the chamber in a timely manner, pressure was released from the fluorescein solution and applied to the non-fluorescein solution. Within 1 min, the fluorescence signal diminished completely, confirming the complete replenishment of fresh solution to the cell chamber. Even after perfusion of fluorescein through channel x, when resuming perfusion through channel y, there was no detectable leakage of fluorescein into the chamber. Such evidence confirmed that the microfluidic perfusion chip for Ca^{2+} imaging is appropriate for maintaining precise control over the cellular environment by allowing rapid changes in glucose or peptide delivery to the cells.

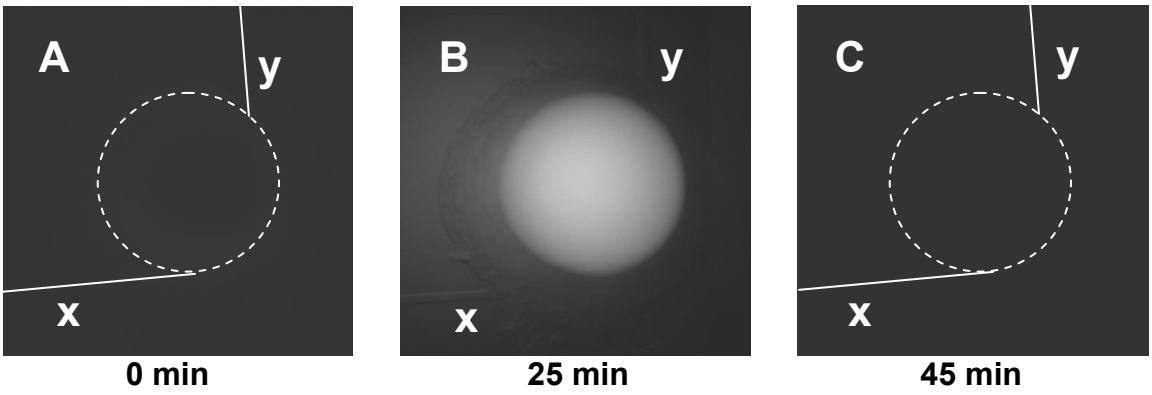

Figure 3.2. Perfusion and buffer replenishment in microfluidic Ca^{2+}-imaging chip. Images were collected while perfusing cellular buffer not containing ((A) and (C)) or containing (B) 200 nM fluorescein into the cell chamber on the chip. The cell chamber is depicted with a dashed-line circle in ((A) and (C)). For clarity in (A) and (C), channels are highlighted with a white line. Fluorescein-containing buffer was perfused through channel "x", and non-fluorescein-containing buffer was perfused through channel "y".

Membrane Disruption Induced by $hIAPP_{1-19}$ and $rIAPP_{1-19}$ in POPG Vesicles.

Our collaborators performed initial investigations to study the extent of membrane disruption induced by $hIAPP_{1-19}$ and $rIAPP_{1-19}$ peptides were performed by monitoring the leakage of carboxyfluorescein from large unilamellar POPG vesicles as a function of the concentration of POPG (Figure 3.3). Carboxyfluorescein concentration was high (40 mM) in intact vesicles, and the carboxyfluorescein fluorescence was self-quenched. The peptides' membrane-disruption on the vesicle allowed carboxyfluorescein to escape, thereby eliminating the self-quenching effect and increasing the carboxyfluorescein fluorescence. The peptide-to-lipid ratio was varied by the addition of POPG vesicles not containing carboxyfluorescein (empty vesicles) while the peptide and carboxyfluorescein-containing vesicle concentrations did not change.

The dye leakage assay results indicate that $hIAPP_{1-19}$ strongly induced membrane disruption at 1 μM at pH 7.5 (Figure 3.3A, as demonstrated by the high fraction of dye leakage from POPG vesicles. One μM $rIAPP_{1-19}$, however, is nonlinearly dependent on the peptide-to-lipid ratio at pH 7.5. The membrane-disrupting activity of $rIAPP_{1-19}$ peptide is nearly as high as $hIAPP_{1-19}$ at high peptide-to-lipid molar ratios, but as the peptide-to-lipid ratio is decreased, the membrane disrupting effect of $rIAPP_{1-19}$ drops off suddenly once the critical peptide-to-lipid ratio is surpassed (approximately 1:100).

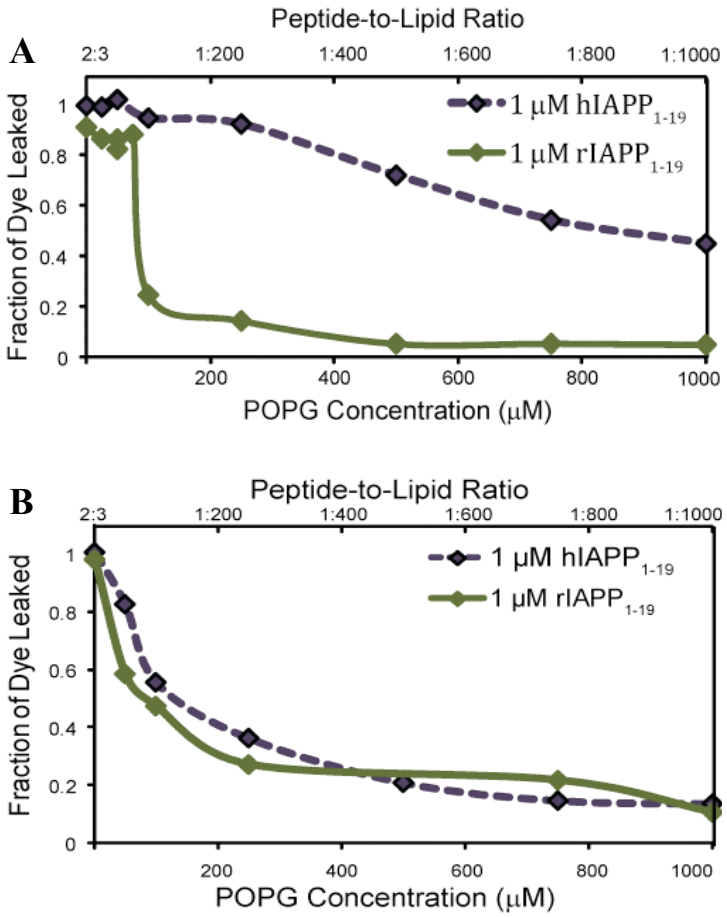

Figure 3.3. Liposome leakage induced by $hIAPP_{1-19}$ (blue diamonds) and the $rIAPP_{1-19}$ fragment (green diamonds) at pH 7.5 (A) and pH 6.0 (B). The various peptide-to-lipid ratios were created by adding 1 μM solutions of either $rIAPP_{1-19}$ or $hIAPP_{1-19}$ to POPG liposomes containing 1.5 μM carboxyfluorescein and a sufficient amount of POPG liposomes not containing carboxyfluorescein to create the desired peptide-to-lipid molar ratio. The fluorescence was recorded 100 s after peptide injection and was normalized to the maximum possible signal to calculate the dye leakage fraction following addition of detergent. Reproduced with permission from reference 106.

The $hIAPP_{1-19}$ structure differs from the $rIAPP_{1-19}$ structure only by the H18R substitution. The pH of the extracellular matrix is approximately 7.3, which is slightly alkaline. At pH 7.3, H18 is deprotonated while R18 remains charged. Previous reports demonstrated the hIAPP fibrillizes more rapidly in an acidic environment where H18 is charged.[107, 108] To examine the membrane-disrupting effects of the ionization state of H18, the dye leakage assay was repeated at pH 6.0 using 1 μM $hIAPP_{1-19}$. The assay

results were compared to both the vehicle disruption assays performed with 1 μM $hIAPP_{1-19}$ and 1 μM $rIAPP_{1-19}$ at pH 7.5, as well as to the leakage assays performed with 1 μM $rIAPP_{1-19}$ at pH 6.0 (Figure 3.3B) The $hIAPP_{1-19}$ causes significantly more disruption at lower peptide-to-lipid ratios at pH 7.5 than at pH 6.0. Furthermore, the extent of disruption induced by $hIAPP_{1-19}$ at pH 6.0 is comparable to $rIAPP_{1-19}$, indicating $hIAPP_{1-19}$ disrupts membranes via a similar mechanism as $rIAPP_{1-19}$ at pH 6.0 but not at pH 7.3 where histidine is deprotonated. Comparison of the results in Figures 3.3A and 3.3B suggests the ionization state of H18 is critical for membrane disruption.

In fact, His18 has previously been implicated in the rate of assembly of amyloid fibers, with amyloid fiber formation proceeding much more slowly when His18 is protonated at a low pH.[108] The R18H substitution in the rIAPP1-37 is sufficient to induce slight amyloidogenic properties in the typically nonamyloidogenic peptide.

Comparison of the Binding Affinity of $hIAPP_{1-19}$ and $rIAPP_{1-19}$ for POPG Vesicles. The differences in the extent of $hIAPP_{1-19}$- and $rIAPP_{1-19}$-induced membrane disruption indicate a difference in the extent of membrane binding of the peptides. To assess the extent of membrane binding of $rIAPP_{1-19}$ and $hIAPP_{1-19}$ to POPG vesicles, a series of circular dichroism (CD) experiments were performed. CD, a version of light absorption spectroscopy that measures the difference in absorbance of right- and left-circularly polarized light by a substance, is a popular tool used to approximate the conformational changes of peptides. Despite the fact that conformational changes that occur after membrane binding can complicate quantitative analysis, CD is a well established technique for investigating peptide membrane binding.[109] A series of CD spectra were collected of varying concentrations of $hIAPP_{1-19}$ and $rIAPP_{1-19}$ and varying

amounts of POPG vesicles. The CD spectra (data not shown) indicate that both $hIAPP_{1-19}$ and $rIAPP_{1-19}$, like the full-length peptide, exist in a random coil conformation in solution and adopt an alpha-helical conformation upon binding to the membrane, agreeing with previous structural reports of IAPP.[74, 110] Nevertheless, distinct differences exist in the binding curves of $hIAPP_{1-19}$ and $rIAPP_{1-19}$ titrated with increasing concentrations of POPG vesicles (Figure 3.4). $rIAPP_{1-19}$ is nearly as effective at binding to the lipid membranes as its human counterpart at saturating concentrations of POPG, but it is less effective at lower concentrations. The binding of full-length hIAPP and rIAPP is a cooperative process with membrane binding proceeding considerably more efficiently upon the formation of small aggregates of IAPP on the membrane.[110] Full-length rIAPP, differs from full-length hIAPP, however, since the nucleation of small aggregates by rat IAPP is noticeably lessened compared to that of hIAPP.[110] The lower affinity of $rIAPP_{1-19}$ for the membrane at lower concentrations of POPG indicates the $rIAPP_{1-19}$, like $rIAPP_{1-37}$, is less capable of forming small aggregates necessary to enhance membrane binding.

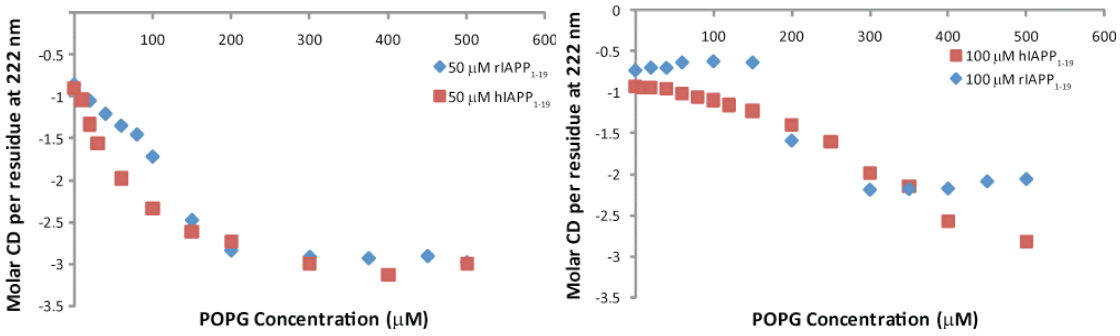

Figure 3.4. Binding of $rIAPP_{1-19}$ and $hIAPP_{1-19}$ to vesicles as approximated by CD spectroscopy. Plots of the molar CD per residue at 222 nm for 50 μM $hIAPP_{1-19}$ and $rIAPP_{1-19}$ (A) and 100 μM $hIAPP_{1-19}$ and $rIAPP_{1-19}$ (B) with the indicated concentrations of POPG. Data were collected in 10 mM sodium phosphate buffer, pH 7.3. Reproduced with permission from reference 106.

Membrane Disruption Induced by $hIAPP_{1-19}$ and $rIAPP_{1-19}$ in Pancreatic Islets. The vesicle disruption assays suggest $hIAPP_{1-19}$ strongly disrupts phospholipid membranes; however, the $rIAPP_{1-19}$ also disrupts membranes if the peptide-lipid-ratio is sufficiently high. These results agree with data from a previous study that demonstrated $hIAPP_{1-19}$, which is non-amyloidogenic when membrane-bound, disrupted POPG vesicles to a similar extent as the highly amyloidogenic hIAPP $peptide_{1-37}$.[79] Additionally, differential scanning calorimetry (DSC) was used to investigate the modes in which the two peptide fragments bind to model membranes. The addition of $hIAPP_{1-19}$ had minimal impact on the thermodynamics of the gel to liquid-crystalline phase transition, indicating the lipid-lipid interactions that stabilize the membrane are largely intact. The results, summarized in Figure 3.5A may suggest the peptide fragment binds in a transmembrane orientation in an aggregated state, similar to the suggested binding orientation for $hIAPP_{1-37}$.[110-112] $rIAPP_{1-19}$ only minimally reduces the enthalpy change of the main phase transition at low concentrations, as illustrated in Figure 3.5B. However, the peptide has a significant effect on the pretransition peak reflective of the rippled gel-to-gel phase transition, shifting it to higher temperatures and dramatically increasing the height of the peak for membranes containing 0.5 mol % $rIAPP_{1-19}$. Unlike the human version of the peptide fragment, $rIAPP_{1-19}$ induced a significantly different gel to liquid-crystal-line phase transition of the membranes at higher concentrations of the peptide, as evidenced by a reduction in height and a split into two peaks. A split of the phase transition peak is suggestive of lipid domain formation, with one peak corresponding to peptide-enriched domains of lipids and the other to peptide-poor domains of lipids.[113, 114] The results suggest that $rIAPP_{1-19}$ exhibits greater perturbation of the lipid bilayer and indicate that

the rat version of the peptide fragment may be bound to the surface of the bilayers and not in the active conformation necessary to form pores. The findings are consistent with the membrane orientation of IAPP peptides determined from NMR studies.[105]

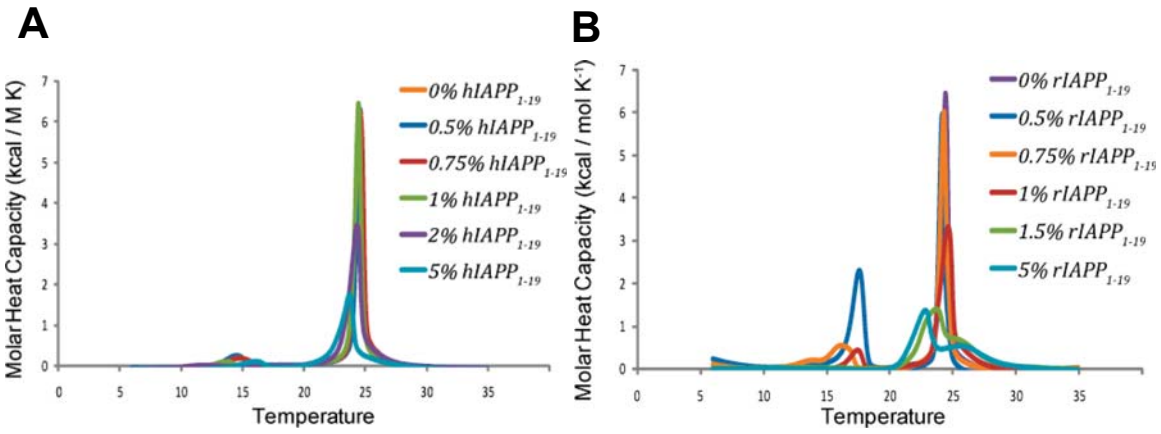

Figure 3.5 Membrane-disrupting effects of $hIAPP_{1-19}$ and $rIAPP_{1-19}$ as observed by differential scanning calorimetry. Differential scanning calorimetry of the pretransition and the main gel to liquid-crystalline phase transition of DMPC/DMPG (7/3) vesicles at the indicated molar ratio of (A) $hIAPP_{1-19}$ and (B) $rIAPP_{1-19}$ to lipid. Peptide and lipids were codissolved in a chloroform/ethanol solution, dried, and resuspended in 10 mM sodium phosphate buffer, pH 7.3, with 150 mM NaCl. Reproduced with permission from reference 106.

Despite the complementary results of the *in vitro* studies, all previously-mentioned assays were performed under non-physiological conditions (low ionic strength, high content of anionic lipids) to maximize peptide binding. The IAPP-induced damage could be more accurately assessed by performing experiments on live cells in more physiologically-relevant conditions. A previous report demonstrated that $hIAPP_{1-37}$ disrupted the Ca^{2+} homeostasis of neuroblastoma cells via a conformation-dependent manner.[81] Demuro *et al*. reported that the addition of monomeric hIAPP and mature fibers of hIAPP had little effect on intercellular Ca^{2+} levels but the addition of a prefibrillar oligomeric form of hIAPP caused the influx of Ca^{2+} into the cells. The extent of Ca^{2+} influx induced by prefibrillar oligomeric hIAPP was dependent on the hIAPP

concentration, with a maximal response at 12 μg/mL and an EC_{50} of approximately 3.5 μg/mL.[81] The hIAPP-induced membrane disruption allowed leakage of calcein dye from the cells, suggesting the prefibrillar oligomeric hIAPP does not simply disrupt Ca^{2+} homeostasis via the activation of the voltage-sensitive, L-type Ca^{2+} channels,[81] as has been reported for the fibrillar form of hIAPP.[115]

To assess the toxicity of $hIAPP_{1-19}$ and $rIAPP_{1-19}$ on pancreatic islets, we performed a similar experiment to that mentioned above by monitoring the influx of Ca^{2+} into single islets upon the addition of $hIAPP_{1-19}$ and $rIAPP_{1-19}$. The membrane-disrupting effects of the $hIAPP_{1-19}$ and $rIAPP_{1-19}$ peptide fragments, as well as the full-length $rIAPP_{1-37}$ peptide are summarized in Figure 3.6. The extent of disruption can be measured by comparing the rise in intracellular Ca^{2+} concentration in islets upon introduction of the peptides. Both $hIAPP_{1-19}$ and $rIAPP_{1-19}$ are toxic at relatively low concentrations, as measured by their ability to disrupt the cellular membrane and allow the influx of Ca^{2+} into the cell. However, $hIAPP_{1-19}$ is significantly more effective than $rIAPP_{1-19}$ at disrupting the islet membrane, complementing the dye leakage assay results. Full-length rIAPP prepared in the same manner does not induce the influx of intracellular Ca^{2+} into the cell, in agreement with the low cytotoxicity of $rIAPP_{1-37}$ reported in previous studies.[81, 116, 117]

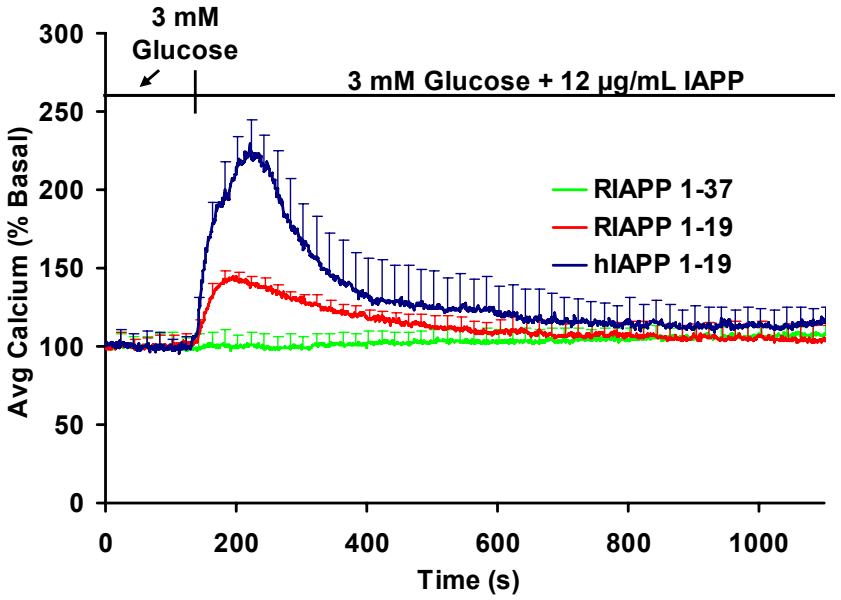

Figure 3.6. Membrane permeabilization in pancreatic islets induced by IAPP. Whole mouse pancreatic islets were loaded 45 minutes prior to the experiment with 2 µM of the Ca^{2+}-sensitive dye fura-2 AM. At 140 seconds (indicated by a vertical line at the top), 12 µg/ml $hIAPP_{1-19}$, $rIAPP_{1-19}$, or $rIAPP_{1-37}$. The values given are the average of 5 islet samples; error bars indicate standard error of the mean. Reproduced with permission from reference 106.

Interestingly, the rise in intracellular Ca^{2+} upon perfusion of the peptide fragments was followed by an immediate and somewhat gradual decrease in Ca^{2+}. A number of phenomena could be responsible for the apparent decrease. Leakage of fura-2 from the islets could lead to an apparent decrease in Ca^{2+}; however, the sum of the total fluorescence in the islet did not decrease significantly over time (data are not shown), confirming that there was minimal dye leakage from the islets. It is possible that Ca^{2+} was sequestered quickly upon flux into the islets, resulting in an apparent loss of Ca^{2+}. Additionally, the IAPP-induced pores may not be stable in the membranes. There are reports that zinc can protect against the cytotoxicity of another amyloid peptide, amyloid-β, possibly by inducing precipitation of the peptide.[118] Insulin is secreted as a hexamer with zinc, and the rise in Ca^{2+} typically results in exocytosis of insulin. Insulin dissociates from zinc within 60 s following exocytosis,[119] so it seems possible that zinc

may be partially responsible for the decrease in Ca^{2+}. Finally, it has not yet been confirmed that that the increase in Ca^{2+} is not due to activation of the voltage-sensitive Ca^{2+} channels on the cellular membranes. If the influx of Ca^{2+} is a result of the opening of the Ca^{2+} channels on the membrane, the apparent decrease in Ca^{2+} levels could be due solely to deactivation of the Ca^{2+} channels. Treatment of the cells with a Ca^{2+} channel blocker, such as nifedipine or cobalt, would confirm whether the influx of Ca^{2+} is due to IAPP-induced membrane disruption or due only to increased permeability of Ca^{2+} channels. However, Demuro *et al*. used cobalt to confirm that the previously observed membrane-disrupting effects of amyloid-β on neuroblastoma cells were not due to increased permeability of Ca^{2+} channels,[81] suggesting the membrane-disrupting effects of IAPP are not due to activation of Ca^{2+} channels but rather to IAPP-induced pore formation on the membranes. While several potential causes of the apparent decrease in Ca^{2+} levels have been suggested, further investigations are necessary to characterize the mechanism of the apparent decrease in intracellular Ca^{2+}.

Conclusions

The $hIAPP_{1-19}$ peptide is of interest in amyloidogenic protein research due to its membrane-disrupting effects. The human peptide fragment disrupts artificial anionic membranes to a similar extent as the full-length human IAPP peptide but is not amyloidogenic once bound to a membrane in an active alpha-helical form.[79] The impairment of $hIAPP_{1-19}$ to aggregate provides a valuable tool for investigating the properties of the full-length IAPP, whose rapid and complex aggregation process significantly complicates typical biophysical studies. The full-length rat version of the peptide is non-amyloidogenic and nontoxic, suggesting that the amyloid fibers, rather

than other oligomeric states, of the human full-length peptide may play a crucial role in IAPP's toxicity of β-cells in the context of type 2 diabetes.

Due to the similarities in the sequences in the 1-19 region of the rat and human versions of IAPP, the membrane-disrupting effect of $hIAPP_{1-19}$ is unexpected. The results presented in this work demonstrating the membrane-disrupting effects of IAPP on islets corroborated findings from previously reported studies investigating the membrane-disrupting effects of IAPP on model membranes. The results presented here suggest an important role for His18 in the early stages of aggregation and membrane binding. Our results show, for the relatively non-amyloidogenic but toxic 1-19 fragments of the peptide, that the His18 residue also plays a key role in controlling the toxicity of the peptide by modulating the interactions of IAPP with the phospholipid membrane.

CHAPTER 4

INVESTIGATION OF LEPTIN SIGNALING IN ISLETS USING PANCREAS-SPECIFIC LEPTIN RECEPTOR KNOCK-OUT MICE

Introduction

The mechanisms that result in β-cell failure and increase the incidence of diabetes in obese individuals are not fully elucidated, and it is possible that the adipose-derived hormone leptin plays a key role. Leptin, a 16 kDa hormone predominantly secreted from white adipose tissue,[82] regulates energy balance and metabolism by acting on neurons in the brain to regulate appetite.[83] In addition to their presence on the hypothalamus, leptin receptors are widely distributed throughout peripheral organs, indicating that leptin has actions aside from its effects on the central nervous system.[84, 85] For instance, leptin receptors are expressed on pancreatic β-cells, suggesting a potential effect of leptin on insulin action[120]; however, leptin's effect on β-cells is not fully understood. There are several reports that leptin acts to inhibit insulin secretion through multiple signaling pathways in β-cells, as summarized in Figure 4.1.[86] The inhibition of insulin release by leptin, combined with the known adipogenic effects of insulin, suggests the existence of an insulin/leptin feedback loop.[86] Because leptin is primarily secreted from white adipose tissue, plasma leptin levels are proportional to fat mass in humans and other animals.[121] According to the proposed insulin/leptin feedback loop, an increase in adipose tissue and leptin would reduce insulin production and direct less energy to the formation of adipose tissue.[86] Despite the strong evidence for the inhibitory effects of

leptin on insulin secretion,[122-125] several discrepancies exist in the literature. One study reported that leptin enhances insulin secretion[126] while others suggest that it has no effect.[127-129] The observed lack of inhibition of leptin, however, seem to be an artifact of administering leptin in the presence of BSA, and thus leptin is generally believed to be inhibitory on insulin release.[87]

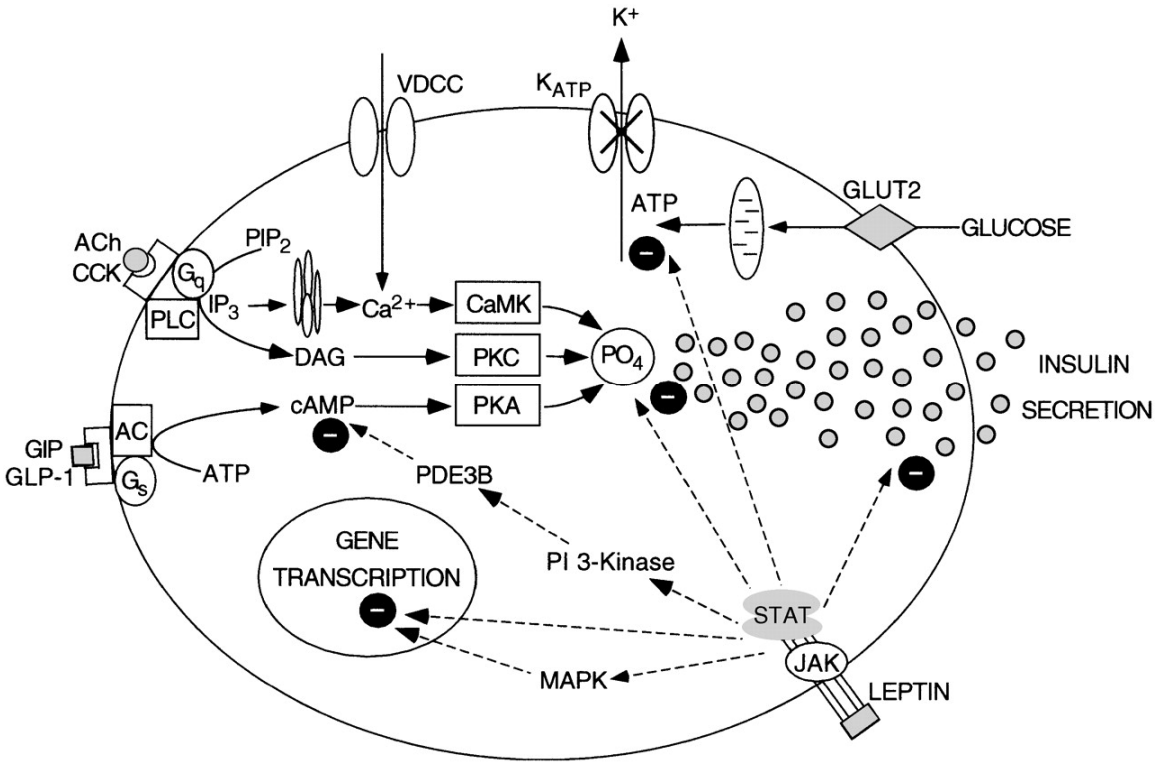

Figure 4.1. Proposed effects of leptin signaling in the pancreatic β-cell. Leptin inhibits insulin secretion through multiple signaling pathways in β-cells. Reproduced with permission from reference 86.

To examine more closely the factors that link obesity and diabetes, Kulkarni and coworkers used the Cre-*LoxP* approach to create pancreas-specific leptin receptor knock-out (ObRKO) and corresponding control (ObRlox) mice. It was previously demonstrated that the knock-outs (KO) showed significantly higher levels of both Ca^{2+} flux and insulin release compared to control islets, indicating that a lack of leptin signaling in islets from lean animals enhances glucose-stimulated insulin secretion (GSIS). Furthermore, GSIS

from control islets was significantly less when the islets were perfused with elevated glucose and 10 nM leptin compared to those perfused with only glucose, whereas neither insulin release from nor Ca^{2+} flux into KO islets differed with leptin treatment. The results demonstrate an inhibitory effect of leptin on insulin secretion. These phenomena are illustrated with averaged plots in Figure 4.2.

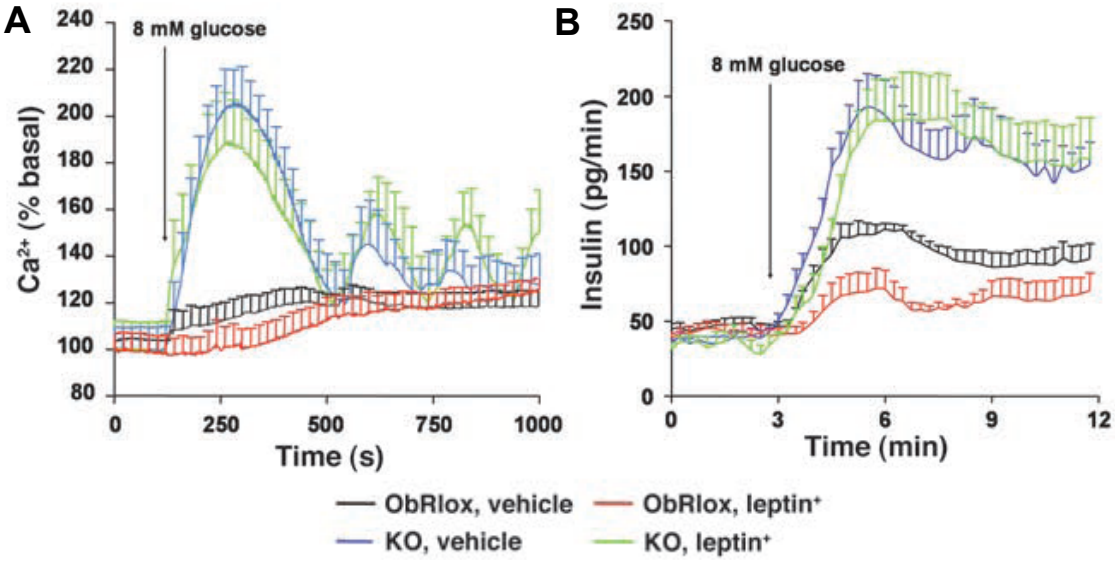

Figure 4.2 Enhanced early-phase Ca^{2+} and insulin secretion in pancreas-ObR-KO mice. Representative traces of intracellular Ca^{2+} flux (A) and insulin secretion (B) measured in single size-matched islets isolated from male ObRlox and KO mice with or without 100 nM (A) or 10 nM (B) leptin. *n* = 6 islets from 3 individual mice in each group. Reproduced with permission from reference 91.

In agreement with the improved GSIS, the ObRKO mice exhibited improved glucose tolerance due to enhanced acute-phase insulin secretion and greater β-cell mass due to greater size and increased expression and phosphorylation of p70 S6 kinase. The evidence demonstrates greater insulin signaling in β-cells, corroborating the idea of the insulin/leptin feedback loop. However, challenging the KO mice with a high-fat diet (HFD) unexpectedly resulted in reduced early-phase glucose-stimulated insulin secretion,

poor compensatory islet growth, and enhanced glucose intolerance in the KOs compared with the controls. The results suggest a potential role for leptin in preparing cells to handle lipids; without leptin signaling, the HFD is harmful.

The above-mentioned results suggest that altered leptin action in islets could contribute to obesity-associated diabetes. To further examine the influence of leptin on islet function, we designed and performed a series of experiments to study leptin signaling in β-cells by monitoring Ca^{2+} flux into and insulin secretion from islets isolated from both ObRlox and ObRKO mice. By exposing islets to various environments, we were able to probe potential signaling pathways in β-cells.

Experimental Section

Animals and Genotyping. Experiments were performed using ObRKO and ObRlox mutant mice, produced using the Cre-*loxP* system, as previously described in detail.[91, 130] The mice were from the C57BL/6 strain and were generously supplied to us by Kulkarni and coworkers. All animals were housed in specific pathogen–free facilities and maintained on a 12 hour light/dark cycle and fed standard rodent chow.

Preparation of 10 mM Palmitate. The stock solution of palmitate bound to BSA was prepared using the following method. The palmitate was dissolved in a modified Krebs-Ringer bicarbonate (KRB) medium containing 20 mM HEPES (N[2-hydroxyethyl]piperzine-N'-[2-ethanesulfonic acid]), 118 mM NaCl, 5.4 mM KCl, 2.4 mM Ca^{2+}, 1.2 mM KH_2PO_4 supplemented with fatty acid-free BSA (10 g/100 mL) to produce a 10 mM palmitate stock solution. 10 mM NaOH was added to the KRB solution to aid in dissolution of the palmitate. The solution was stirred gently at 37 ˚C for

12 hours, allowing time for the dissolution of palmitate and for the palmitate to bind to the BSA. The pH of the palmitate solution was adjusted to 7.4 using sodium hydroxide, and the stock solution was filtered through a 0.2 μm filter and, to prevent oxidation, stored at -20 ˚C. Palmitate concentration (of the nonesterified fatty acid) in the resulting medium was measured with a NEFA C kit (Wako Chemicals, Richmond, VA). The palmitate stock solution was diluted in RPMI culture medium or in KRB to obtain 10 mM palmitate; the final concentration of BSA was approximately 0.56%.

Islet Isolation Protocol. Pancreatic islets were obtained from 20 to 30 g male CD-1 mice as previously described.[102] Briefly, mice were sacrificed by cervical dislocation and collagenase type XI was injected into the pancreas through the main pancreatic duct. The pancreas was removed and incubated in 5 mL of a collagenase solution at 37 °C. Islets that were used for experiments were 100-200 μm in diameter, had an intact islet membrane, and were oblong to spherical in shape. Islets were placed in tissue culture dishes and incubated in RPMI 1640 containing 10% fetal bovine serum, 100 U/mL of penicillin, and 100 μg/mL of streptomycin at 37 °C, 5% CO_2, pH 7.4. Islets were used 1-6 days following isolation.

Chip Fabrication. The microfluidic devices used for monitoring Ca^{2+} flux and insulin secretion were fabricated using a previously described method.[52, 98] Briefly, chips were prepared using photolithography and wet chemical etching.

Intracellular Ca^{2+} Measurements. Ca^{2+} flux measurements were performed on islets after a 40 min incubation with 2 μM of the fluorescent Ca^{2+}-sensitive dye, fura-2. Afterward, individual islets were loaded into an open cell chamber on a microfluidic chip. Islet media and stimulants were perfused over the islet at a rate of 0.6 μL/min. The chip

was placed atop the stage of a Nikon Diaphot 300 microscope. The instrumentation used to monitor intracellular Ca^{2+} concentration is described in more detail in Appendix B. Briefly, the fura-2 was alternately excited using a filter wheel with 340 and 380 nm-light from a Xenon-arc lamp. The fluorescence emission from both excitation wavelengths was collected through a 510 ± 10 nm bandpass filter. Images of the islet were collected at 1 Hz and the intensity over the islet area was integrated using Metamorph software. Intracellular Ca^{2+} concentration was calculated by determining the ratio of the emission intensity at 340 and 380 nm excitation wavelengths after calibration of the system.

Insulin Secretion Measurements. Insulin release from islets was monitored in parallel using a capillary electrophoresis-based immunoassay performed on a microfluidic chip. The chip operation was based on techniques described in more detail elsewhere.[99] During insulin monitoring, solution sampled from the islet reservoirs was mixed with 50 nM fluorescein isothiocyanate-labeled insulin (FITC-insulin) (Molecular Probes, Eugene, OR) and 40 nM anti-insulin antibody (Ab) (BioDesign Int'l, Saco, ME) in 20 mM Tricine, 1 mM EDTA, 50 mM NaCl, Tween 20, and BSA (pH 7.4). A gating electrophoresis buffer (150 mM Tricine, 20 mM NaCl, pH 7.4) was placed in the gate and waste reservoirs. The gate reservoirs were grounded with a high voltage relay (Kilovac, Santa Barbara, CA). When the relay was opened, sample from each reaction channel was allowed to flow onto the subsequent separation channels. Afterward, the gate was returned to ground, and separation occurred. Immunoassays were performed every 10 s, and immunoassay products were separated in the electrophoresis channels and detected using multiplexed fluorescence detection.

The device was conditioned before experiments by electrophoretically flowing 0.1 M NaOH through the channels, followed by deionized water, and finally the experimental solution. All solutions were filtered to prevent introduction of particulates to the chip and to prevent degradation of the solutions. A single islet was then placed in the islet reservoir and perfused with a balanced salt solution (125 mM NaCl, 5.9 mM KCl, 1.2 mM $MgCl_2$, 2.4 mM $CaCl_2$, 25 mM tricine, and 0.7 mg mL^{-1} bovine serum albumin (BSA), adjusted to pH 7.4) containing varying amounts of glucose, leptin, palmitic acid, or glibenclamide.

Statistics. All data are presented here as mean ± SEM and were analyzed using an unpaired 2-tailed Student's *t* test or analysis of variance (ANOVA) as appropriate. The null hypothesis was rejected at a *P* value of 0.05.

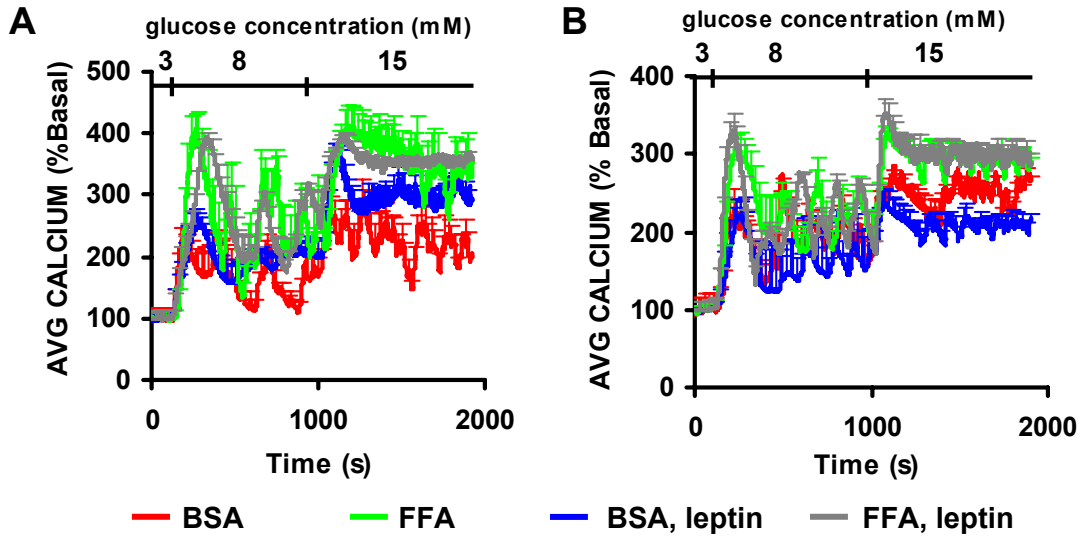

Figure 4.3. Effects of acute FFA exposure on ObRlox (A) and KO (B) islets. Data sets are from islets perfused with 8 mM and then 15 mM glucose (± 10 nM leptin) containing 0.5 mM palmitic acid (FFA) or FFA-free BSA control cell media (BSA). Error bars are ± SEM. Each data set is n ≥ 5 islets.

Results

Acute and Chronic Exposure to Fatty Acid. Acute free fatty acids experiments were performed by monitoring intracellular Ca^{2+} while perfusing the islets with either 8 mM or 15 mM glucose and 0.5 mM palmitic acid (± 10 nM leptin), and results are illustrated in Figure 4.3. In both KO and control islets, Ca^{2+} flux was significantly ($P < 0.05$) enhanced with acute stimulation with FFA and both 8 and 15 mM glucose compared to the KO and control islets not treated with FFA. Interestingly, in both islet types, treatment with leptin resulted in only a moderate and insignificant ($P < 0.05$) inhibition of Ca^{2+} flux. Traces from GSIS experiments (data not shown) showed similar results. It is believed that the previously demonstrated inhibitory effect of leptin is diminished in the FFA experiments due to the presence of a high concentration of bovine serum albumin (BSA) in the perfusion buffer, as previous studies have also reported this phenomenon.[87] The high BSA concentration is necessary for the appropriate FFA action

on the islets, but it is reported that up to 98 % of plasma leptin in humans is bound to serum proteins.[131] Such a condition would result in a weakened inhibition from endogenous leptin in the presence of BSA.

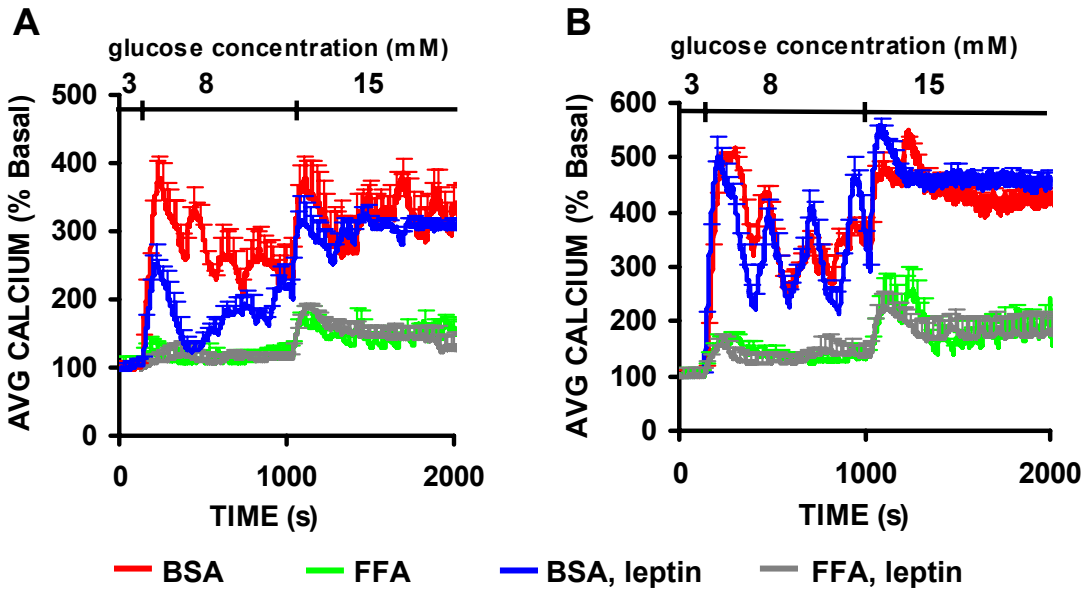

Figure 4.4. Effects of chronic FFA exposure on ObRlox (A) and KO (B) islets. Data sets are from islets incubated for 48 h in either 0.5 mM palmitic acid (FFA) or control cell media (BSA). Islets were then perfused with 8 mM glucose and then 15 mM glucose (± 10 nM leptin). Error bars are ± SEM. For all sets, n ≥ 5 islets.

The effect of chronic FFA on islets was studied by incubating islets for 48 h with 0.5 mM palmitic acid and then monitoring intracellular Ca^{2+} while perfusing the islets with glucose (± 10 nM leptin). Results from the chronic FFA experiments are illustrated in Figure 4.4. During perfusion with both 8 mM and 15 mM glucose, Ca^{2+} flux into both control and KO islets was significantly ($P < 0.05$) decreased after chronic exposure to FFA compared to islets incubated with only FFA-free BSA. While there was a significant ($P < 0.05$) inhibition of Ca^{2+} flux into control islets incubated with FFA-free BSA after leptin treatment during perfusion with 8 mM glucose, no inhibition was

observed from control islets incubated in 0.5 mM palmitic acid, nor was an effect from leptin treatment observed in KO islets in either incubation media.

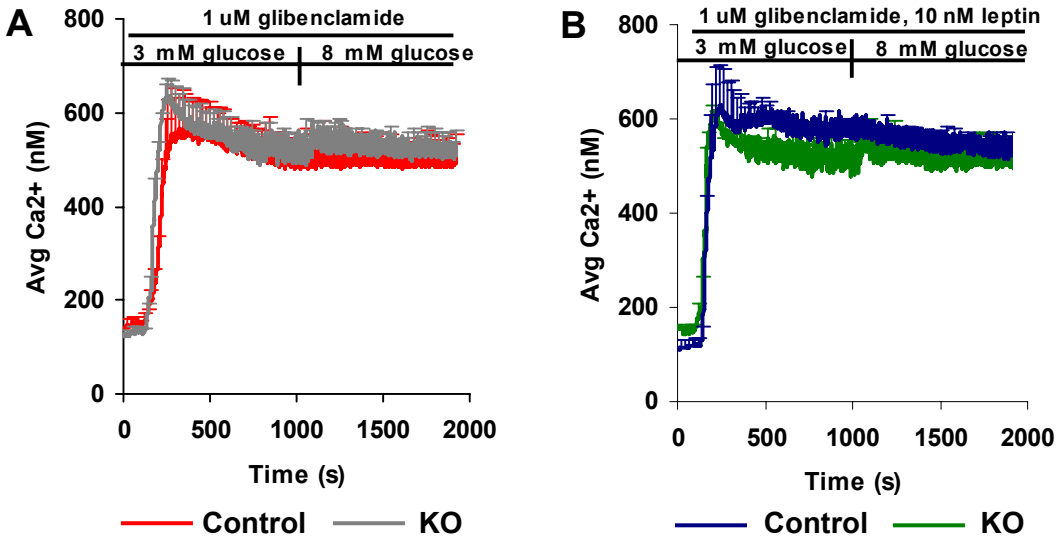

Figure 4.5. Ca^{2+} influx from ObRlox and KO islets stimulated with glibenclamide with or without 8 mM glucose with leptin (A) and without leptin (B). Error bars are ± SEM. For all data sets, n ≥ 5.

Stimulation of Islets with Sulfonylurea. To examine the possible interaction of leptin signaling pathways and K_{ATP} channel-independent secretion, insulin release and Ca^{2+} flux were monitored from ObRlox and KO islets stimulated with the sulfonylurea, glibenclamide, in either 3 mM or 8 mM glucose with or without the presence of 10 nM leptin. Sulfonylureas bind to K_{ATP} channels, inhibiting efflux of potassium. Insulin release from KO islets perfused with 1 μM glibenclamide was markedly higher ($P < 0.05$) than release from ObRlox islets perfused with the same concentration of glibenclamide, with or without the presence of leptin (data not shown). While there was no significant difference in insulin release from KO islets after leptin treatment, there appeared to be a mild, though insignificant, inhibitory effect of leptin on insulin secretion from ObRlox

islets in the presence of 8 mM glucose. The results for Ca^{2+} flux experiments using the same protocol are summarized in Figure 4.5. There was no difference in intracellular Ca^{2+} levels between ObRlox and KO islets with or without leptin treatment. The data suggest that the differences in measured insulin levels are not due to enhanced Ca^{2+} flux into the cells and that the triggering pathways is not significantly affected by the lack of leptin signaling. .

Discussion

Comparison with *in vivo* Observations. The effects of pancreas-specific leptin receptor removal were explored by our collaborating researchers; assessments included both *in vivo* and *in vitro* experiments. *In vitro* data were compared to results from *in vivo* experiments (live animal insulin secretion assays and glucose tolerance tests) performed for investigations of potential mechanisms involving leptin signaling in beta cells. Previously mentioned observations showing enhanced insulin secretion from and Ca^{2+} flux into KO islets complement data collected from experiments on living animal models. The acute-phase insulin secretory response to glucose KO mice of both male and female sexes was enhanced compared with control mice (Figure 4.6A). As a result, upon i.p. glucose challenge, glucose excursion from KO mice was significantly lower, consistent with improved glucose tolerance (Figure 4.6B). These *in vivo* data are consistent with data showing enhancement of both Ca^{2+} flux in and insulin secretion from KO mice due to the lack of leptin signaling in islets.

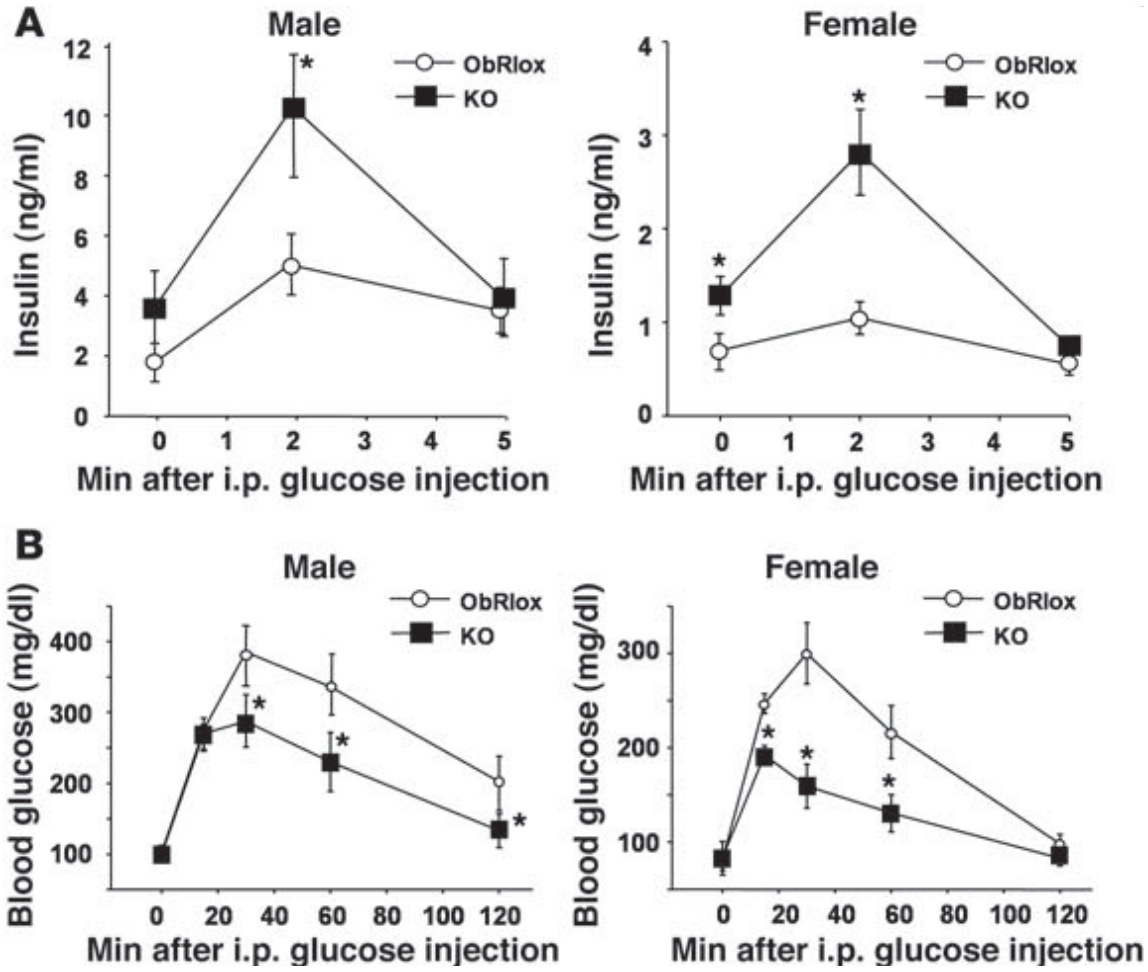

Figure 4.6. Early-phase insulin release and glucose tolerance were enhanced in pancreas-ObRKO mice compared to ObRlox controls. (A) Plasma insulin levels after i.p. glucose injection (3 g kg^{-1} body weight) in 6-month old male and female mice of both types. (B) Blood glucose levels after i.p. injection of glucose (2 g kg^{-1} body weight) in 6-month old male and female mice of both types. For all plots, *P < 0.05 compared to ObRlox controls and n ≥ 6. Error bars are ± SEM. Reproduced with permission from reference 91.

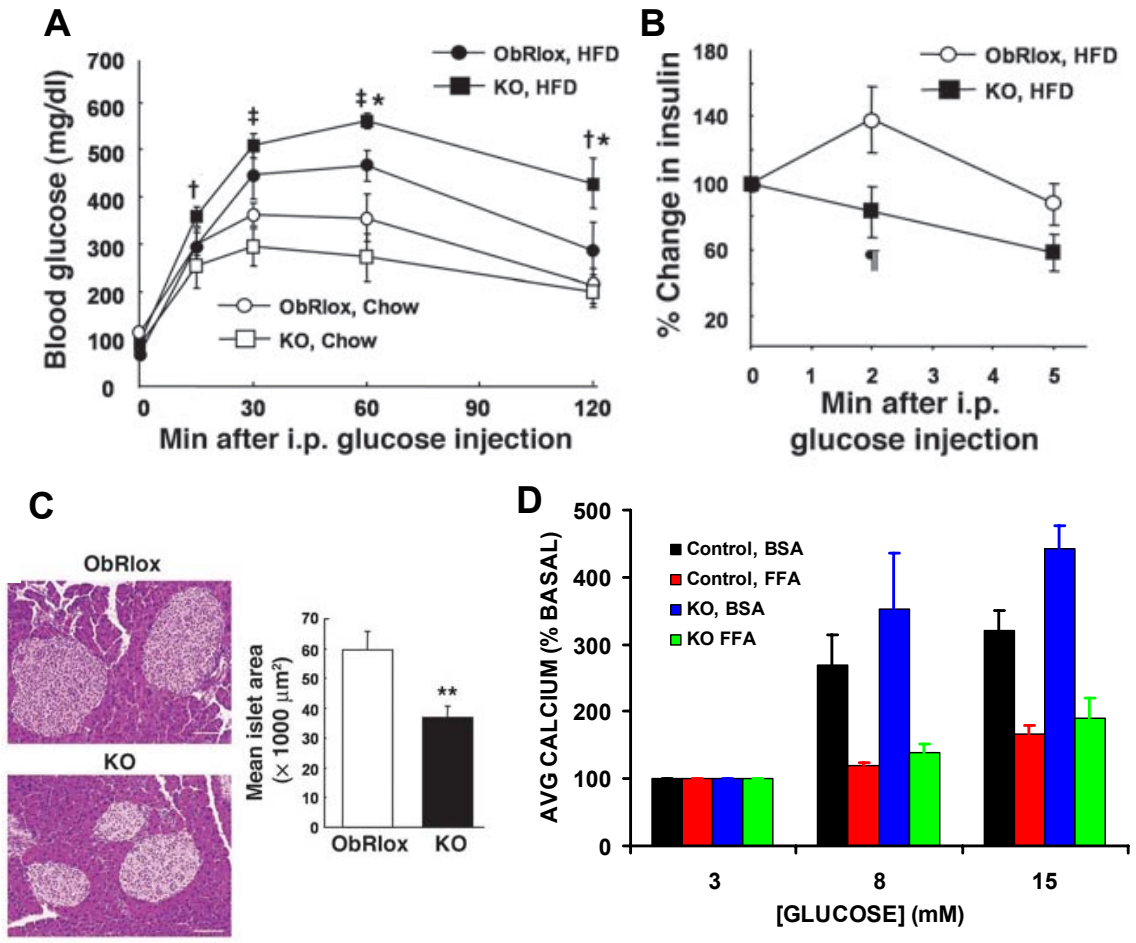

Figure 4.7. Effects of diet-induced obesity on islet function and size. (A) Glucose tolerance test results for 4-month-old male mice fed regular chow (Chow) or high fat diet (HFD), n = 5; †P < 0.05, ‡P < 0.01 for KO mice on HFD versus KO mice on Chow, n = 5 (KO) or 3 (Chow). (B) Change in plasma insulin levels after i.p. glucose injection (3 g kg^{-1} body weight) in mice on HFD for 12 weeks. ¶P = 0.07; n = 4. (C) Left: Hematoxylin and eosin staining in representative pancreas sections of ObRlox and KO mice on HFD for 12 weeks. Scale bars = 100 µm. Right: mean average islet area from n ≥ 10 islets from 5 mice for each genotype. Error bars are SEM. **P < 0.01 versus ObRlox. (D) Plot comparing mean intracellular Ca^{2+} levels from islet data presented in Figure 4.4 (results summarized here are only treatments without the presence of leptin). *P < 0.05. Error bars are ± SEM. (A), (B), and (C) are reproduced with permission from reference 91.

To investigate whether the enhanced insulin secretion observed in the KOs on a normal chow diet protects the KOs from the effects of HFD-induced obesity, the control and KO mice were fed an HFD or normal chow diet for 12 weeks. As a result of the high fat feeding, mice in both groups were demonstrated significant and similar weight gain and exhibited insulin resistance compared with ObRlox and KO mice fed a normal chow

diet (data not shown). Unexpectedly, however, the KO mice fed a HFD showed impaired glucose tolerance, partially due to a decreased acute insulin response to glucose compared with the ObRlox controls (Figures 4.7A and 4.7B). Furthermore, control mice on HFD developed islet hyperplasia to compensate for insulin resistance compared with mice on normal chow; however, KO mice showed a significantly reduced islet mass after being fed an HFD (Figure 4.7C), suggesting the KO mice may be more susceptible to lipotoxic effects.

Data collected from islet experiments complement the *in vivo* observations. Figure 4.7D summarizes the average Ca^{+} flux in both ObRlox and KO islets following 48 h incubation in either BSA or FFA. As expected, Ca^{+} flux in both islet types significantly decreased after FFA treatment, and the percent decrease was similar for both types. However, GSIS from KO islets decreased by 48 % and 54 % for 8 and 15 mM glucose stimulations, respectively, whereas GSIS from ObRlox islets decreased by only 21 % and 37 % (data not shown). The GSIS results suggest that KO islets may be more susceptible to FFA-induced lipotoxic effects due to inferior lipid regulation mechanisms. The discrepancy in the Ca^{+} flux and GSIS results also indicate that the differences in GSIS after FFA incubation are not due solely to decreased Ca^{2+} flux into the cells.

Proposed Mechanisms of Leptin Effects on Islets. In addition to its role in islet function and survival, leptin has been reported to regulate lipid metabolism and storage in β-cells, and it is also known that lipid accumulation in islets impairs secretory function and viability. The results shown in Figure 4.7 suggest leptin may be partially responsible for regulating lipid metabolism. It is possible that the decreased acute-phase secretory response and islet size in the KO mice on the HFD may be due to secondary

effects of lipid overload in the islets as a result of inhibited leptin signaling. The consequential lipotoxic effect on islets is a potential mechanism for the impaired glucose tolerance in the KO mice. Figure 4.8 summarizes the proposed pathway for leptin signaling in the development of diabetes. The coupling of leptin signaling and lipid metabolism and their contribution to insulin resistance in β-cells in the circumstance of obesity is yet to be fully elucidated, and further investigation is necessary.

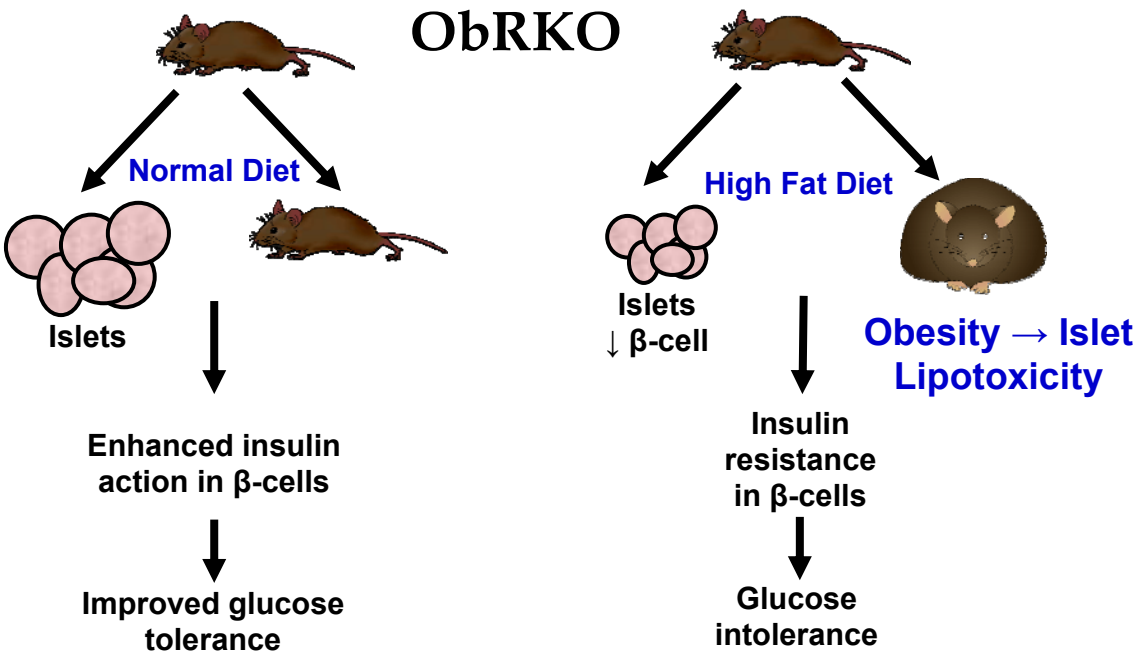

Figure 4.8. Proposed pathway for leptin signaling in islets in the development of obesity-associated diabetes. ObRKO mice fed a normal diet resulted in enhanced insulin action in β-cells and improved glucose tolerance, but the same mice fed a high fat diet exhibited insulin resistance in β-cells and glucose intolerance. Adapted with permission from reference 91.

To further investigate leptin signaling pathways in islets, KO and ObRlox islets were treated with the sulfonylurea, glibenclamide. KO islets treated with glibenclamide exhibit similar Ca^{2+} flux compared with ObRlox islets; however, KO islets secrete more insulin in response to glibenclamide than their control counterparts. The different effects

in Ca^{2+} flux and insulin secretion suggest that that the differences in measured insulin levels are not due to enhanced Ca^{2+} flux into the cells. The results suggest leptin signaling pathways are coupled with the metabolic amplifying pathway of insulin secretion.

Conclusions

We report that GSIS and Ca^{2+} flux is enhanced in KO islets acutely exposed to free fatty acids (FFAs), while both physiological responses are inhibited in KO islets chronically exposed to the same concentration of FFAs. Additionally, when incubated in normal conditions, the KO islets exhibited enhanced GSIS and Ca^{2+} flux compared to the ObRlox mice. These data support previous evidence of a lipotoxic effect on islet function with chronic FFA exposure. In fact, it directly supports the *in vivo* results in which ObRKO mice were fed a HFD and exhibited decreased glucose tolerance with a blunted insulin response. Jointly, the results provide further evidence for an insulin/leptin feedback loop and provide implications for β-cell failure in obesity. Additionally, KO islets treated with the sulfonylurea, glibenclamide, exhibit similar Ca^{2+} flux compared with controls, while KO islets secrete more insulin in response to glib than their control counterparts. The results from the glibenclamide experiments suggest leptin signaling pathways are coupled with glucose-dependent, K_{ATP} channel-independent methods of insulin secretion. The described effects are not fully elucidated, and further investigation involving leptin signaling in β-cells is warranted.

CHAPTER 5

NANOSCALE FIBER OPTIC OXYGEN SENSOR FOR MONITORING METABOLISM OF LIVING ISLETS OF LANGERHANS

Introduction

Pancreatic islets of Langerhans are small microorgans that are composed of 2000-4000 cells, 80% of which are insulin-secreting β-cells.[5] At elevated levels of glucose, β-cells are stimulated to secrete insulin. Insulin is then carried by the bloodstream throughout the body, and it works to maintain the level of glucose flux in the liver and adipocytes.[132] Glucose-stimulated insulin secretion (GSIS) involves metabolism of the sugar to generate appropriate intracellular signaling events. While the coupling of metabolism with insulin secretion is not yet clear, the present model suggests that glucose is rapidly transported into the β-cell through glucose transporter-2, after which time glycolysis occurs. Glycolysis produces ATP and the mitochondrial substrates, NADH and pyruvate. Mitochondrial respiration then produces a large amount of ATP. The further increase in the ATP/ADP ratio activates K_{ATP} channels causing the cell to depolarize, opening L-type Ca^{2+} channels, and allowing Ca^{2+} to enter. The rise in intracellular Ca^{2+} concentration leads to the subsequent triggering of insulin secretion.[6]

Because of the link between β-cell metabolism and insulin secretion, the relationship between oxygen consumption, insulin secretion, and other biochemical events of β-cells and islets is of interest.[93] It has been reported that, in islets, intracellular Ca^{2+} concentration, membrane potential, glucose consumption, insulin secretion, and

oxygen consumption all exhibit rhythmical patterns with the same period (approximately 5.4 min).[93] Furthermore, it was reported that loss or impairment of these oscillations are an early sign of type 2 diabetes.[15-17] The precise mechanisms that result in oscillations or their impairment are not well understood. To further investigate the oscillations and the possibility that metabolic oscillations drive insulin secretion oscillations, our lab developed electrochemical sensors for measuring oxygen consumption by islets. The electrode demonstrated sufficient sensitivity to monitor changes in oxygen concentration as the electrode was moved toward and inserted into an islet using a micromanipulator (Figure 5.1A).[93] Additionally, the electrochemical sensor was used to monitor oscillations in oxygen concentration in islets; samples of intraislet oxygen traces are shown in Figure 5.1B.[93]

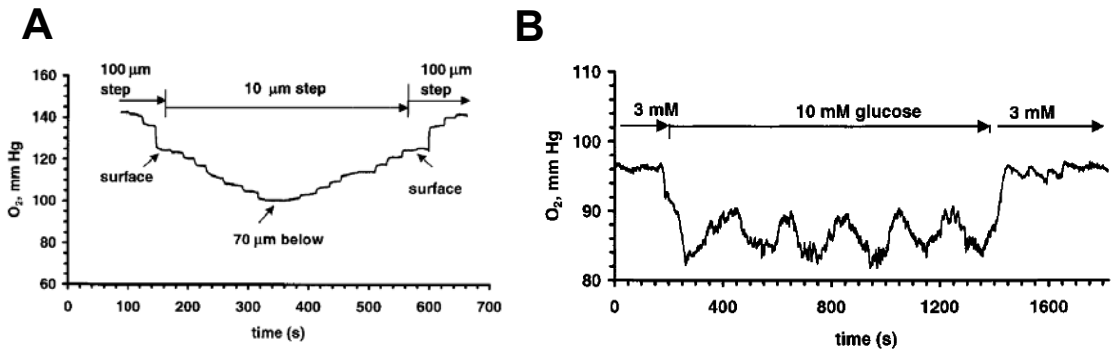

Figure 5.1. Detection of oxygen consumption by islets via electrochemical sensors. (A) Oxygen level near or in an islet incubated in 3 mM glucose. Oxygen was monitored as the electrode was moved into and out of the islet. (B) Oxygen concentration at the center of an islet as glucose was changed from 3 to 10 mM. Reproduced with permission from reference 93.

While the electrochemical oxygen sensor developed in our lab demonstrated excellent sensitivity and was used to perform high spatial resolution experiments with high temporal resolution, the sensor suffered from two significant drawbacks. First,

fabrication of the sensor was tedious and time-consuming, and production of batches of consistent oxygen electrodes required much skill. Second, our lab routinely monitors insulin secretion by islets using microfluidic electrophoresis chips. Because of the link between metabolism and insulin secretion, it is desirable to simultaneously monitor both oxygen consumption by and insulin secretion from a single islet on the electrophoresis device. The feasibility of coupling the electrochemical electrode measurements with electrophoretic-based insulin secretion measurements is not known; it may be necessary to isolate the electric field of the electrochemical oxygen measurements from the field applied to drive electroosmotic flow. A simple-to-fabricate optical sensor could alleviate both concerns associated with the electrochemical sensor. As a result, we developed a fiber optic oxygen sensor for monitoring oxygen consumption by islets.

The use of optical oxygen sensors as an alternative to electrochemical sensors has received much attention in recent years. Optical oxygen sensors may be advantageous compared to conventional electrochemical methods, since they are simple to fabricate, are not easily fouled, and minimize consumption of oxygen when sensing.[94, 133-136] Additionally, as already described, oxygen sensing at low intracellular levels via electrochemical methods introduces a chemical perturbation, which may result in inaccurate measurements. Optical oxygen sensors typically consist of an oxygen sensitive fluorophore entrapped in a film membrane or matrix. Recently reported optodes are based on the quenching of luminescence of the emitting state in the presence of oxygen. The oxygen sensitivity of the free dye depends on several factors, including quenching efficiency and triplet state lifetime. Although the sensitivity of the free dye is primarily determined by the quenching efficiency and triplet state lifetime, the sensitivity

of an optical oxygen sensor, based on the same free dye, may be highly correlated with the membrane's homogeneity and oxygen's permeability through the membrane.

Reports have demonstrated that, even when using the same indicator dye, an optode will show different sensing responses depending on the membrane characteristics, including but not limited to density, viscosity, and hydrophobicity.[137-140] Therefore, the best optical sensors capitalize on both the intrinsic properties of the indicator dye and the matrix characteristics. The selection of an appropriate oxygen sensing dye requires a dye with a high luminescence quantum yield, a long excited state lifetime, and, a high quenchability by oxygen.[141] Additionally, for cellular applications, longer wavelength excitation and emission properties are advantageous, since background light from cellular autofluorescence is thereby minimized. Several dyes have such favorable properties, but the ruthenium complex[134, 136, 142-144] Ru(II)–tris(4,7-diphenyl-1,10-phenanthroline)2+ ([Ru(dpp)3]2+) has received the most attention.[141]

In addition to the ruthenium complex, it has been documented that phosphorescent porphyrins of platinum, platinum(II) octaethylporphyrin (PtOEP) or platinum(II) octaethylporphine ketone (PtOEPK), have the desirable features of longer luminescence lifetimes (0.06–0.09 ms), convenient excitation and emission wavelengths with large Stokes shifts (100–170 nm), and reasonable luminescence quantum yields (10–50%).[145] There have been many reports on the superiority of platinum porphyrin dyes,[137, 138, 140, 145, 146] and the use of fluorescence lifetime measurements for oxygen sensing.[147, 148] However, the lifetime measurements require complex instrumentation and electronics; simple intensity ratio-based spectroscopic methods provide an attractive alternative. Several reports using oxygen-sensitive dyes demonstrate the advantages of ratiometric

measurements.[149, 150] The versatility of optical fiber sensors of submicron dimensions is well documented.[135, 151, 152]

Plasticized poly(vinyl chloride) (PVC) membranes are homogeneous and gas permeable and have successfully been used to fabricate film-type optodes.[153] By applying a membrane to the end of a fiber, one can prepare submicron-sized PVC fiber optodes.[154] Optical fiber sensors are simple to fabricate using a dip coating method that applies a homogeneous membrane film onto the distal end of the fiber. This method is easily reproduced and the fiber can be re-dipped (after solvent removal) at any time to freshly renew the film. After film renewal, sensing characteristics are retained, and further measurements are possible without re-calibrating the fiber. The lifetime of the fiber is ultimately dictated by the physical rigidity of the tip rather than the chemical properties of the sensing film, and so long as the fairly robust tip is intact, continuous measurements can be made. In addition to the ease of fabrication, the homogeneous hydrophobic PVC membrane, which is highly oxygen permeable, is an ideal matrix for dissolved oxygen sensing. The membrane exhibits minimal leaching of dye components and shows high reproducibility. Finally, the matrix allows for the fabrication of a ratiometric sensor by encapsulating both indicator and reference dye into one membrane. Ratiometric sensors have several advantages over free dye measurements, since they account for variations such as excitation power fluctuations. With tip sizes smaller than conventional microelectrodes, the relative ease of fabrication, and the minimization of chemical perturbations, PVC dipcoated optical fibers may offer a favorable sensing method.

We developed and characterized both cleaved and pulled fiber optic PVC dip-coated dissolved oxygen sensors using PtOEPK as a sensing agent and either OEP (cleaved fiber) or Bodipy 577/618 maleimide (pulled fiber) as a reference dye. The sensitivity of the pulled fiber was demonstrated to be considerably superior to that of the cleaved fiber, and thus the detailed characterization of only the pulled optode is presented in this chapter. Compared to previous optical oxygen sensors, the pulled fiber reported here demonstrated improved reversibility, increased photostability, and increased sensitivity. Also included here are preliminary data collected during an investigation of the use of the optode for monitoring oxygen consumption by islets; these data were collected using the cleaved fiber sensor.

Experimental Section

Design and Fabrication of Sensors. The fiber (Polymicro Technologies Inc., Phoenix, Arizona) was pulled with a micropipette puller (Sutter Instrument Co., Novato, California) equipped with a 25 W infrared CO_2 laser (Synrad Co., Mukilteo, WA) to a tip diameter less than 1 μm. The optode was prepared by repeated (4x) brief dipping of the pulled fibers into an optode film cocktail. The cocktail consisted of the oxygen-sensitive dye, PtOEPK, as well as an oxygen-insensitive dye, BODIPY 577/618 maleimide (Molecular Probes, Eugene, Oregon), for use as an internal standard, or reference dye. The use of a reference dye allows for ratiometric measurements, which can help compensate for changes in signal intensity due to fluctuations in light source intensity, detector sensitivity, or light scattering. Poly(vinyl chloride) (PVC) was added to the cocktail solution to create a polymer film with high oxygen permeability, high chemical

and mechanical stability, and good optical clarity. The plasticizing reagent, bis(2-ethylhexyl sebacate) (DOS), was also included in the cocktail. All cocktail components were dissolved in THF.

Characterization of Sensor. All sensor characterization was performed on the stage of an Olympus inverted fluorescence microscope, IMT-II (Lake Success, NY), equipped with fluorescence optics. A fiber coupler was used to couple the 514 nm line of an Ar^+ laser (Ion Laser Technology, Salt Lake City, UT) to one end of the fiber. The light excited the dyes in the polymer film on the tip of the other end of the fiber. The subsequent emission was collected through the objective of the microscope and passed through a 560 nm long-pass filter (Newport Corp., Irvine, CA). The fluorescence emission was then focused by two Nikon 50 mm *f*/1.8 camera lenses onto the entrance slit of an Acton 150 mm spectrograph (Acton, MA). The light was ultimately detected using a Princeton Instruments 1024x256 liquid N_2-cooled CCD array (Trenton, NJ).

Detection of Oxygen Consumption by Islets. Measurements were performed 2-3 days after islet isolation, when the islets had adhered to the surface of coverslips in the culture dishes. The coverslips with adhered islets were removed from the incubator and rinsed three times with balanced salt solution containing 118 mM NaCl, 5.4 mM KCl, 2.4 mM $CaCl_2$, 1.2 mM $MgSO_4$, 1.2 mM KH_2PO_4, and 5 mM $NaHCO_3$ at pH 7.4. The slips were then placed in the chamber atop the inverted microscope at 37 °C. Measurements were performed by positioning oxygen sensors normal to the islet surface and advancing or retrieving to or from the islet with the use of a micromanipulator. Glucose was added by spiking the solution around the islet, and all measurements were made in quiescent solutions.

Islet Isolation Protocol. Pancreatic islets were obtained from 20 to 30 g male CD-1 mice as previously described.[102] A detailed protocol for the isolation is included in Appendix A. Briefly, mice were sacrificed by cervical dislocation and collagenase type XI was injected into the pancreas through the main pancreatic duct. The pancreas was removed and incubated in 5 mL of a collagenase solution at 37 °C. A Ficoll gradient was used to separate islets from exocrine tissue. Islets that were used for experiments were 100-200 μm in diameter, had an intact islet membrane, and were oblong to spherical in shape. Islets were placed in tissue culture dishes and incubated in RPMI 1640 containing 10% fetal bovine serum, 100 U/mL of penicillin, and 100 μg/mL of streptomycin at 37 °C, 5% CO_2, pH 7.4. Islets were used 1-6 days following isolation.

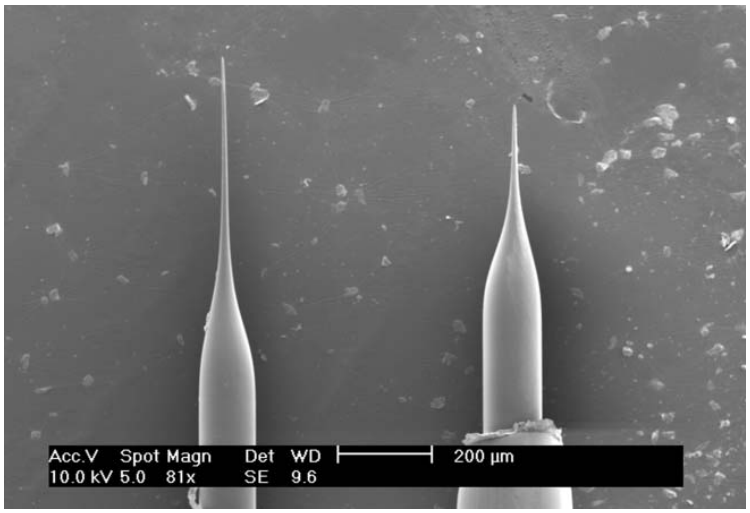

Figure 5.2. Sample SEM image of typical pulled fiber tips. The tips were pulled to submicron dimensions. Tip size and contour was varied by altering parameters such as heat and tension on the fiber puller.

Results and Discussion

Typical pulled fiber sensors, depicted in Figure 5.2, had submicron dimensions tip sizes from 100 to 500 nm. The size and contour of the fiber tip can be varied by changing parameters such as applied heat and tension on the fiber puller to create smaller

diameter sensors, perhaps important for intracellular measurements or for applications in which high spatial resolution is a concern, or to create thicker, more robust sensors.

Fiber Calibration. Figure 5.3 illustrates the fluorescence emission spectra of the fiber optode at different dissolved oxygen (DO) concentrations. As the oxygen concentration in solution increases, the fluorescence intensity of the indicator dye is quenched. The sensor's response to oxygen is expressed in terms of the peak ratio (R), i.e., fluorescence intensity of the indicator dye (F_I), divided by the fluorescence intensity of the reference dye (F_R).

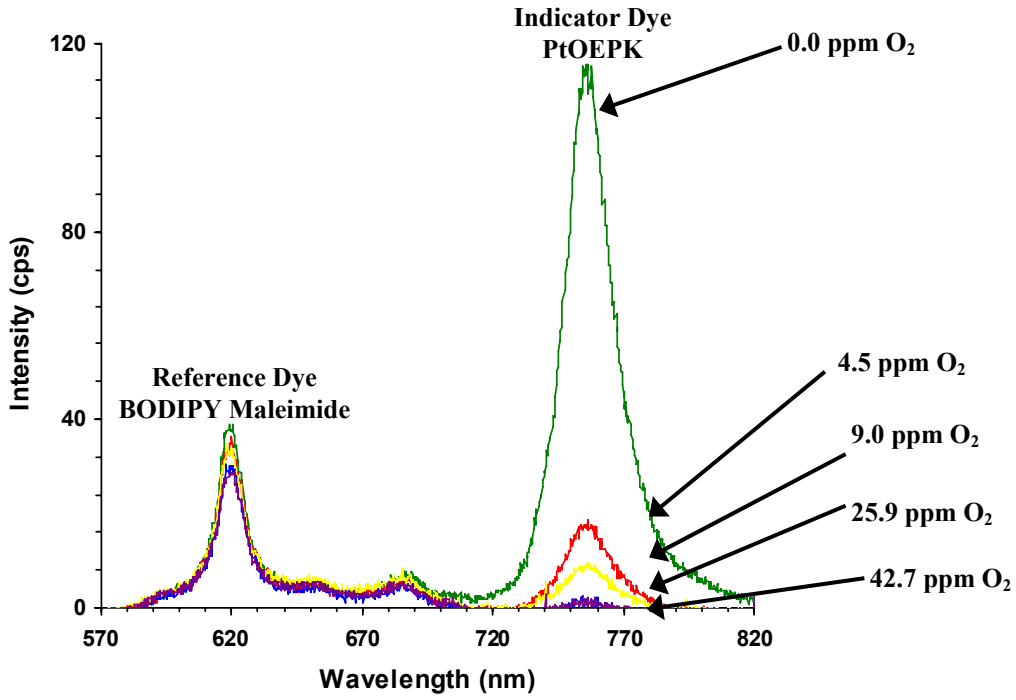

Figure 5.3. Sample spectra of the PVC based fiber optic oxygen sensor in various dissolved oxygen concentrations. The fiber was placed in a sealed sample chamber and excited with an argon ion laser source at 514 nm. The oxygen concentration (~0–42 ppm) was controlled by purging the system with a mixture of nitrogen and oxygen. The resultant luminescence is passed through a dichroic filter and collected with a CCD.

A simple measure of the sensor's sensitivity is given by the overall quenching response to DO (Q_{DO}), defined by

$$Q_{DO} = (R_{N_2} - R_{O_2})R_{N_2} \times 100 \qquad \text{Eq. 1}$$

where R_{N_2} and R_{O_2} are the fluorescence intensity ratio in fully deoxygenated water and in fully oxygenated water, respectively.

The quenching response of the polymer-based oxygen sensors depend upon the indicator dye as well as the polymer matrix. The measured value of Q_{DO} of the fiber sensor was 98%, for the pulled fiber, which is among the highest reported to date (Table 5.1).

Table 5.1. Comparison of the quenching response of various optical oxygen sensors based on silica, ormosil, and PVC matrixes.

Probe	Sensor type	Q_{DO}	Reference
$[(Ru(dpp)_3]^{2+}$	Silica film	30%	155
$[(Ru(dpp)_3]^{2+}$	Ormosil film	56-80%	134
$[(Ru(dpp)_3]^{2+}$	Silica nanoparticle	80%	136
PtOEP	Ormosil nanoparticle	97%	133
PtOEPK	Ormosil nanoparticle	97%	133
PtOEPK	Cleaved PVC fiber	93%	Current work
PtOEPK	Pulled PVC fiber	98%	Current work

Since this oxygen quenching process occurs in a liquid polymer, i.e. homogeneous system, the peak ratio values are used in a linear calibration plot described by the linear Stern-Volmer equation:

$$I_o / I = K_{SV}^{conc}[O_2] = K_{SV}^{gas}\, pO_2 \qquad \text{Eq. 2}$$

where K_{SV}^{conc} and K_{SV}^{gas} are, respectively, the Stern-Volmer constants expressed in terms of solution oxygen concentration and gas phase partial pressure.

Although the Stern-Volmer plot should theoretically be linear for homogeneous solutions, there are usually reports of non-linear Stern-Volmer plots once a dye has been embedded in a polymer sensing film.[139, 140] The deviation from the expected linearity can be attributed to matrix heterogeneity effects, such as oxygen permeability and/or microheterogeneity of the local environment of the dye molecules in the sensing layer. A linear response in the Stern-Volmer plot is desirable.

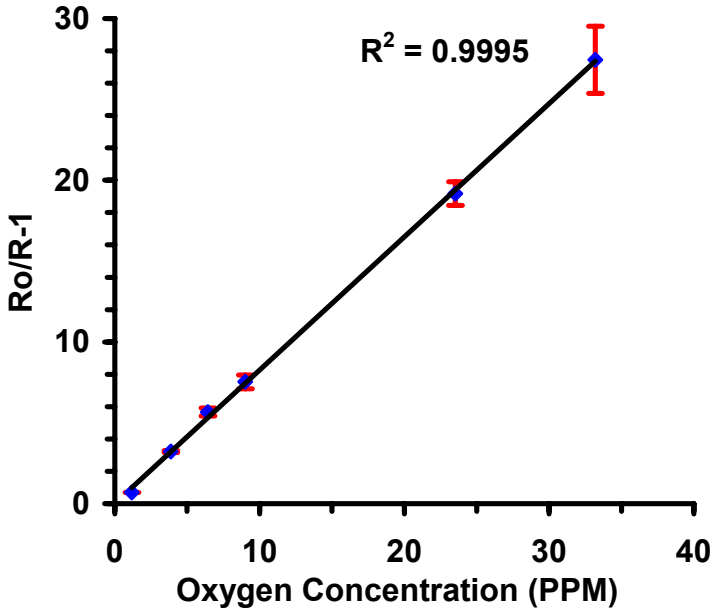

Figure 5.4. Stern-Volmer plot calibration curve response of PtOEPK fiber sensor. Stern–Volmer plot calibration curve response a pulled PtOEPK fiber sensor. The oxygen concentration in a sealed chamber was controlled by purging the system with a mixture of oxygen and nitrogen.

Figure 5.4 shows the Stern-Volmer plot of the fluorescence intensity ratio versus dissolved oxygen concentration for the ratiometric PtOEPK fiber sensor. The pulled sensor has a nearly linear Stern-Volmer plot over the whole range of oxygen concentrations (0% oxygen to 100% oxygen saturated), indicating negligible matrix heterogeneity effects. Previously, the only such reports of complete linearity throughout this region have been from "naked" molecular probes (i.e., dye solutions) or from the recently reported OEP/PtOEPK PEBBLE sensors,[25] likely a result of the increased oxygen permeability. The slope in the Stern-Volmer plot is an indicator of the sensitivity of the sensor. The pulled fiber sensor exhibits over a 2-fold increase in sensitivity at high oxygen concentrations (Table 5.2). This may be a result of a decrease in the thickness of the sensing film, thus reducing the typical distance of oxygen diffusion required to occur prior to analyte binding.

Table 5.2. Comparison of the sensitivity of ormosil PEBBLEs and PVC fiber oxygen sensor. The slope of the Stern-Volmer plot is representative of the sensitivity of a sensor.

Sensor type	Slope
Ormosil PEBBLE	0.78
Unpulled PVC fiber	1.07
Pulled PVC fiber	1.84

Fiber reversibility. The fiber sensor exhibits excellent reversibility over the course of several hours. A fiber was placed in distilled water which was alternatively purged with nitrogen and air. The indicator peak intensity increased and decreased accordingly, returning to the same initial values with only a slight deviation; the reference peak intensity remained constant throughout the experiment (Figure 5.5). Upon inspection of the reversibility plot, it appears that the response time of the fiber is on the

order of 10 minutes; however, the slow increase in indicator peak intensity is actually an artifact of the length of time required to saturate the solution with nitrogen. In order to achieve a nitrogen-saturated water solution, the sample solution must be purged for approximately 10-15 minutes. Therefore the time required for equilibration is limited by the time required to saturate the solution with nitrogen, rather than the response of the sensor. It may be possible to reduce this equilibration time by substituting nitrogen with argon, which is denser, by weight, and more soluble, or by performing measurements in a flow injection apparatus. Additionally, the true response time could be obtained by placing the sensor in two different solutions, each of which is already saturated with the appropriate gases.

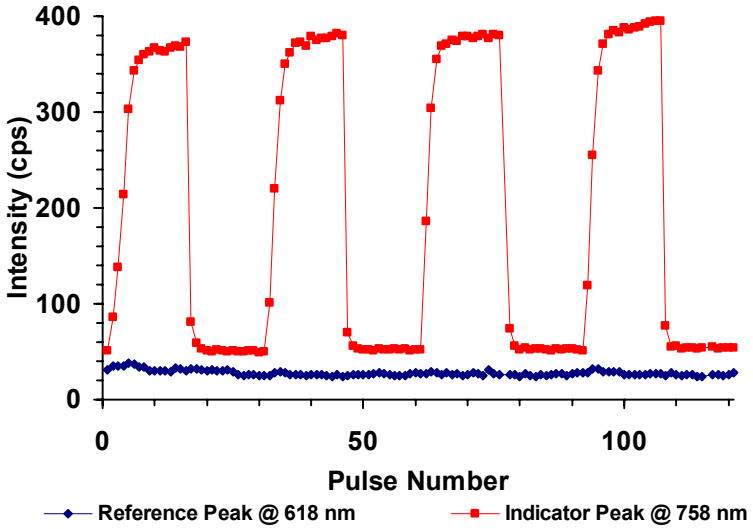

Figure 5.5. Reversibility of PVC oxygen fiber sensor. The fiber is immersed in water and purged alternatively with nitrogen and oxygen. The indicator peak intensity changes according to dissolved oxygen concentration, while the reference peak intensity remains constant. The resultant increase and decrease in peak ratio demonstrates the reversibility of the fiber over 4 hours.

Optode Leaching. Leaching of sensing components is a critical factor in sensor fabrication, and the pulled fiber sensor was tested for leaching of component dyes. The

fiber tip was immersed in solution and the fluorescence was monitored. Because fluorescence is collected solely from the tip of the fiber, if the dye leached from the membrane, a decrease in fluorescence would be observed. Because numerous pulses of the laser to the fiber for many hours may result in photobleaching, the laser was pulsed every 20 min. The pulled fiber exhibited no significant leaching throughout the 9 hour time period in which the leaching experiment was performed (Figure 5.6), as the individual fluorescence intensities of the indicator and reference dye did not change. The leaching experiment was repeated two times, and each time the sensor demonstrated negligible leaching. More importantly, the peak ratio value showed very little fluctuation for the duration of the experiment. Over the 9 hour period the greatest standard deviation of the peak ratio was approximately 4% of the initial value. The small change in peak ratio is negligible compared to fluctuations resulting from the expected changes in dissolved oxygen concentration.

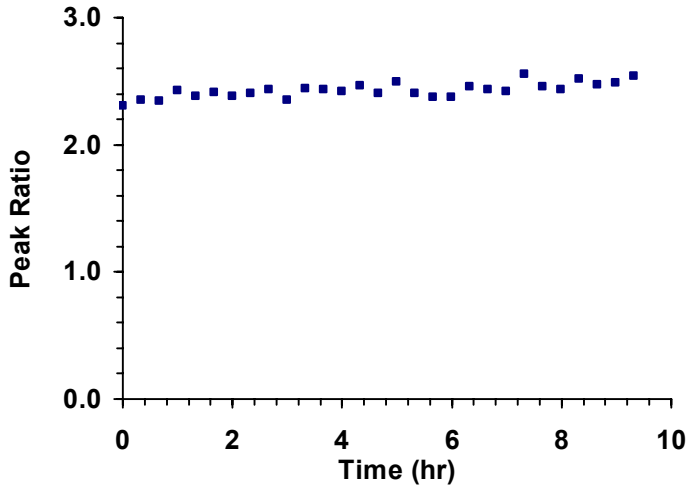

Figure 5.6. Leaching test of the PtOEPK/BODIPY maleimide oxygen fiber sensor. There was little change (±3.6 %) in peak ratio over 9 hours, indicating that only a minimal amount of dye leached from the fiber film.

Photostability. The photostability of a sensor can be the ultimate limiting factor of optical sensing methods.[156] To determine the extent of dye photobleaching, the fiber tip was immersed in solution and the fluorescence was monitored. The pulled fiber could be excited with excitation powers in the range of 5 μW – 40 μW without extensive photobleaching after 1000 pulses of 200 ms each (Figure 5.7).

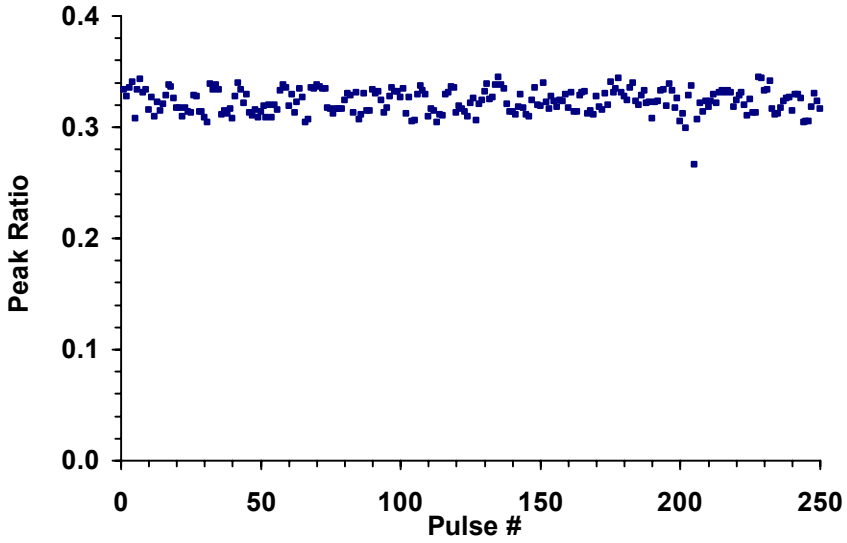

Figure 5.7. Photobleaching test of the PtOEPK/BODIPY maleimide oxygen fiber sensor. There was little change (±0.3 %) in peak ratio over 2 hours, indicating that the fluorescent dyes are photostable.

Oxygen Consumption by Single Islets. The characterization experiments discussed above suggested that the oxygen sensors possess the properties necessary to monitor oxygen consumption by islets. To demonstrate the utility of this sensor, a series of simple experiments were performed at single islets. The initial experiments were designed to characterize the oxygen gradient around single mouse islets. Figure 5.8 illustrates a dissolved oxygen concentration trace for a typical experiment in which the sensor was moved from a position 100 μm from the islet to 0 μm from the islet while the islet was incubated in a quiescent solution with 3 mM glucose. The decrease in the

dissolved oxygen level in Figure 5.8 reflects the oxygen consumption by the islet at 3 mM glucose.

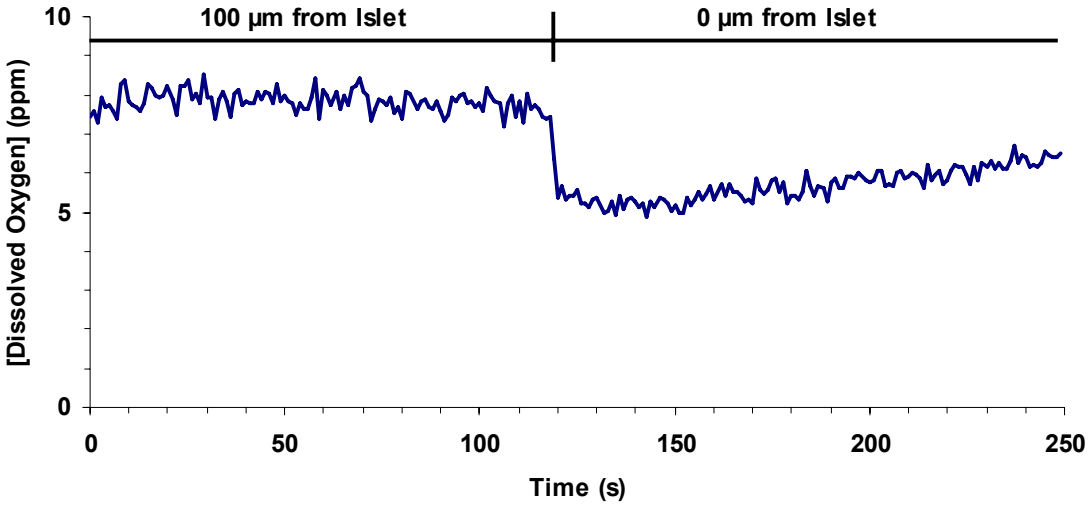

Figure 5.8. Recording of dissolved oxygen concentration at and near an islet. The decrease in dissolved oxygen at the islet reflects oxygen consumption by the islet. These data were obtained with a cleaved fiber sensor; it is expected sensitivity would be enhanced 4X with a pulled fiber sensor.

The dynamic changes in oxygen level as a function of changing conditions or stimulations are of interest, so the sensor was used to measure oxygen consumption by a single islet at basal and stimulatory glucose concentrations. Figure 5.9 demonstrates the expected change in oxygen level that occurs at islets after stimulation with 20 mM glucose. The oxygen level decreased as the glucose level was increased since increasing glucose caused an increase in metabolism and oxygen consumption.

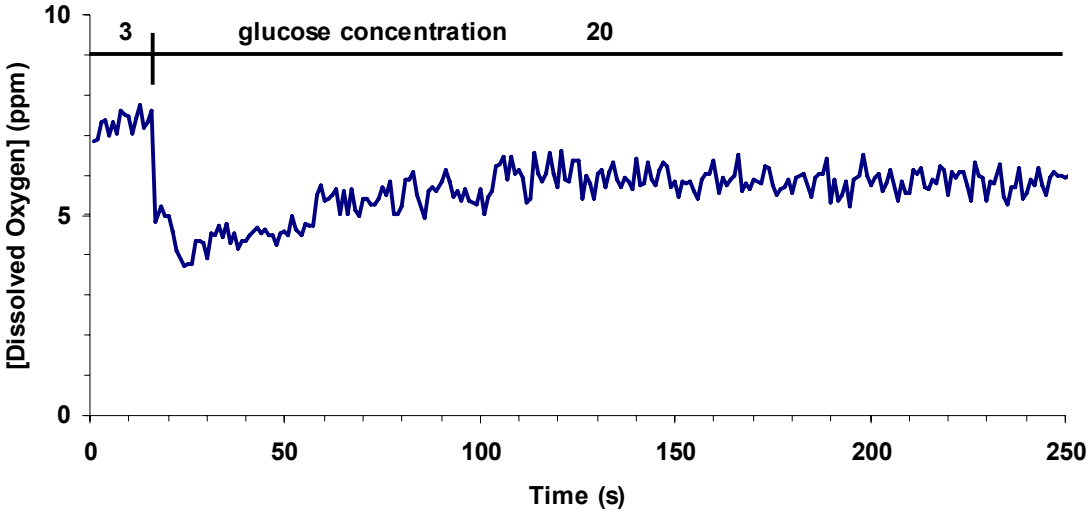

Figure 5.9. Oxygen measurement at surface of islet upon glucose stimulation. Decrease in dissolved oxygen concentration indicates an increase in O_2 consumption by the islet after stimulation with 20 mM glucose. These data were obtained with a cleaved fiber sensor; it is expected sensitivity would be enhanced 4X with a pulled fiber sensor.

Conclusions

The developed dissolved oxygen fiber optic sensor is ratiometric, demonstrates linear behavior, and is sufficiently sensitive for monitoring oxygen concentrations at living cells. The combination of the permeable polymer, the PVC, and the hydrophobic nature of the membrane result in an excellent overall quenching response to dissolved oxygen, as well as a linear response over the entire range of roughly 0 to 100% oxygen-saturated water. The fiber optic sensor has excellent reversibility and photostability and is resistant to leaching over 10 h. The characterized fiber sensor also provides the spatial resolution necessary for simultaneous measurements of multiple analytes in submicron domains and is expected provide an adequate platform for measurements in biological samples. The sensor offers significant promise for measurement of real-time oxygen

consumption by islets. Further work is necessary to demonstrate the practical capabilities and limitations for islet measurements.

CHAPTER 6

SUMMARY AND FUTURE DIRECTIONS

Summary

The overall objective of this work was to develop, use, and refine analytical instrumentation and methods to monitor chemical events at islets of Langerhans. Novel analytical tools and techniques were developed and applied to study insulin secretion and Ca^{2+} flux in living islets of Langerhans. Although this work was directed at studying islets, the developed analytical technology can be used to study other biological cells or systems.

Long-term Microfluidic Electrophoresis Device. The first tool developed was a microfluidic device for long-term electrophoresis operation. In the device, buffers were continuously perfused in the chip via a pressure-driven perfusion system to allow sampling of fresh buffers and reagents from reservoirs on the chip. A vacuum system was used to remove excess fluid from the reservoirs to maintain a volume of approximately 100 μL. Electroosmotic flow was employed to continuously sample buffers, and portions of this sample were serially injected and electrophoretically separated. A voltage-gated relay rated for 1 billion cycles was used to perform repeated injections. To demonstrate the electrophoretic stability of the device, injections and separations of Rhodamine 110 were performed over a period of 24 hours. Over 14,400 electropherograms were collected; a 4 % RSD of the Rhodamine 110 peak height was

calculated from the electropherograms. Change in migration time of the peak was negligible as less than 1 % RSD in the Rhodamine 110 peak migration time was observed.

The microfluidic electrophoresis chip was applied to monitoring insulin secretion from pancreatic islets for 24 h. The device enabled the observation of never-before-seen long-term insulin secretion dynamics from several individual islets. The data suggest that single islets may exhibit ultradian insulin secretion oscillations (2 to 4 h) and that the ultradian oscillations may be due to increased amplitude of more rapid secretory oscillations (4 to 6 minutes).

Investigation of Membrane-Disrupting Effects of Islet Amyloid Polypeptide. A microfluidic chip for housing and perfusion of islets was developed to perform intracellular Ca^{2+} measurements. Results from fluorescence imaging experiments demonstrated the feasibility of maintaining precise control of the islet environment. The small volume of the microenvironment around the islet enabled rapid changes in concentrations of glucose, peptides, or other stimulants to be applied to the islet. The Ca^{2+} monitoring chip was used to investigate the membrane disrupting effects of islet amyloid polypeptide, a 37-residue peptide secreted with insulin by β-cells. The aggregation of the peptide into either amyloid fibers or small soluble oligomers has been implicated in the death of β-cells by disrupting the cellular membrane. Unlike the human version of the peptide, the rat version is nonamyloidogenic and nontoxic. The rat and human versions differ by only one peptide, Arg18 in the rat version and His18 in the human version. In collaboration with the Ramamoorthy lab, a series of experiments were performed to probe the toxicity and membrane-disrupting effects of the peptide. An influx of Ca^{2+} to islets is indicative of membrane disruption, so the Ca^{2+} imaging chip

served as a tool to monitor the membrane disrupting effects of various forms of the peptides. The Ca^{2+} imaging results, corroborated by results from experiments performed on model membranes, identify an important role of the 18^{th} residue of the peptide for the demonstrated membrane-disrupting effects.

Investigation of Leptin-Signaling in Islets. The intracellular Ca^{2+} chip was also used in a collaborative effort to probe leptin signaling in islets. The presence of leptin receptors on β-cells suggests a role of leptin and leptin signaling on insulin secretion. By monitoring a number of parameters, including islet cell mass, insulin secretion, and intracellular Ca^{2+} concentration, islets from pancreas-specific leptin receptor knock-out mice were compared with control islets. Unexpectedly, challenging the KO mice with a high-fat diet resulted in glucose-stimulated insulin secretion, suggesting that leptin signaling helps to accommodate for the potentially harmful effects of a HFD. The effects of leptin, palmitic acid, and glibenclamide on intracellular Ca^{2+} concentration and insulin release were explored. The results from the investigation demonstrate the inhibitory effect of leptin on Ca^{2+} flux into islets and on glucose-stimulated insulin secretion and suggest a role of leptin-signaling on islet behavior. GSIS from KO islets chronically exposed to palmitate was more affected than GSIS from control islets exposed to palmitate. The GSIS corroborated evidence from *in vivo* experiments that suggested a role of leptin signaling in regulating fatty acid metabolism. However, differences in the Ca^{2+} flux after chronic exposure to fatty acids were very similar for both islet types. The evidence indicates that the suggested role of leptin in regulating fatty acid metabolism is not due to increased permeability of Ca^{2+} into β-cells.

Fiber Optic Oxygen Sensor. Insulin secretion from β-cells is primarily driven by metabolism, and oscillations in oxygen consumption by islets have been observed to correlate with insulin release levels. Studies have shown oscillations of oxygen consumption by islets using conventional electrochemical methods, but optical oxygen sensors may provide a useful alternative to electrochemical measurements for use with islets. Optical sensors are simple to fabricate, do not consume oxygen, and may be easily coupled with electrophoresis or other microfluidic measurements. We designed a fiber optic oxygen sensor with the end purpose of exploring how β-cell metabolism and glucose-stimulated insulin secretion are linked. The submicron-tipped sensor demonstrated good reversibility, good stability, and high sensitivity compared with previously-reported optical oxygen sensors. Such characteristics, along with the potential for high special resolution using pulled fiber sensors, make the sensor a potentially good candidate for measuring oxygen consumption by islets, but further work is necessary to determine whether the optode is sufficiently sensitive to monitor oscillations in oxygen consumption.

Future Directions

Improvement of Perfusion and Insulin Secretion Sampling from Islets on Long-term Electrophoresis Device. The insulin secretion results collected on the long-term electrophoresis chip presented in Chapter 2 of this dissertation demonstrate the capabilities of the chip for monitoring insulin secretion. The perfusion and sampling system is based on designs on designs previously used in our lab.[52, 98] However, later evaluation of the perfusion system demonstrated that some nonuniformity in

concentration of the perfused solution existed while the islet was present in the chamber.[99] The evidence indicated that there may be variations in the concentration of stimulant around the islet, resulting in inaccurate insulin secretion analyses. As a result, our lab developed an improved perfusion and sampling method in which the possibility of uneven islet stimulation and biased insulin sampling was eliminated.[99] In the redesigned system, the islet is sealed in the chamber with a polydimethylsiloxane (PDMS) plug, and all perfusate from the islet was driven using hydrodynamic flow toward the mixing cross on the chip. Because the flow from the islet chamber was too fast for proper mixing with immunoreagents, the majority of the flow was directed elsewhere using an on-chip flow-split. A side view of the modified perfusion and sampling design is shown in Figure 6.1B and an enlarged image of the flow-split channel design is shown in Figure 6.1C. Implementation of the modified perfusion and sampling design onto the long-term electrophoresis chip would provide increased accuracy in insulin secretion studies.

Although the islets studied in Chapter 2 of this work exhibited insulin secretion dynamics for over 24 h, the islets were perfused only with glucose and a pH-adjusted balanced salt solution. To further explore the longer-term phenomena of insulin secretion, it is more appropriate to perfuse the islets with actual culture media, such as RPMI 1640. RPMI 1640 contains several nutrients in addition to glucose, including amino acids and other vitamins necessary for maintain health of cultured islets. Perfusion with nutrient-rich media is particularly necessary for explorations of effects of various culture conditions. Our lab previously performed short-term perfusion experiments using RPMI.[52] Because the physiological media buffering systems is based on bicarbonate and

intended to be used in a 5% CO_2 atmosphere, the RPMI was supplemented with HEPES adjusted to pH 7.4. It is not clear whether the addition of HEPES is sufficient to maintain pH for longer-term measurements, and it may be necessary to maintain a 5% CO_2 environment around the islets if RPMI 1640 is selected as a perfusion medium.

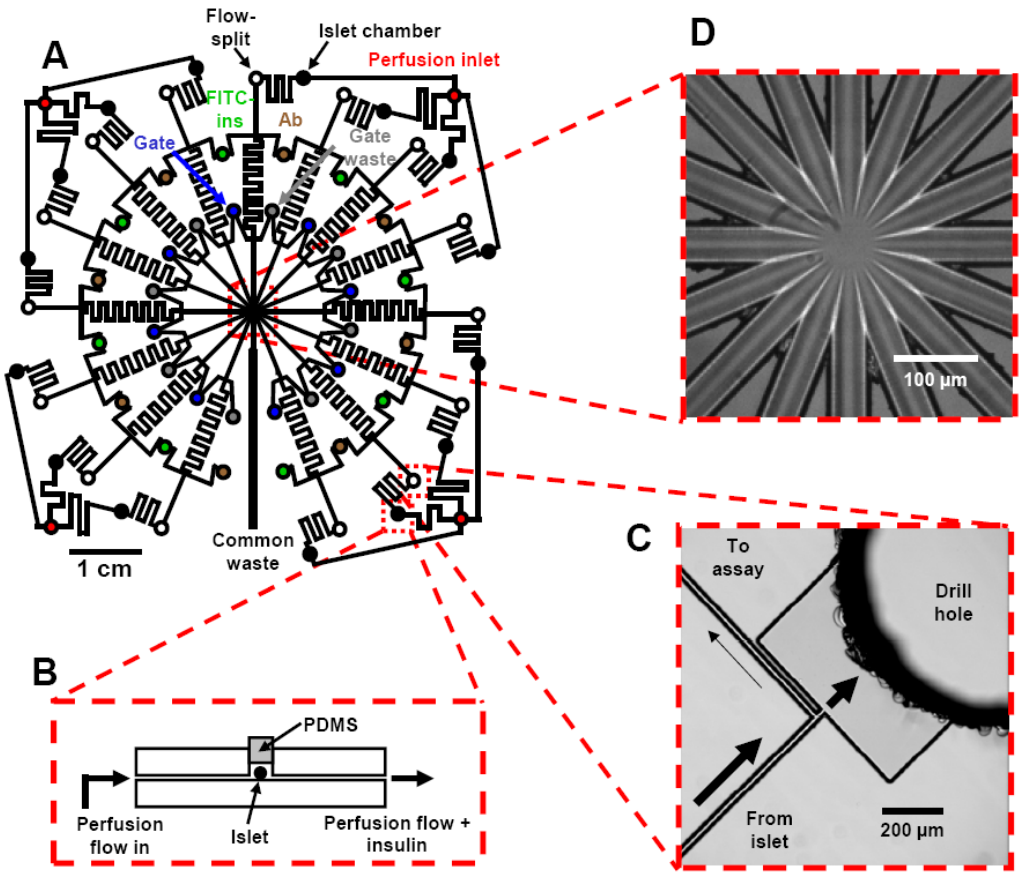

Figure 6.1. Microfluidic device for parallel analysis of 15 individual islets. (A) Microfluidic channel design for performing 15 simultaneous insulin immunoassays. Channels are indicated by black lines and circles represent fluidic reservoirs or connections. (B) Sideview of the modified perfusion and sampling design. Islets are loaded into the chamber, which is then sealed with a PDMS plug. (C) Brightfield image of the flow-split channel design. Due to the high fluidic resistances in the channel leading to the assay, the bulk of the perfusate is directed through the widened channel toward the drilled access hole. (D) Enlarged brightfield image of the detection zone. The 15 electrophoresis channels converge at a single point, and flow from the electrophoresis channels ultimately flows out through a single waste channel, which is shown in the bottom center of the image. Reproduced with permission from reference 99.

The bulk of the insulin secretion studies completed in our lab are performed by increasing glucose from a low, non-stimulatory concentration (~3 mM) to a higher,

stimulatory glucose concentration (> 10 mM). The step-wise format of the glucose changes is not likely to mimic *in vivo* conditions, in which plasma glucose will increase in response to a meal and decrease during fasting. While the step-wise changes may be sufficient for short-term studies, it may be of interest to investigate a more physiologically relevant glucose pattern in long-term insulin studies. A programmable syringe pump or high performance liquid chromatography pump could be used to more gradually apply changes in glucose concentration to an islet. Additionally, the pump could be used to increase and decrease the glucose concentration in a pattern to mimic meal-induced plasma glucose changes *in vivo*.

Microfluidic Device for Long-term Insulin Secretion Studies in Parallel. In addition to improving islet perfusion and insulin secretion sampling on the long-term electrophoresis chip, it would be advantageous to increase the throughput of the chip. Our lab previously developed a microfluidic electrophoresis device for high-throughput, automated, online monitoring of insulin secretion from single islets in parallel.[99] The parallel chip design is illustrated in Figure 6.1A, is based on the radial geometry in the center of the chip, as depicted in the enlarged brightfield image in Figure 6.1D.[99] Higher throughput analyses made possible by parallel measurements results in reduced time and cost of the measurements. Furthermore, parallel measurements are isolated islets are advantageous by enabling insulin studies of several islets at precisely the same time after isolation. The parallel insulin immunoassay chip allowed for the simultaneous analysis of 15 individual islets with 10 s temporal resolution, correlating to the completion of 5,400 assays in one hour, but was capable of operation no longer than 1 to 2 h. The long-term microfluidic device presented in Chapter 2 of this dissertation demonstrated insulin

secretion dynamics with high temporal resolution (6 s) for 24 h. The electrophoresis chip enabled the completion of 14,400 insulin immunoassays in 24 h. A modified long-term chip capable of 15 channel parallel analysis could enable the completion of 129,600 assays in one hour. This device would incorporate the ideas that make long-term chip operation modifications onto the parallel microchip design. On the short-term parallel chip, one fluidic inlet is used to perfuse 3 to 4 islets. Likewise, on the long-term parallel microchip, all buffers and reagents will be continuously introduced to the chip via pressure driven flow through one fluidic inlet per 3 to 4 channels on the chip. The addition of reservoirs and fluidic connections necessary to implement the long-term modifications will require expansion of the parallel chip design. Otherwise, spatial constraints would prevent the placement of appropriate reservoirs and fluidic connections above the drilled fluidic access holes. The long-term parallel chip design will drastically increase throughput on studies of the long-term insulin secretion dynamics described in Chapter 1.

Microfluidic System for Co-culture of Adipocytes and Islets. Obesity has long been associated with type 2 diabetes, but scientists have struggled to directly define the link the two epidemics.[157] In obese individuals, a chronic imbalance between fat consumption and utilization increases the mass of adipose tissue through an increase in the number or size of adipocytes.[158] Adipose tissue is widely distributed throughout the body but occurs most prominently under the skin, in the abdominal cavity, and in skeletal muscle.[159] In time of metabolic need, adipocytes hydrolyze triacylglycerols to fatty acids and glycerol through the action of hormone-sensitive lipase.[160] In obese individuals, blood fatty acid levels tend to be elevated. Short-term treatment of β-cells with fatty

acids stimulates insulin secretion, while chronic exposure results in impaired insulin secretion.[161] This observation provides an important potential link between obesity and impaired insulin secretion in type 2 diabetes. Adipocytes also secrete cytokines, such as leptin, the absence of which leads to obesity and insulin resistance, and adiponectin, which enhances insulin secretion in some cases, that influence β-cell function.[159] Consequently, it is essential to understand the endocrine and metabolic interactions between islets and adipocytes.

Nearly all *in vitro* studies on insulin secretion and other islet parameters are performed on isolated islets; however, *in vivo* islets and β-cells are in chemical communication with many other cell types, such as adipocytes, whose interactions can have a significant effect on islet function. Although it has been well documented that secretion from adipocytes may affect insulin secretion from islets[159], no studies have simultaneously investigated both fast and slow dynamics of the interactions. Microfluidics offers the opportunity to improve the study of islet-adipocyte communication by allowing precise control of how the interactions between the adipocytes and islets take place, enabling islets and adipocytes to be separated for subsequent proteomic or metabolomic analysis, and permitting the two cell types to be directly monitored while in co-culture. More specifically, a multi-cell co-culture system would readily allow the study of how adipocytes alter events in islets, including insulin secretory dynamics and GSIS.

Our lab has developed a microfluidic chip platform for culture and analysis of adipocytes via enzyme assay-based analysis of their secretions.[162] The platform was composed of two separate microfluidic chips. The first microfluidic chip (Figure 6.2),

which was designed for culturing and perfusing the adipocytes, was reversibly sealed to facilitate reloading of cells and reuse of the chip. Computational modeling demonstrated the adipocytes were not exposed to high sheer during perfusion. Flow from the first chip was then directed to a separate chip on which an enzyme assay was performed to detect glycerol secretion from the adipocytes.

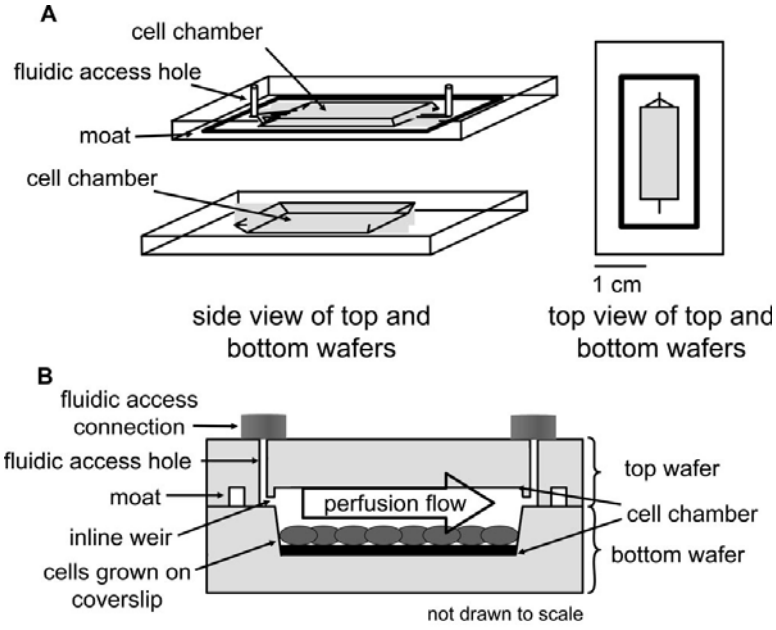

Figure 6.2. Microfluidic device for adipocytes culture and perfusion. (A) Adipocyte perfusion chamber. Adipocytes were cultured between two glass wafers which were reversibly sealed. The figure on the right depicts the top-view of the culture chip. (B) Side-view of the adipocyte perfusion chip. The adipocyte chamber housed 50,000 cells, which were held in place with a weir design. Media and/or stimulants flowed over the cells, and resulting secretions were directed out of the chip through a fluidic access connection. Reproduced with permission from reference 162.

A multi-cell communication platform can be developed by linking the adipocyte culture chip and the long-term electrophoresis chip for insulin secretion studies (described in Chapter 2). In the co-culture system, illustrated in Figure 6.3, adipocytes will be cultured between two glass wafers as already described. Perfusate from the adipocytes will be directed onto the long-term insulin assay chip through a capillary and a

fluidic access connection, and the perfusate will ultimately flow over a single islet in the long-term device.

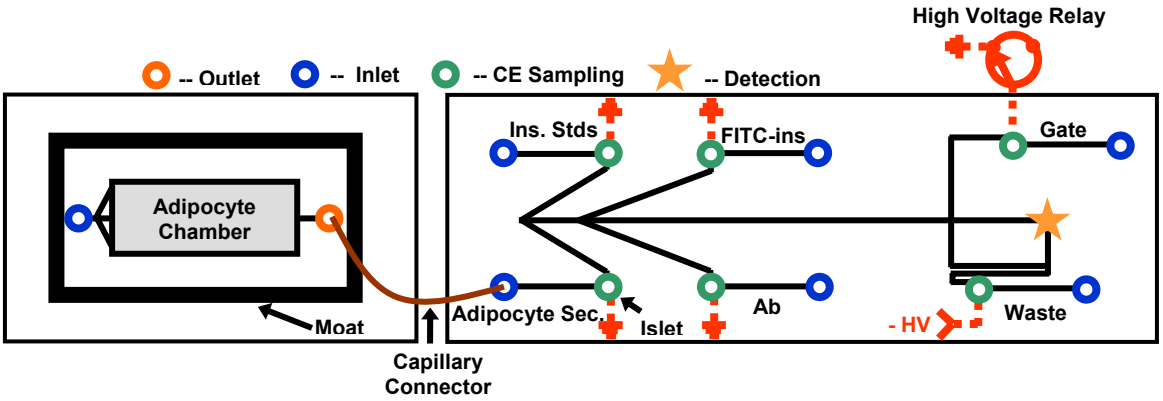

Figure 6.3. Microfluidic platform for investigating adipocyte-modified insulin secretion. Adipocytes will be cultured and continuously perfused in the adipocyte culture chip. Adipocyte perfusate will be directed onto the long-term insulin immunoassay chip through a fluid access connection and will ultimately flow over the islet. Resulting insulin secretion dynamics will be observed with 6 s temporal resolution via the insulin immunoassay.

The microfluidic co-culture system will be used to monitor short- and long-term insulin secretion from islets exposed to adipocyte secretions. To monitor short term effects, the adipocytes will be cultured on the chip, after which time an islet would be added for acute exposure to fatty acids. To explore the effects of chronic exposure of islets to adipocyte secretions, the flow from the adipocytes will be perfused over the islet for 48 h; afterward GSIS may be examined. It will be necessary to optimize the concentration of adipocyte secretions and glucose flowing over the islet to best mimic *in vivo* conditions. A flow-spit can be added to adipocyte perfusate to allow for appropriate perfusion flow rate over the islet and to enable fraction collection; the fractions could be analyzed off-line to determine the concentration of free fatty acids, glycerol, and other adipocytokines such as leptin. The microfluidic system will allow, for the first time, the

monitoring and control of dynamics between adipocytes and islets in a variety of different conditions.

APPENDIX A

ISOLATION AND CULTURE OF PANCREATIC ISLETS OF LANGERHANS

Islet Isolation. Pancreatic islets analyzed in Chapters 3, 5, and 6 were isolated from 20 – 40 g CD-1 mice obtained from Charles River. Islets analyzed in Chapter 4 were from obtained from Brandeis University (Waltham, MA, USA). Prior to islet isolation, several items were autoclaved to achieve sterilization. Autoclaved materials included 6 Pasteur pipettes, 2 500 mL bottles, 1 100 mL bottle, and 2 siliconized scintillation vials. The scintillations vials were siliconized with Sigmacote (Sigma-Aldrich).

Further preparation entailed making several solutions. First 1 L of concentrated (10X) Hanks Balanced Salt Solution (HBSS) was prepared; HBSS consisted of 1.360 M NaCl, 54 mM KCl, 4.1 mM NaH_2PO_4, and 100 mM HEPES, and the pH of the solution was adjusted to 7.4 via NaOH. Next, stock solutions of 100 mM glucose, 1 M $CaCl_2$, 1 M $MgCl_2$, 20 % Halothane (diluted in mineral oil) and 70 % EtOH were prepared. Immediately prior to isolation, additional solutions were prepared. 1 L of Mg-HBSS was prepared by mixing 100 mL of 10X HBSS, 50 mL of 100 mM glucose, and 1 mL of 1 M $MgCl_2$, diluting to 1 L and adjusting pH to 7.4 using NaOH. 100 mL of the MG-HBSS was removed, filtered into a sterile 100 mL bottle using a 0.22 μm filter (Nalgene), and stored on ice. A Ca-HBSS solution was prepared by adding 1.34 mL of 1 M $CaCl_2$ to the remaining 900 mL of Mg-HBSS. The Ca-HBSS mixture was filtered using the same 0.22

μm filter into 2 500 mL bottles and stored on ice. Next, a collagenase solution was prepared in a 50 mL sterile centrifuge tube by adding 10.5 mg of collagenase (Sigma-Aldrich) (per mouse); immediately before dissection, 15 mL Mg-HBSS (per mouse) were added to the collagenase. Finally, RPMI 1640 physiological media were prepared by mixing 500 mL of RPMI 1640 (Invitrogen), 50 mL fetal bovine serum (FBS) (Invitrogen), and 5.5 mL penicillin-streptomycin (Invitrogen). The mixture was filtered through a 0.22 μm filter into sterilized bottles and stored at 4 ˚C. Preparation was completed by placing the dissection materials atop the lab bench as shown in Figure A.1.

Figure A.1. Lab bench preparation for isolation of islets.

Following preparation, a transfer pipette was used to deliver approximately 1 mL of 20 % halothane to a dessicator. One mouse was placed in the dessicator until unconscious. Afterward, the mouse was sacrificed using cervical dislocation (as demonstrated in Figure A.2) and placed in 70 % EtOH.

Figure A.2. Sacrifice of mouse by cervical dislocation. Anesthetized mouse was removed from the dessicator. Pressure was applied behind the neck of the mouse while the tailed was pulled.

After removing the mouse from the EtOH, pronged forceps were used to grasp abdominal skin, and an incision was made in the lower abdomen with 5.5" dissection scissors, as shown in Figure A.3A. Care should be taken to remove all abdominal skin, as demonstrated in Figure A.3B.

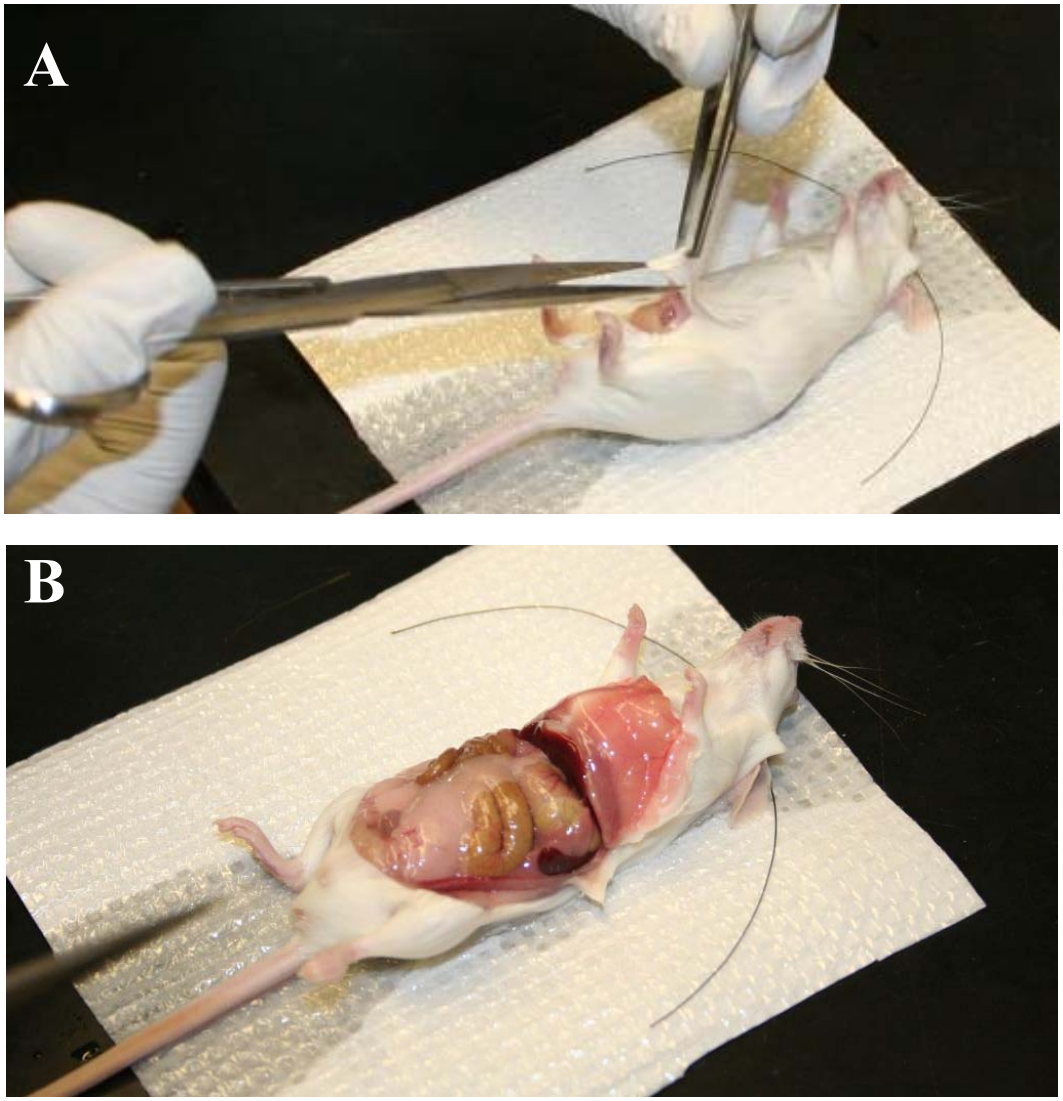

Figure A.3. Incision of abdominal cavity. (A) Initial incision was made by using pronged forceps to grasp skin. (B) After initial incision, skin was carefully cut toward outside of abdominal cavity to open cavity as wide as possible.

Following incision, the internal organs were placed to one side of the mouse with sterile cotton swabs. The common bile duct, which is illustrated along with other critical anatomy for islet isolation in Figure A.4, was tied off with suture and fine point forceps. Tying of the suture is demonstrated in Figure A.5.

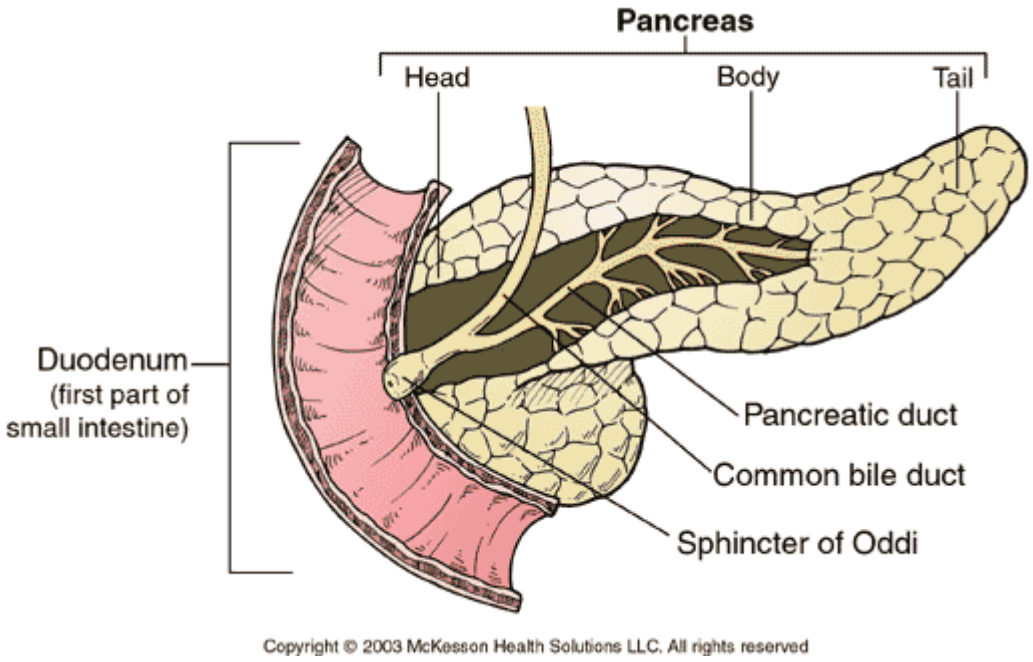

Figure A.4. Illustration of anatomy pertinent to islet isolation. Suture was used to prevent flow through the common bile duct, and injections were made into the pancreas via the spinchter of Oddi, which is on the duodenum. Reproduced with permission from reference [163].

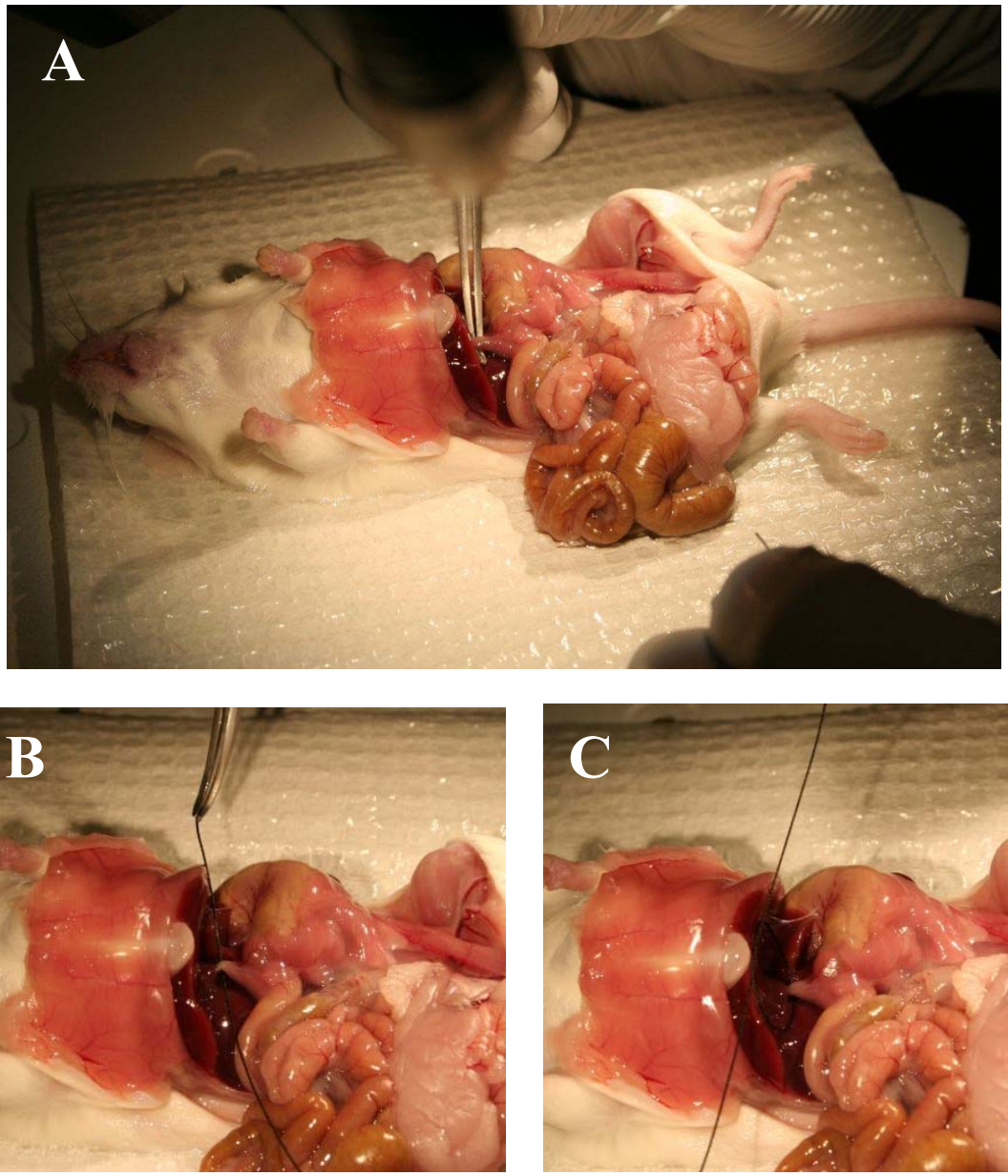

Figure A.5. Tying of the common bile duct with suture. (A) Curved, fine-point forceps were used to lift common bile duct. (B) The suture was gently threaded beneath the common bile duct. (C) Forceps and fingers were used to tie the suture in a single knot.

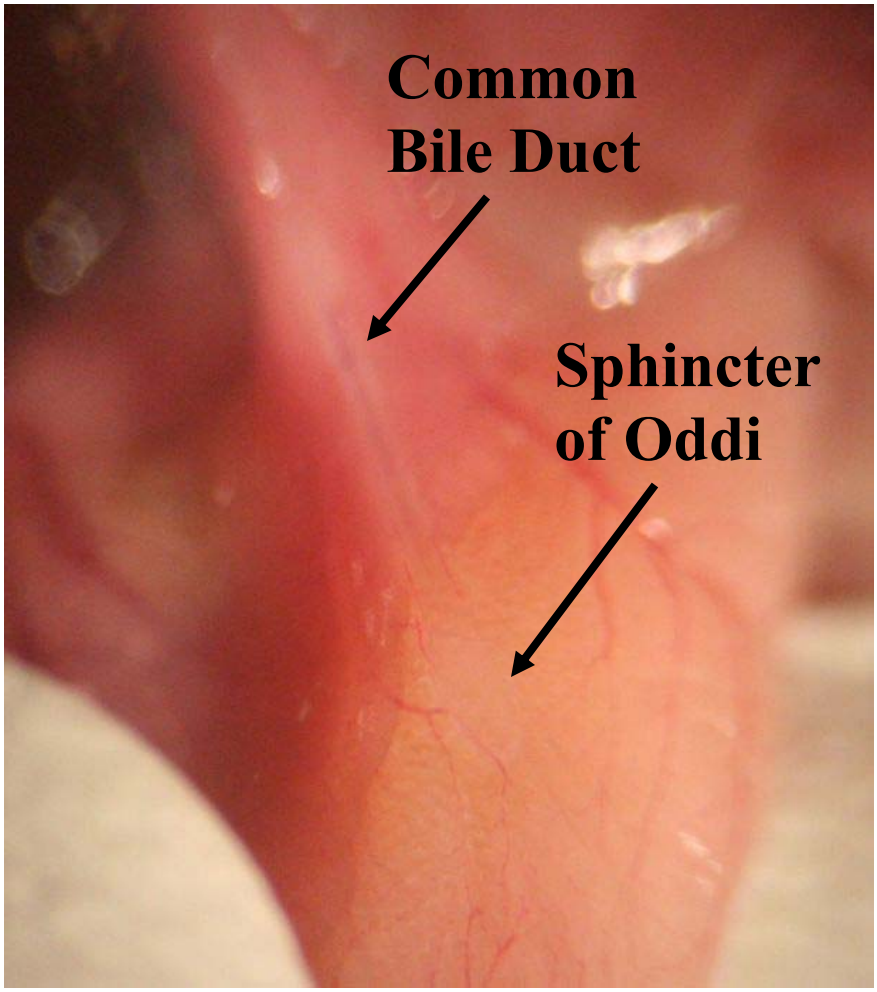

Figure A.6. Close-up view of common bile duct and sphincter of Oddi. Needle was inserted horizontally through the sphincter of Oddi.

Next, a 30 gauge needle was used injected into the Sphinchter of Oddi (labeled in Figures A.4 and A.6 to deliver approximately 2-4 mL of the collagenase solution into the pancreatic duct; the injection is shown in Figure A.7.

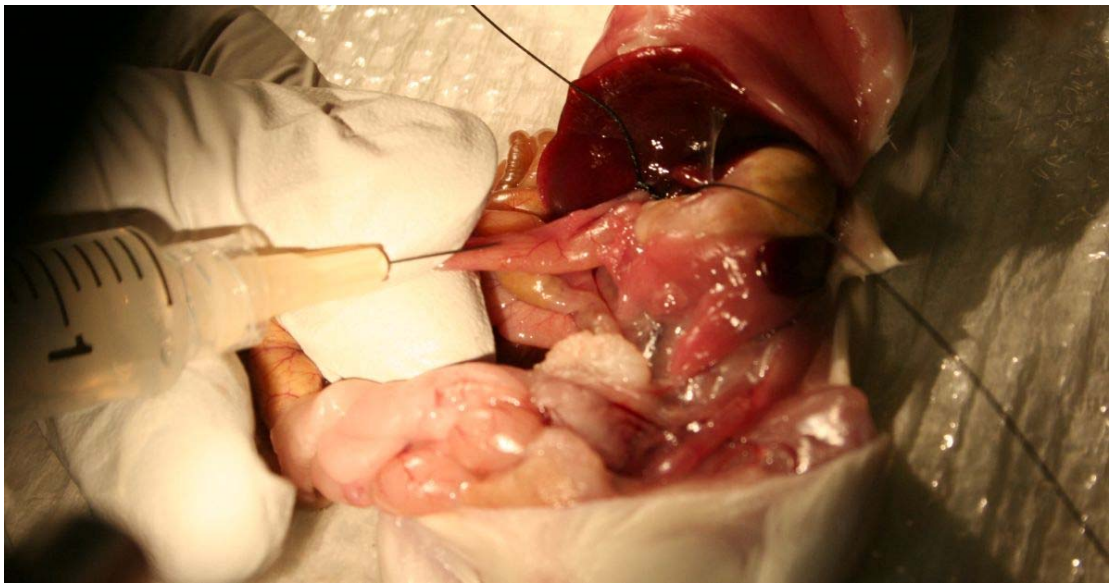

Figure A.7. Injection of collagenase through sphincter of Oddi. Syringe needle was directed through the sphincter of Oddi.

As the pancreas was filled with collagenase, it expanded and formed a marble-like appearance, as shown in Figure A.8.

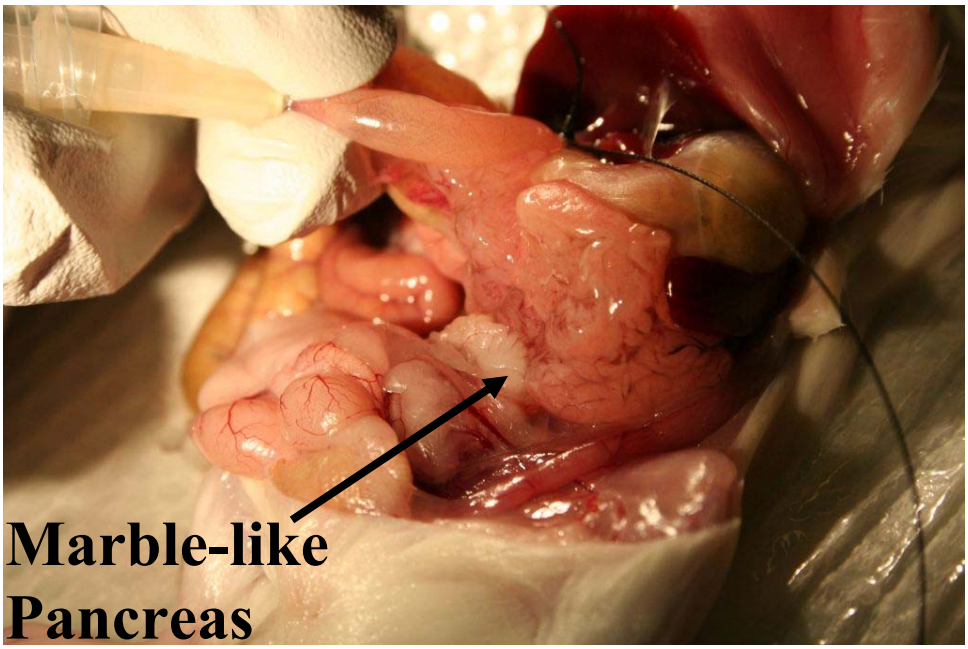

Figure A.8. Expansion of pancreas upon injection. Following injection of 2-4 mL of collagenase through the sphincter of Oddi, the pancreas took on a marble-like appearance.

Following injection, 4.5" dissection scissors and plain forceps were used to remove the pancreas from the mouse's abdominal cavity. The pancreas was then placed in a siliconized scintillation vial, the vial was filled with approximately 4-5 mL of collagenase solution, and the pancreas was minced with the 4.5" scissors. The vial was then shaken vigorously for approximately 3 s and placed in a water bath at 37 ˚C until digested. After approximately 4 minutes in the water bath, the vial was shaken again, and the digestion was checked for progress every 2 min. Once the digestion was nearly complete, the vial was checked more frequently. Figure A.9 shows various stages of digestion.

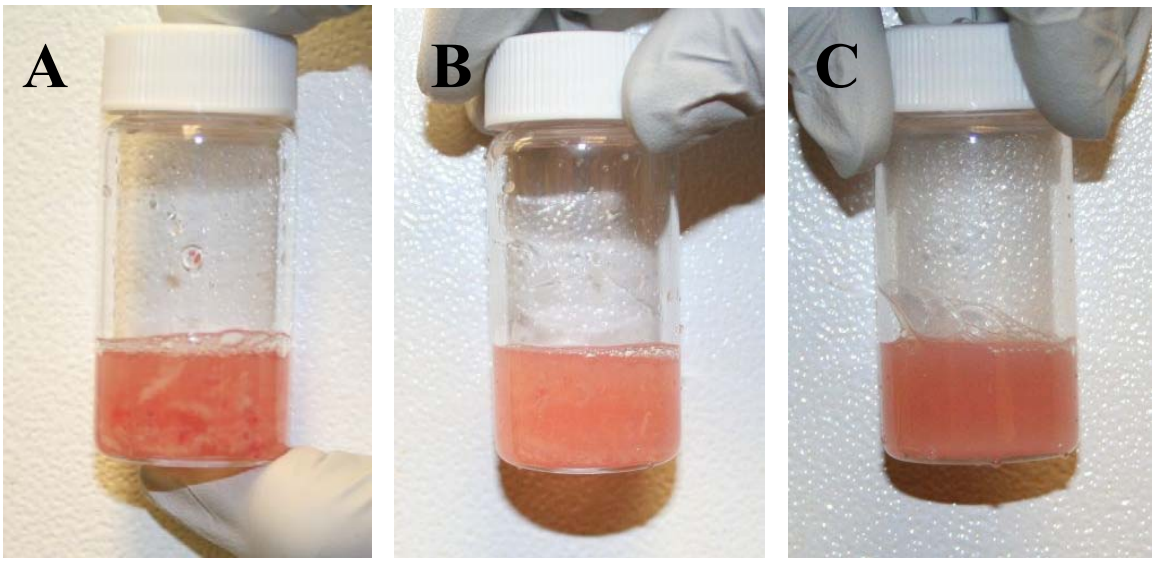

Figure A.9. Digestion of pancreas. (A) Minced pancreas in collagenase before digestion. (B) Partially-digested pancreas. (C) Fully-digested pancreas. After removal of pancreas, the pancreas-containing vial was placed in a water bath at 37 C. Pancreas was digested until mixture was cloudy and few large masses of pancreatic tissue remained (C).

After digestion was complete, 15 mL of Mg-HBSS was added to the vial. The vial was shaken and the contents of the vial were poured into a 50 mL centrifuge tube. The rinse process was repeated by adding 15 mL of Mg-HBSS to the scintillation vial, shaking the vial, and pouring the contents into the same 50 mL centrifuge tube. The contents of the centrifuge tube were then allowed to settle for 4 min. The vial was then topped off to 50 mL with Ca-HBSS and triturated with a sterile transfer pipette. The trituration process is demonstrated in Figure A.10. The contents of the vial were again allowed to stand for 4 min.

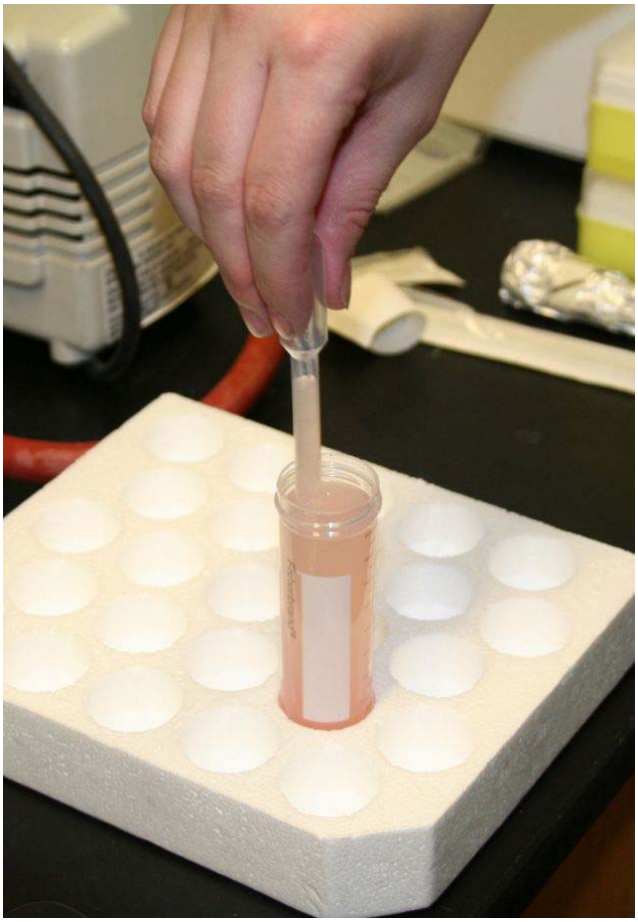

Figure A.10. Washing of islets following pancreas digestion. Solution was triturated with a sterile transfer pipette.

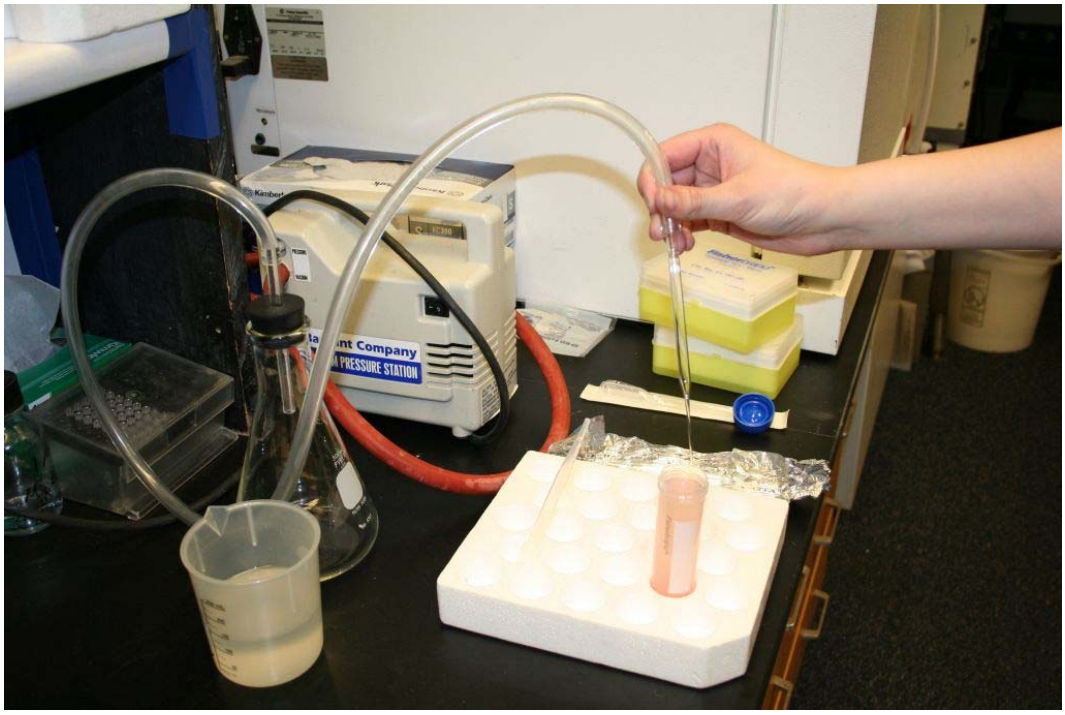

Figure A.11. Vacuum apparatus used for supernatant removal. Supernatant was removed with a sterile Pasteur pipette connected to a vacuum trap.

After settling for 4 min, the supernatant was removed to 10-15 mL with sterilized glass Pasteur pipettes using a vacuum trap apparatus, as demonstrated in Figure A.11. Ca-HBSS was then added to 40 mL again, and the solution was triturated and allowed to settle for 4 min. The rinsing procedure was repeated 5 times or until the tissue solution was relatively clear, as shown in Figure A.12.

Figure A.12. Supernatant removal following final islet washing step. Islets were washed until supernatant was relatively clear with few particulates.

After the final supernatant removal, the centrifuge tube was gently swirled to form a homogenous tissue solution. Figure A.13 shows the centrifuge tube contents after 4 minutes of settling (A.13A) and the contents after gentle mixing to form a more homogenous solution (A.13B).

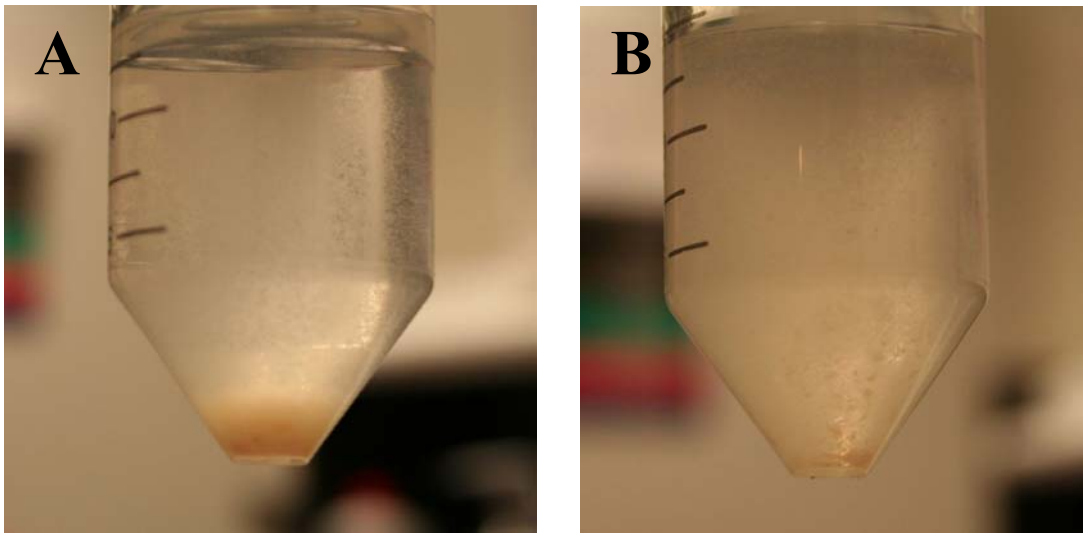

Figure A.13. Islet tissue following final washing step. (A) Settled islets following supernatant removal. (B) Mixed islet solution. Contents of centrifuge tube were gently swirled to create a homogeneous solution.

The solution was poured though a 100 µm cell strainer into a 60 mm petri dish. To transfer all remaining tissue, 5-10 mL of fresh Ca-HBSS were poured into the centrifuge tube, the tube was swirled, and again, the contents of the tube were poured through the cell strainer. The cell strainer was then inverted over an empty 60 mm petri dish (Figure A.14A), and a sterile transfer pipette and Ca-HBSS were used to rinse off islets and remaining tissue from the inside of the cell strainer (Figure A.14B).

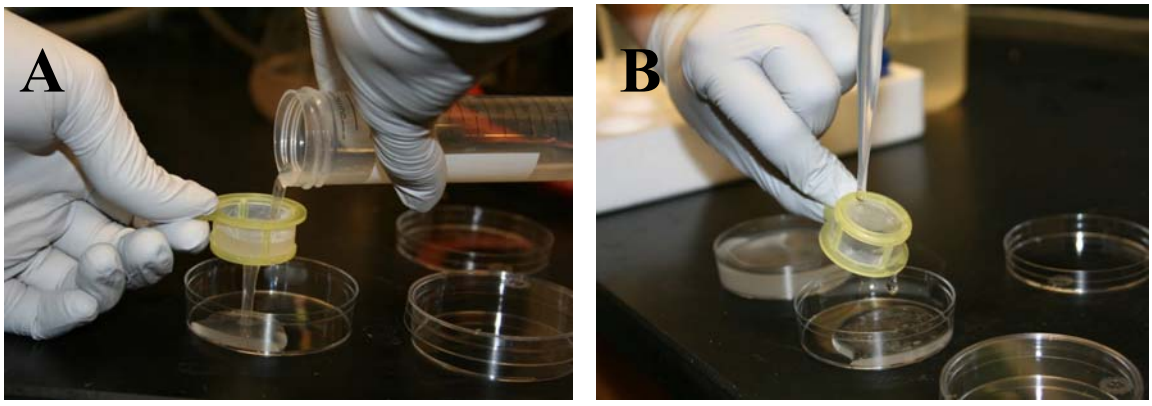

Figure A.14. Separation of islets from smaller tissue debris. (A) Solution was poured through a 100 µm filter. (B) Islets were removed from the filter by rinsing with Ca-HBSS and a sterile transfer pipette.

Once the islets were removed from the cell strainer, they were transferred to a sterile cell hood, where islet plating occurred. Figure A.15 shows an image of the petri dish containing islets and other cell debris immediately after filtering through the cell strainer.

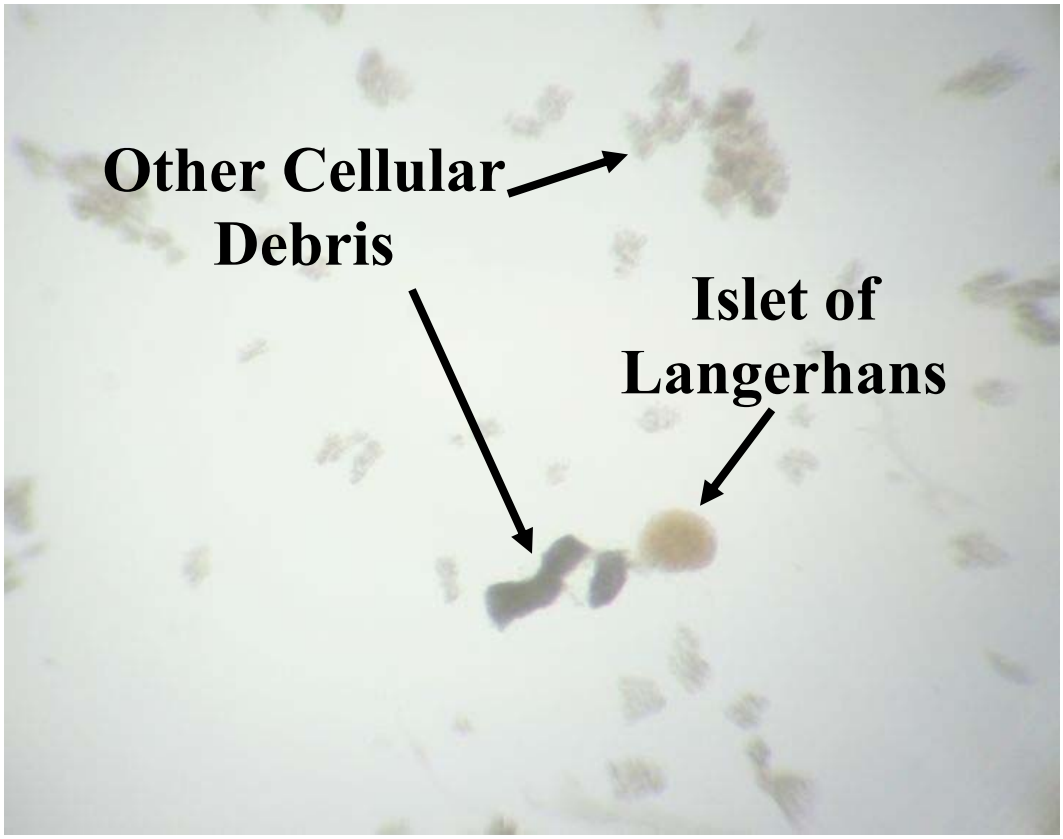

Figure A.15. Photomicrograph of isolated islet of Langerhans and other cellular debris. Islets appeared pink and round with smooth edges.

Islets 100-300 μm in diameter and oblong-to-spherical in shape were picked individually under a light microscope in a cell hood (shown in Figure A.16) using a 100 μL pipette and sterile pipette tips (pre-autoclaved). The picked islets were immediately pipetted into RPMI 1640 media supplemented with 10 % FBS, 100 U/mL of penicillin, and 100 μg/mL of streptomycin. Islets were picked and transferred into fresh RPMI 1640 media until no debris was present. No more than 25 islets were placed in a 60 mm cell dish for

culture. Picked islets were maintained at 37 °C, 5 % CO_2, and pH 7.4. Islets were used 1-7 days following isolation. Figure A.17 depicts a batch of approximately 20 healthy islets that have been cultured for 36 h.

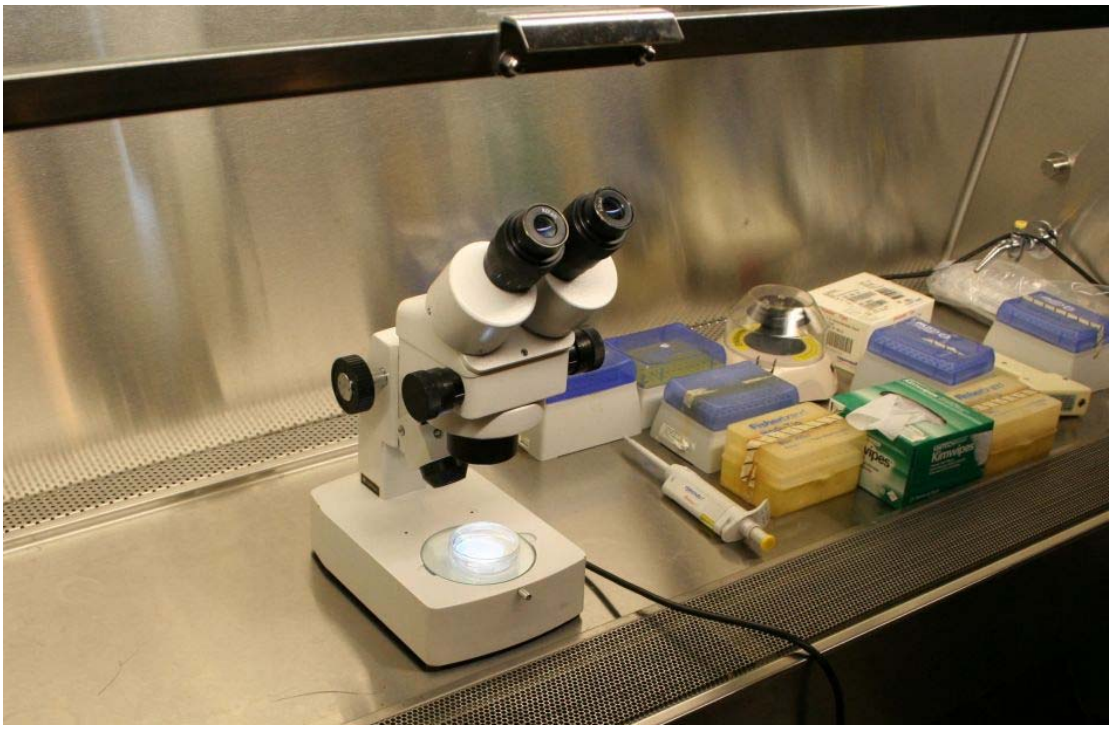

Figure A.16. Sterile hood for cell manipulation.

Figure A.17. Photomicrograph of approximately 20 healthy islets contained in a petri dish in culture media.

Importance of Sterility. Because all culture is performed in a physiologically friendly environment (i.e. plentiful salts and nutrients, 37 ˚C, pH 7.4, etc), it is imperative to use sterile cell culture techniques since multiple infection types are possible and difficult to eliminate. Sterile technique should begin prior to the isolation. All materials that touch cells in the isolation process should be sterile. Additionally, all solutions in which cells are bathed should be sterile filtered using a 0.22 μm filter prior to use. When using the cell hood, it is important to wear gloves and sterilize them with 70 % EtOH before entering the hood. All items should be wiped with 70 % EtOH prior to placement in the cell hood. Before bringing cells into the hood, use EtOH to sterilize all surfaces with which cell culture dishes may come into contact. As mentioned above, pipette tips should be autoclaved prior to placement in the cell hood, and should the pipette tip

contact any surface in the hood other than cell solutions, it should be promptly disposed of and replaced with a new pipette tip.

Once cells are picked and placed in cell culture dishes, the dishes should be wiped with 70 % EtOH prior to placement in an incubator. Gloves should be worn and cleaned with 70 % EtOH prior to removing cells from or placing cells in the incubator. Prior to cell placement in the incubator, sterilized (autoclaved), deionized water should be added to the water pan in the incubator.

When an infection arises in the incubator, all disposable contents of the incubator should be placed in bleach and disposed. The non-disposable components should be autoclaved, if possible. The inside of the incubator should be wiped with bleach (up to 20 %) or another sterilization solution. Because bleach is corrosive, care should be taken to thoroughly rinse the bleach from the incubator. If the infection remains, a cell culture expert should be contacted for further assistance in sterilizing the incubator.

APPENDIX B

INTRACELLULAR CALCIUM MEASUREMENTS

Fura-2. Intracellular Ca^{2+} imaging experiments were performed on islets loaded with the Ca^{2+}-sensitive dye, fura-2. Fura-2 is a fluorescent, ratiometric, cell-permeant dye capable of binding Ca^{2+}.[69] The excitation wavelength shifts from 380 nm to 340 nm upon Ca^{2+} binding. Figure B.1 shows the excitation spectra for 1 μM fura-2 collected at 20 ˚C in buffers with free Ca^{2+} concentrations ranging from 1 nM to 10 μM.[69]

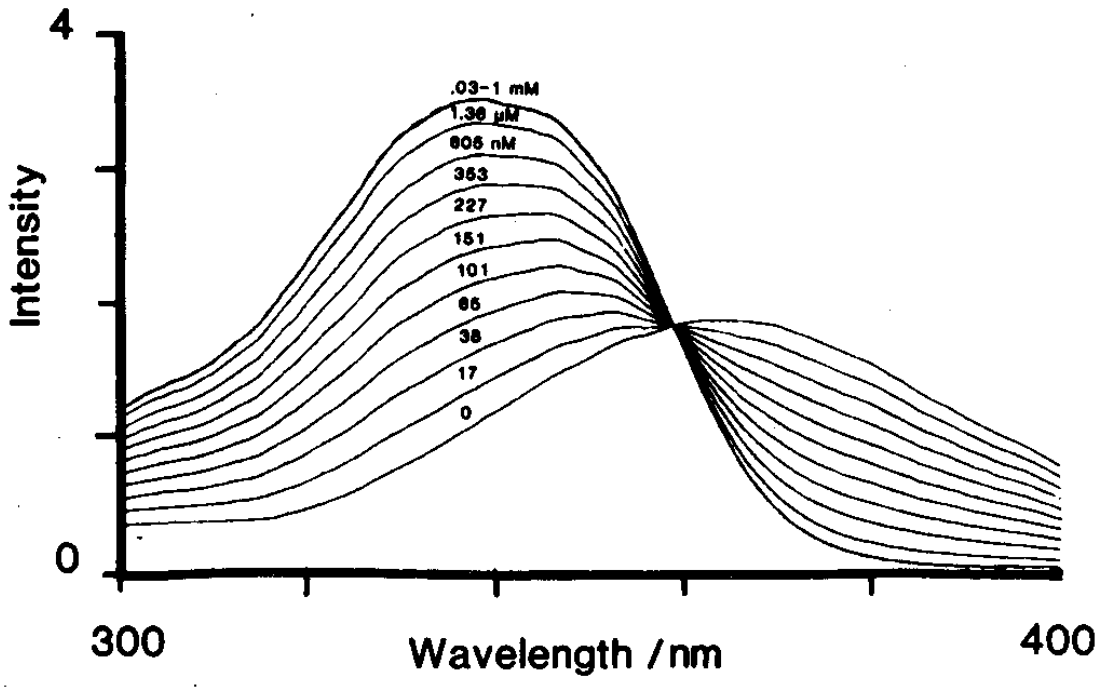

Figure B.1. Excitation spectra for 1 μL fura-2. Spectra were collected at 20 ˚C in buffers with free Ca^{2+} values ranging from 1 nM to 10 μM. The excitation bandwidth was 1.9 nm and the emission was collected at 510 ± 4.6 nm. The fluorescence excitation spectra shift to shorter wavelengths with increasing Ca^{2+} concentration. Reproduced with permission from reference [69].

System Calibration. To calibrate the system, two solutions were prepared. First, an R_{min} (0 nM Ca^{2+}) solution was prepared by dissolving 1.4 mg of the Ca^{2+} chelator, ethylene glycol tetraacetic acid (EGTA) in 3 mL Kreb's ringer buffer (KRB) (without Ca^{2+}) and 4.5 μL of the stock fura-2 salt solution. The mixture produces a solution of KRB with 1 mM EGTA and ~2 μM fura-2 salt. An R_{max} solution (1 mM Ca^{2+}) was prepared by mixing 3 mL of KRB (without Ca^{2+}), 3 μL of 1 M $CaCl_2$, and 4.5 μL of stock solution of fura-2 salt. The mixture produces a KRB solution with 1 mM Ca^{2+}, and ~2 μM fura-2 salt.

All Ca^{2+} imaging experiments were performed on a microfluidic device, which enabled precise control of the environment surrounding the cells. Beginning with R_{min}, one at a time, the solutions were placed in the islet reservoir and all perfusion reservoirs. Vacuum was applied to the islet chamber and used to pull the solutions through the channels. The according solution was then replaced in the islet chamber, and the chip was placed atop the stage of a Nikon Diaphot 300 microscope. The free fura-2 and the complex formed between Ca^{2+} and fura-2 were alternately excited, via a filter wheel, by 340 nm (complex dye) and 380 nm (free dye) with light from a Xenon-arc lamp. The 340 and 380 nm light was directed to the microscope with a liquid light guide. The excitation light was then reflected with a 505 nm dichroic mirror and was focused through a 20X microscope objective onto the islet reservoir (exposure time was 50-100 ms). The fluorescence emission from both excitation wavelengths was collected through a 520 ± 10 nm bandpass filter. Figure B.2 shows a schematic of the Ca^{2+} imaging instrumentation. A region of interest was drawn in both the image collected with 340 nm excitation and the image collected with 380 nm excitation of the reservoir, and the

intensities over the region were integrated using Metamorph software. The intensity at 340 was divided by the intensity at 380 to determine ratio R_{min} and ratio R_{max}. The resulting R_{min} and R_{max} values were recorded in Metamorph and used later to determine the intracellular Ca^{2+} concentration in single islets.

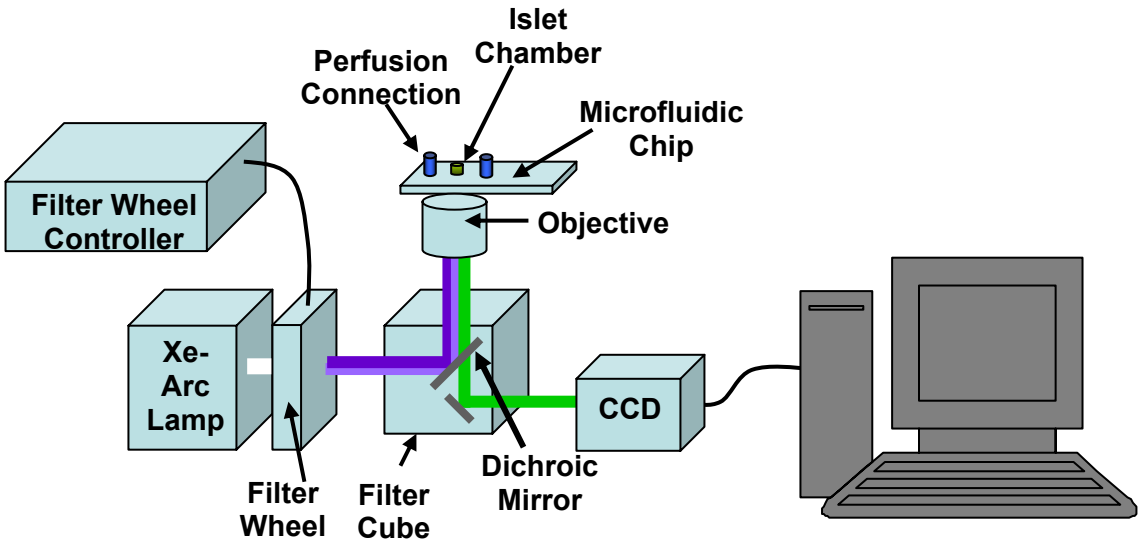

Figure B.2. Instrumentation schematic for Ca^{2+} imaging. A Xe-arc lamp was used as a broad-field light source. A filter wheel was used to alternately select 340 and 380 nm light for excitation. The excitation light was directed into a filter cube in a Nikon Diaphot 300 microscope via a liquid light guide, was directed up via a 505 nm dichroic mirror though a 20 X objective. The fluorescence emission was collected through the same objective, passed through a 520 ± 10 nm emission filter, and collected with a CCD.

Intracellular Ca^{2+} Imaging. To perform Ca^{2+} imaging experiments on pancreatic islets, islets were first loaded with the dye by incubation for 45 min with 2 μM fura-2 at 37 ˚C. The fura-2 was dissolved in DMSO to create a stock concentration of 1 mM. All Ca^{2+} imaging experiments were performed on a microfluidic chip to allow precise control of the islet's environment. Prior to loading the islet on the chip, the device's microfluidic channels were rinsed via vacuum with water, followed by 3 mM glucose KRB. Next, 50 μL of fresh 3 mM glucose KRB were added to the islet chamber on the chip. The rinsing steps were performed during the dye-loading process.

Following incubation with fura-2, the islet was handpicked under a light microscope with a 10-100 μL pipette and sterile pipette tips. The islet was transferred to a cell dish holding 3 mM glucose KRB to rinse off RPMI 1640 (10 mM glucose) from the islet. The islet was again picked along with 3 mM glucose KRB (total volume was 50 μL) and transferred to the islet chamber. A gel loader pipette tip was used to gently guide the islet from the surface of the chip to the drilled access hole, which is on level with microfluidic perfusion channels. After the islet was loaded onto the microfluidic device, the chip was transferred to the stage of the microscope. A gas-driven pressure perfusion system was used to perfuse the islet with media and stimulants at a rate of 0.6 μL/min. To maintain the cells at physiological temperature (37 ˚C), a thin-film resistive heater was placed underneath the chip.

Images of the islet were collected at 1 Hz, and the intensity over the islet area was integrated using Metamorph imaging software. Metamorph was used to calculate the ratio of the emission at 340 and 380 nm, and after calibration of the system, eq. 1 was used to determine the intracellular Ca^{2+} concentration.

$$\left[Ca^{2+}\right] = K_d \left[\frac{R - R_{\min}}{R_{\max} - R}\right]\left[\frac{S_{f2}}{S_{b2}}\right] \qquad \text{eq. 1}$$

where K_d = effective dissociation constant, 224 nM at 37 ˚C (from literature), R = experimental ratio, R_{min} = ratio in zero free Ca^{2+}, R_{max} = ratio in saturated Ca^{2+}, S_{f2} = fluorescence intensity at 380 nm with zero Ca^{2+}, and S_{b2} = fluorescence intensity at 380 nm with saturated Ca^{2+}.

REFERENCES

(1) http://diabetes.org, Accessed December 7, 2008.
(2) Allen, R. D. M.; Nankivell, B. J.; Hawthorne, W. J.; O'Connell, P. J.; Chapman, J. R. *Transplant. Proc.* **2001**, *33*, 3485-3488.
(3) Kahn, C. R. *Diabetes* **1994**, *43*, 1066-1084.
(4) US Department of Health and Human Services: Atlanta, G., 2007.
(5) Kulkarni, R. N. *Int. J. Biochem. Cell Biol.* **2004**, *36*, 365-371.
(6) Henquin, J. C. *Diabetes* **2000**, *49*, 1751-1760.
(7) Gilon, P.; Shepherd, R. M.; Henquin, J. C. *J. Biol. Chem.* **1993**, *268*, 22265-22268.
(8) Nunemaker, C. S.; Wasserman, D. H.; McGuinness, O. P.; Sweet, I. R.; Teague, J. C.; Satin, L. S. *American Journal of Physiology-Endocrinology and Metabolism* **2006**, *290*, E523-E529.
(9) Porksen, N.; Nyholm, B.; Veldhuis, J. D.; Butler, P. C.; Schmitz, O. *Am. J. Physiol. Endocrinol. Metab.* **1997**, *273*, E908-E914.
(10) Schmitz, O.; Arnfred, J.; Nielsen, O. H.; Becknielsen, H.; Orskov, H. *Acta Endocrinol.* **1986**, *113*, 559-563.
(11) Schmitz, O.; Juhl, C. B.; Hollingdal, M.; Veldhuis, J. D.; Porksen, N.; Pincus, S. M. *Metab. Clin. Exp.* **2001**, *50*, 41-46.
(12) Peiris, A. N.; Stagner, J. I.; Vogel, R. L.; Nakagawa, A.; Samols, E. *J. Clin. Endocrinol. Metab.* **1992**, *75*, 290-294.
(13) Porksen, N.; Munn, S.; Steers, J.; Vore, S.; Veldhuis, J.; Butler, P. *Am. J. Physiol. Endocrinol. Metab.* **1995**, *269*, E478-E488.
(14) Porksen, N.; Munn, S.; Steers, J.; Veldhuis, J. D.; Butler, P. C. *Diabetes* **1996**, *45*, 1317-1323.
(15) Lang, D. A.; Matthews, D. R.; Burnett, M.; Turner, R. C. *Diabetes* **1981**, *30*, 435-439.
(16) Paolisso, G.; Sgambato, S.; Torella, R.; Varricchio, M.; Scheen, A.; Donofrio, F.; Lefebvre, P. J. *J. Clin. Endocrinol. Metab.* **1988**, *66*, 1220-1226.
(17) Hollingdal, M.; Juhl, C. B.; Pincus, S. M.; Sturis, J.; Veldhuis, J. D.; Polonsky, K. S.; Porksen, N.; Schmitz, O. *Diabetes* **2000**, *49*, 1334-1340.
(18) Orahilly, S.; Turner, R. C.; Matthews, D. R. *N. Engl. J. Med.* **1988**, *318*, 1225-1230.
(19) Schmitz, O.; Porksen, N.; Nyholm, B.; Skjaerbaek, C.; Butler, P.; Veldhuis, J. D.; Pincus, S. M. *Am. J. Physiol.-Endocrinol. Metab.* **1997**, *272*, E218-E226.
(20) Simon, C.; Brandenberger, G. *Diabetes* **2002**, *51*, S258-S261.
(21) Shapiro, E. T.; Tillil, H.; Polonsky, K. S.; Fang, V. S.; Rubenstein, A. H.; Vancauter, E. *J. Clin. Endocrinol. Metab.* **1988**, *67*, 307-314.
(22) Simon, C.; Brandenberger, G.; Follenius, M. *J. Clin. Endocrinol. Metab.* **1987**, *64*, 669-674.

(23) Sturis, J.; Scheen, A. J.; Leproult, R.; Polonsky, K. S.; Vancauter, E. *J. Clin. Invest.* **1995**, *95*, 1464-1471.
(24) Sturis, J.; Vancauter, E.; Blackman, J. D.; Polonsky, K. S. *J. Clin. Invest.* **1991**, *87*, 439-445.
(25) Omeara, N. M.; Sturis, J.; Vancauter, E.; Polonsky, K. S. *J. Clin. Invest.* **1993**, *92*, 262-271.
(26) Simon, C.; Brandenberger, G.; Follenius, M.; Schlienger, J. L. *Diabetologia* **1991**, *34*, 435-440.
(27) Sturis, J.; Polonsky, K. S.; Shapiro, E. T.; Blackman, J. D.; Omeara, N. M.; Vancauter, E. *Diabetologia* **1992**, *35*, 681-689.
(28) Merl, V.; Peters, A.; Oltmanns, K. M.; Kern, W.; Hubold, C.; Hallschmid, M.; Born, J.; Fehm, H. L.; Schultes, B. *Metab. Clin. Exp.* **2004**, *53*, 1449-1453.
(29) Peschke, E.; Peschke, D. *Diabetologia* **1998**, *41*, 1085-1092.
(30) Picinato, M. C.; Haber, E. P.; Carpinelli, A. R.; Cipolla-Neto, J. *J. Pineal Res.* **2002**, *33*, 172-177.
(31) Polonsky, K. S.; Given, B. D.; Hirsch, L. J.; Tillil, H.; Shapiro, E. T.; Beebe, C.; Frank, B. H.; Galloway, J. A.; Vancauter, E. *N. Engl. J. Med.* **1988**, *318*, 1231-1239.
(32) Polonsky, K. S.; Given, B. D.; Vancauter, E. *J. Clin. Invest.* **1988**, *81*, 442-448.
(33) Vancauter, E.; Shapiro, E. T.; Tillil, H.; Polonsky, K. S. *Am. J. Physiol.* **1992**, *262*, E467-E475.
(34) Vancauter, E.; Blackman, J. D.; Roland, D.; Spire, J. P.; Refetoff, S.; Polonsky, K. S. *J. Clin. Invest.* **1991**, *88*, 934-942.
(35) Muhlbauer, E.; Wolgast, S.; Finckh, U.; Peschke, D.; Peschke, E. *FEBS Lett.* **2004**, *564*, 91-96.
(36) Gilon, P.; Jonas, J. C.; Henquin, J. C. *Diabetologia* **1994**, *37*, 1007-1014.
(37) Tsuboi, T.; Ravier, M. A.; Parton, L. E.; Rutter, G. A. *Diabetes* **2006**, *55*, 1057-1065.
(38) Van de Casteele, M.; Kefas, B. A.; Cai, Y.; Heimberg, H.; Scott, D. K.; Henquin, J. C.; Pipeleers, D.; Jonas, J. C. *Biochem. Biophys. Res. Commun.* **2003**, *312*, 937-944.
(39) Stein, D. T.; Stevenson, B. E.; Chester, M. W.; Basit, M.; Daniels, M. B.; Turley, S. D.; McGarry, J. D. *J. Clin. Invest.* **1997**, *100*, 398-403.
(40) Zhou, Y. P.; Grill, V. E. *J. Clin. Invest.* **1994**, *93*, 870-876.
(41) Muoio, D. M.; Newgard, C. B. *Nat. Rev. Mol. Cell Biol.* **2008**, *9*, 193-205.
(42) Poitout, V., Canary Isl, SPAIN, Mar 05-07 2008; Portland Press Ltd; 901-904.
(43) Almanza-Perez, J. C.; Blancas-Flores, G.; Garcia-Macedo, R.; Alarcon-Aguilar, F. J.; Cruz, M. *Gac. Med. Mex.* **2008**, *144*, 535-542.
(44) Spiegel, K. *Int. J. Pediatr. Obes.* **2008**, *3*, 27-28.
(45) Rampersaud, E.; Mitchell, B. D.; Naj, A. C.; Pollin, T. I. *Curr Diabetes Rev* **2008**, *4*, 329-339.
(46) Romao, I.; Roth, J. *J. Am. Diet. Assoc.* **2008**, *108*, S24-S28.
(47) Guilherme, A.; Virbasius, J. V.; Puri, V.; Czech, M. P. *Nat. Rev. Mol. Cell Biol.* **2008**, *9*, 367-377.
(48) Lenzen, S.; Joost, H. G.; Hasselblatt, A. *Diabetologia* **1976**, *12*, 495-500.

(49) Eaton, R. P.; Allen, R. C.; Schade, D. S.; Erickson, K. M.; Standefer, J. *J. Clin. Endocrinol. Metab.* **1980**, *51*, 520-528.
(50) Tao, L.; Kennedy, R. T. *Anal. Chem.* **1996**, *68*, 3899-3906.
(51) Roper, M. G.; Shackman, J. G.; Dahlgren, G. M.; Kennedy, R. T. *Anal. Chem.* **2003**, *75*, 4711-4717.
(52) Shackman, J. G.; Dahlgren, G. M.; Peters, J. L.; Kennedy, R. T. *Lab Chip* **2005**, *5*, 56-63.
(53) Davidsson, R.; Boketoft, A.; Bristulf, J.; Kotarsky, K.; Olde, B.; Owman, C.; Bengtsson, M.; Laurell, T.; Emneus, J. *Anal. Chem.* **2004**, *76*, 4715-4720.
(54) Kimura, H.; Yamamoto, T.; Sakai, H.; Sakai, Y.; Fujii, T. *Lab Chip* **2008**, *8*, 741-746.
(55) Kennedy, R. T. *Anal. Chim. Acta* **1999**, *400*, 163-180.
(56) Yeung, E. S. *J. Chromatogr. A* **1999**, *830*, 243-262.
(57) Mayer, B. X. *J. Chromatogr. A* **2001**, *907*, 21-37.
(58) Thomas, B. R.; Ghodbane, S. *J. Liq. Chromatogr.* **1993**, *16*, 1983-2006.
(59) Shafaati, A.; Clark, B. J., Bradford, United Kingdom, Jul 13-14 1993; Royal Soc Chemistry; 481-483.
(60) Strege, M. A.; Lagu, A. L. *J. Liq. Chromatogr.* **1993**, *16*, 51-68.
(61) Altria, K. D. *Chromatographia* **1993**, *35*, 493-496.
(62) Mayer, B. X.; Muller, M. *Lc Gc North America* **2000**, *18*, 694-+.
(63) Siren, H.; Jumppanen, J. H.; Manninen, K.; Riekkola, M. L. *Electrophoresis* **1994**, *15*, 779-784.
(64) Yang, J.; Rose, S.; Hage, D. S. *J. Chromatogr. A* **1996**, *735*, 209-220.
(65) Jumppanen, J. H.; Riekkola, M. L. *Anal. Chem.* **1995**, *67*, 1060-1066.
(66) Frenz, J.; Wu, S. L.; Hancock, W. S. *J. Chromatogr.* **1989**, *480*, 379-391.
(67) Gas, B.; Stedry, M.; Kenndler, E. *Electrophoresis* **1997**, *18*, 2123-2133.
(68) Mayer, B. X.; Muller, M. *LC-GC Europe* **2001**, 2-7.
(69) Tsien, R. Y.; Rink, T. J.; Poenie, M. *Cell Calcium* **1985**, *6*, 145-157.
(70) Chao, P. H. G.; West, A. C.; Hung, C. T. *Am. J. Physiol. Cell Physiol.* **2006**, *291*, C718-C725.
(71) Donahue, S. W.; Donahue, H. J.; Jacobs, C. R. *J. Biomech.* **2003**, *36*, 35-43.
(72) Tran, L.; Farinas, J.; Ruslim-Litrus, L.; Conley, P. B.; Muir, C.; Munnelly, K.; Sedlock, D. M.; Cherbavaz, D. B. *Anal. Biochem.* **2005**, *341*, 361-368.
(73) Mohammed, J. S.; Wang, Y.; Harvat, T. A.; Oberholzer, J.; Eddington, D. T. *Lab Chip* **2009**, *9*, 97-106.
(74) Jayasinghe, S. A.; Langen, R. *Biochemistry* **2005**, *44*, 12113-12119.
(75) Clark, A.; Nilsson, M. R. *Diabetologia* **2004**, *47*, 157-169.
(76) Hoppener, J. W. M.; Lips, C. J. M. *Int. J. Biochem. Cell Biol.* **2006**, *38*, 726-736.
(77) Lorenzo, A.; Yankner, B. A., Zurich, Switzerland, Feb 17-19 1995; New York Acad Sciences; 89-95.
(78) Quist, A.; Doudevski, L.; Lin, H.; Azimova, R.; Ng, D.; Frangione, B.; Kagan, B.; Ghiso, J.; Lal, R. *Proc. Natl. Acad. Sci. U. S. A.* **2005**, *102*, 10427-10432.
(79) Brender, J. R.; Lee, E. L.; Cavitt, M. A.; Gafni, A.; Steel, D. G.; Ramamoorthy, A. *J. Am. Chem. Soc.* **2008**, *130*, 6424-6429.
(80) Yoshiike, Y.; Kayed, R.; Milton, S. C.; Takashima, A.; Glabe, C. G. *NeuroMol. Med.* **2007**, *9*, 270-275.

(81) Demuro, A.; Mina, E.; Kayed, R.; Milton, S. C.; Parker, I.; Glabe, C. G. *J. Biol. Chem.* **2005**, *280*, 17294-17300.
(82) Auwerx, J.; Staels, B. *Lancet* **1998**, *351*, 737-742.
(83) Ahima, R. S.; Prabakaran, D.; Mantzoros, C.; Qu, D. Q.; Lowell, B.; MaratosFlier, E.; Flier, J. S. *Nature* **1996**, *382*, 250-252.
(84) Hoggard, N.; Mercer, J. G.; Rayner, D. V.; Moar, K.; Trayhurn, P.; Williams, L. M. *Biochem. Biophys. Res. Commun.* **1997**, *232*, 383-387.
(85) Lollmann, B.; Gruninger, S.; StrickerKrongrad, A.; Chiesi, M. *Biochem. Biophys. Res. Commun.* **1997**, *238*, 648-652.
(86) Kieffer, T. J.; Habener, J. F. *Am. J. Physiol. Endocrinol. Metab.* **2000**, *278*, E1-E14.
(87) Kulkarni, R. N.; Wang, Z. L.; Wang, R. M.; Hurley, J. D.; Smith, D. M.; Ghatei, M. A.; Withers, D. J.; Gardiner, J. V.; Bailey, C. J.; Bloom, S. R. *J. Clin. Invest.* **1997**, *100*, 2729-2736.
(88) Poitout, V.; Rouault, C.; Guerre-Millo, M.; Reach, G. *Diabetes Metab.* **1998**, *24*, 321-326.
(89) Lee, G. H.; Proenca, R.; Montez, J. M.; Carroll, K. M.; Darvishzadeh, J. G.; Lee, J. I.; Friedman, J. M. *Nature* **1996**, *379*, 632-635.
(90) Baetens, D.; Stefan, Y.; Ravazzola, M.; Malaisselagae, F.; Coleman, D. L.; Orci, L. *Diabetes* **1978**, *27*, 1-7.
(91) Morioka, T.; Asilmaz, E.; Hu, J.; Dishinger, J. F.; Kurpad, A. J.; Elias, C. F.; Li, H.; Elmquist, J. K.; Kennedy, R. T.; Kulkarni, R. N. *J. Clin. Invest.* **2007**, *117*, 2860-2868.
(92) Jung, S. K.; Kauri, L. M.; Qian, W. J.; Kennedy, R. T. *J. Biol. Chem.* **2000**, *275*, 6642-6650.
(93) Jung, S. K.; Gorski, W.; Aspinwall, C. A.; Kauri, L. M.; Kennedy, R. T. *Anal. Chem.* **1999**, *71*, 3642-3649.
(94) Rosenzweig, Z.; Kopelman, R. *Anal. Chem.* **1995**, *67*, 2650-2654.
(95) Park, E. J.; Reid, K. R.; Tang, W.; Kennedy, R. T.; Kopelman, R. *J. Mater. Chem.* **2005**, *15*, 2913-2919.
(96) Ohno, K.; Tachikawa, K.; Manz, A. *Electrophoresis* **2008**, *29*, 4443-4453.
(97) Andersson, H.; van den Berg, A. *Sens. Actuators, B* **2003**, *92*, 315-325.
(98) Dishinger, J. F.; Kennedy, R. T. *Anal. Chem.* **2007**, *79*, 947-954.
(99) Dishinger, J. F.; Reid, K. R.; Kennedy, R. T. *Anal. Chem.* **2009**, *81*, 3119-3127.
(100) Ueki, K.; Okada, T.; Hu, J.; Liew, C. W.; Assmann, A.; Dahlgren, G. M.; Peters, J. L.; Shackman, J. G.; Zhang, M.; Artner, I.; Satin, L. S.; Stein, R.; Holzenberger, M.; Kennedy, R. T.; Kahn, C. R.; Kulkarni, R. N. *Nat. Genet.* **2006**, *38*, 583-588.
(101) Shackman, J. G.; Watson, C. J.; Kennedy, R. T. *J. Chromatogr. A* **2004**, *1040*, 273-282.
(102) Pralong, W. F.; Bartley, C.; Wollheim, C. B. *EMBO J.* **1990**, *9*, 53-60.
(103) Quist, A.; Doudevski, L.; Lin, H.; Azimova, R.; Ng, D.; Frangione, B.; Kagan, B.; Ghiso, J.; Lal, R., Baltimore, MD, Feb 14-18 2004; Natl Acad Sciences; 10427-10432.
(104) Porat, Y.; Kolusheva, S.; Jelinek, R.; Gazit, E. *Biochemistry* **2003**, *42*, 10971-10977.

(105) Nanga, R. P. R.; Brender, J. R.; Xu, J. D.; Veglia, G.; Ramamoorthy, A. *Biochemistry* **2008**, *47*, 12689-12697.
(106) Brender, J. R.; Hartman, K.; Reid, K. R.; Kennedy, R. T.; Ramamoorthy, A. *Biochemistry* **2008**, *47*, 12680-12688.
(107) Jaikaran, E.; Higham, C. E.; Serpell, L. C.; Zurdo, J.; Gross, M.; Clark, A.; Fraser, P. E. *J. Mol. Biol.* **2001**, *308*, 515-525.
(108) Abedini, A.; Raleigh, D. P. *Biochemistry* **2005**, *44*, 16284-16291.
(109) Ladokhin, A. S.; White, S. H. *J. Mol. Biol.* **1999**, *285*, 1363-1369.
(110) Knight, J. D.; Hebda, J. A.; Miranker, A. D. *Biochemistry* **2006**, *45*, 9496-9508.
(111) Knight, J. D.; Miranker, A. D. *J. Mol. Biol.* **2004**, *341*, 1175-1187.
(112) Mishra, R.; Bulic, B.; Sellin, D.; Jha, S.; Waldmann, H.; Winter, R. *Angew. Chem., Int. Ed.* **2008**, *47*, 4679-4682.
(113) Epand, R. M. *Biophys. Chem.* **2007**, *126*, 197-200.
(114) Epand, R. F.; Schmitt, M. A.; Gellman, S. H.; Epand, R. M. *Biochim. Biophys. Acta* **2006**, *1758*, 1343-1350.
(115) Casas, S.; Novials, A.; Reimann, F.; Gomis, R.; Gribble, F. M. *Diabetologia* **2008**, *51*, 2252-2262.
(116) Huang, C. J.; Haataja, L.; Gurlo, T.; Butler, A. E.; Wu, X. J.; Soeller, W. C.; Butler, P. C. *Am. J. Physiol. Endocrinol. Metab.* **2007**, *293*, E1656-E1662.
(117) Janson, J.; Ashley, R. H.; Harrison, D.; McIntyre, S.; Butler, P. C. *Diabetes* **1999**, *48*, 491-498.
(118) Cuajungco, M. *Brain Res. Rev.* **2003**, *41*, 44-56.
(119) Gold, G.; Grodsky, G. M. *Experientia* **1984**, *40*, 1105-1114.
(120) Kieffer, T. J.; Heller, R. S.; Habener, J. F. *Biochem. Biophys. Res. Commun.* **1996**, *224*, 522-527.
(121) Considine, R. V.; Sinha, M. K.; Heiman, M. L.; Kriauciunas, A.; Stephens, T. W.; Nyce, M. R.; Ohannesian, J. P.; Marco, C. C.; McKee, L. J.; Bauer, T. L.; Caro, J. F. *N. Engl. J. Med.* **1996**, *334*, 292-295.
(122) Emilsson, V.; Liu, Y. L.; Cawthorne, M. A.; Morton, N. M.; Davenport, M. *Diabetes* **1997**, *46*, 313-316.
(123) Fehmann, H. C.; Peiser, C.; Bode, H. P.; Stamm, M.; Staats, P.; Hedetoft, C.; Lang, R. E.; Goke, B. *Peptides* **1997**, *18*, 1267-1273.
(124) Ookuma, M.; Ookuma, K.; York, D. A. *Diabetes* **1998**, *47*, 219-223.
(125) Pallett, A. L.; Morton, N. M.; Cawthorne, M. A.; Emilsson, V. *Biochem. Biophys. Res. Commun.* **1997**, *238*, 267-270.
(126) Tanizawa, Y.; Okuya, S.; Ishihara, H.; Asano, T.; Yada, T.; Oka, Y. *Endocrinology* **1997**, *138*, 4513-4516.
(127) Leclercq-Meyer, V.; Malaisse, W. J. *Mol. Cell. Endocrinol.* **1998**, *141*, 111-118.
(128) LeclercqMeyer, V.; Malaisse, W. J. *Med. Sci. Res.* **1997**, *25*, 257-259.
(129) LeclercqMeyer, V.; Considine, R. V.; Sener, A.; Malaisse, W. J. *Biochem. Biophys. Res. Commun.* **1996**, *229*, 794-798.
(130) Gu, H.; Marth, J. D.; Orban, P. C.; Mossmann, H.; Rajewsky, K. *Science* **1994**, *265*, 103-106.
(131) Sinha, M. K.; Opentanova, I.; Ohannesian, J. P.; Kolaczynski, J. W.; Heiman, M. L.; Hale, J.; Becker, G. W.; Bowsher, R. R.; Stephens, T. W.; Caro, J. F. *J. Clin. Invest.* **1996**, *98*, 1277-1282.

(132) Hite, M. F.; Kahn, C. R. *J. Biol. Chem.* **1994**, *269*, 1-4.
(133) Koo, Y. E. L.; Cao, Y. F.; Kopelman, R.; Koo, S. M.; Brasuel, M.; Philbert, M. A. *Anal. Chem.* **2004**, *76*, 2498-2505.
(134) McDonagh, C.; MacCraith, B. D.; McEvoy, A. K. *Anal. Chem.* **1998**, *70*, 45-50.
(135) Preininger, C.; Klimant, I.; Wolfbeis, O. S. *Anal. Chem.* **1994**, *66*, 1841-1846.
(136) Xu, H.; Aylott, J. W.; Kopelman, R.; Miller, T. J.; Philbert, M. A. *Anal. Chem.* **2001**, *73*, 4124-4133.
(137) Amao, Y.; Miyashita, T.; Okura, I. *React. Funct. Polym.* **2001**, *47*, 49-54.
(138) DiMarco, G.; Lanza, M. *Sens. Actuators, B* **2000**, *63*, 42-48.
(139) Hartmann, P.; Trettnak, W. *Anal. Chem.* **1996**, *68*, 2615-2620.
(140) Douglas, P.; Eaton, K. *Sens. Actuators, B* **2002**, *82*, 200-208.
(141) Mills, A.; Thomas, M. *Analyst* **1997**, *122*, 63-68.
(142) Chen, X.; Zhong, Z. M.; Li, Z.; Jiang, Y. Q.; Wang, X. R.; Wong, K. Y. *Sens. Actuators, B* **2002**, *87*, 233-238.
(143) John, G. T.; Klimant, I.; Wittmann, C.; Heinzle, E. *Biotechnol. Bioeng.* **2003**, *81*, 829-836.
(144) Reece, J. S.; Miller, M. J.; Arnold, M. A.; Waterhouse, C.; Delaplaine, T.; Cohn, L.; Cannon, T. *Appl. Biochem. Biotechnol.* **2003**, *104*, 1-11.
(145) Mills, A.; Lepre, A. *Anal. Chem.* **1997**, *69*, 4653-4659.
(146) Lee, S. K.; Okura, I. *Spectrochim. Acta. A. Mol. Biomol. Spectrosc.* **1998**, *54*, 91-100.
(147) Papkovsky, D. B.; Ponomarev, G. V.; Trettnak, W.; Oleary, P. *Anal. Chem.* **1995**, *67*, 4112-4117.
(148) Trettnak, W.; Kolle, C.; Reininger, F.; Dolezal, C.; Oleary, P. *Sens. Actuators, B* **1996**, *35-36*, 506-512.
(149) O'Riordan, T. C.; Buckley, D.; Ogurtsov, V.; O'Connor, R.; Papkovsky, D. B. *Anal. Biochem.* **2000**, *278*, 221-227.
(150) Papkovsky, D. B.; Ovchinnikov, A. N.; Ogurtsov, V. I.; Ponomarev, G. V.; Korpela, T. *Sens. Actuators, B* **1998**, *51*, 137-145.
(151) Tan, W. H.; Shi, Z. Y.; Kopelman, R. *Anal. Chem.* **1992**, *64*, 2985-2990.
(152) Tan, W. H.; Shi, Z. Y.; Smith, S.; Birnbaum, D.; Kopelman, R. *Science* **1992**, *258*, 778-781.
(153) van der Veen, N. J.; Rozniecka, E.; Woldering, L. A.; Chudy, M.; Huskens, J.; van Veggel, F.; Reinhoudt, D. N. *Chem.--Eur. J.* **2001**, *7*, 4878-4886.
(154) Shortreed, M. R.; Dourado, S.; Kopelman, R. *Sens. Actuators, B* **1997**, *38-39*, 8-12.
(155) Lavin, P.; McDonagh, C. M.; Maccraith, B. D. *J. Sol-Gel Sci. Technol.* **1998**, *13*, 641-645.
(156) Marazuela, M. D.; Moreno-Bondi, M. C. *Anal. Bioanal. Chem.* **2002**, *372*, 664-682.
(157) Gil-Campos, M.; Canete, R.; Gil, A. *Clin. Nutr.* **2004**, *23*, 963-974.
(158) Vachharajani, V.; Granger, D. N. *IUBMB Life* **2009**, *61*, 424-430.
(159) Rosen, E. D.; Spiegelman, B. M. *Nature* **2006**, *444*, 847-853.
(160) Martins-Afferri, M. P.; Festuccia, W. T. L.; Navegantes, L. C. C.; Garofalo, M. A. R.; Botion, L. M.; Kettelhut, I. C.; Migliorini, R. H. *J. Nutr.* **2004**, *134*, 2919-2923.

(161) Bays, H.; Mandarino, L.; DeFronzo, R. A. *J. Clin. Endocrinol. Metab.* **2004**, *89*, 463-478.
(162) Clark, A. M.; Sousa, K. M.; Jennings, C.; MacDougald, O. A.; Kennedy, R. T. *Anal. Chem.* **2009**, *81*, 2350-2356.
(163) http://www.med.umich.edu/1libr/aha/pancreas.gif, Accessed February 12, 2009.